THE APPLICATION OF THE DELANO y-$\bar{y}$ DIAGRAM TO OPTICAL DESIGN

by

Fernando José López-López

A Dissertation Submitted to the Faculty of the

COMITTEE ON OPTICAL SCIENCES

In Partial Fulfillment of the Requirements
For the Degree of

DOCTOR OF PHILOSOPHY

In the Graduate College

THE UNIVERSITY OF ARIZONA

1 9 7 3

THE UNIVERSITY OF ARIZONA

GRADUATE COLLEGE

I hereby recommend that this dissertation prepared under my direction by Fernando José López-López

entitled The Application of the Delano y-$\bar{y}$ Diagram to Optical Design

be accepted as fulfilling the dissertation requirement of the degree of Doctor of Philosophy

Roland V. Shack — 23 FEB 1973

Dissertation Director — Date

After inspection of the final copy of the dissertation, the following members of the Final Examination Committee concur in its approval and recommend its acceptance:*

Orestes N. Stavroudis	23 February 1973
Arden C. Menzel	23 February 1973
R. J. Hilliard	26 February 1973
Robert R. Shannon	26 Feb 73

*This approval and acceptance is contingent on the candidate's adequate performance and defense of this dissertation at the final oral examination. The inclusion of this sheet bound into the library copy of the dissertation is evidence of satisfactory performance at the final examination.

STATEMENT BY AUTHOR

This dissertation has been submitted in partial fulfillment of requirements for an advanced degree at The University of Arizona and is deposited in the University Library to be made available to borrowers under rules of the Library.

Brief quotations from this dissertation are allowable without special permission, provided that accurate acknowledgment of source is made. Requests for permission for extended quotation from or reproduction of this manuscript in whole or in part may be granted by the copyright holder.

SIGNED: Juan Manuel Soto Loyza-Loyza

© COPYRIGHTED

BY

FERNANDO JOSÉ LÓPEZ-LÓPEZ

1973

Dedicado con todo cariño a

$$\frac{\exp(\ln \alpha t)\; n!\; e^{i\pi/2}}{\Gamma(n)\cdot \operatorname{sinc}(\pi/2) \int_0^\infty \frac{dx}{t^2 + a^2 x^2}},$$

a Citlaltzintli

y a Huitzitzilin.

ACKNOWLEDGMENTS

I wish to express my deep and sincere gratitude to all the persons who helped me through the years that took me to complete the work here reported.

First of all to my wife and daughters for their patience and continued faith and concern for my work, (Is your program working, Father?), and to whom this dissertation is dedicated.

To Dr. Aden B. Meinel and his wife Marjorie, long-time friends and advisers, whose constant help made possible for me to come back to Graduate School to pursue the doctoral degree in Optics.

To Dr. Roland V. Shack, for his constant encouragement and guidance in the supervision of this dissertation. His criticisms, always very constructive, were a powerful incentive for this work.

To Dr. Orestes N. Stavroudis and Prof. Robert R. Shannon, members of my comittee, for many invaluable discussions of a mathematical and practical nature that permitted to steer my work in the right direction.

To the Office of Education of the United States Government, for an NDEA Fellowship; the Perkin Elmer Corporation for the Perkin-Elmer Fellowship; and The University of Arizona, for the accompanying Graduate Tuition Scholarship, that allowed me to complete all my course work without financial worries.

To Mr. Hank Gethner of the Digigraphics Laboratory, Control Data Corporation, and Mr. Frank Scott of Perkin-Elmer Corporation, who through the free use of their computing facilities and a travel grant, respectively, made possible the early trial of this idea as a possible topic for a dissertation.

To the Air Force Office of Scientific Research which supported part of this work under Contract No. F04695-67-C-0197, and under Project THEMIS (Contract No. F44620-69-C-0024).

To The University of Arizona, State of Arizona, for the time used at the CDC 6400 Computer.

Finally, to my typist, whose name appears on the Dedication, and without whose help this work would have never been written, not even in rough draft form.

TABLE OF CONTENTS

TABLE OF CONTENTS--Continued

LIST OF ILLUSTRATIONS

LIST OF ILLUSTRATIONS--Continued

LIST OF ILLUSTRATIONS--Continued

LIST OF TABLES

ABSTRACT

The Delano y-$\bar{y}$ diagram, defined as a cartesian plot of the marginal ray height (ordinate) and the chief ray height (abscissa) at every surface of an optical system, provides a powerful tool for the analysis and design of optical systems, as well as for the teaching of geometrical-optics principles. The origin of the y-$\bar{y}$ diagram is based on the constancy of the Lagrange-Helmholtz invariant throughout an optical system, and on the refraction law.

In the present work, by using the tools of analytic geometry, all the first-order (gaussian) properties of an optical system (magnification, cardinal points, powers and focal lengths, separations and radii of curvature, stops and pupils, vignetting, obscurations, etc.) are derived analytically. The use of vectors or complex numbers to represent the points in the diagram, not only permits more elegant derivations, but also facilitates enormously the interpretation of the diagram, and gives the reader a powerful tool for solving practical problems.

This formulation is used for a general analysis of the properties of a thick element in the y-$\bar{y}$ diagram. An exact analytic solution to the problem of generalized bending and thickening of lenses is a direct result of this analysis.

The normalization of the $y-\bar{y}$ diagram for the purposes of comparative analyses of different systems is also investigated.

Finally, a computer program (YYRANCH) is described that implements these ideas into a practical tool allowing the user to analyze the first and third order properties of an optical system and to produce a workable third-order design that will maintain the first-order constraints imposed on such a system; the design variables are $y,\bar{y}$ and the curvatures and thicknesses are given as a result. The graphical monitoring of the program allows the user to follow the design step by step, and to make the appropiate corrections when needed.

CHAPTER 1

INTRODUCTION

Existing optical design computer programs make use of surface curvatures, thicknesses, and refractive indices as design parameters. This choice seems natural because these are the actual physical parameters of the optical system. However, as design variables, curvatures and thicknesses suffer from several disadvantages; for example, it is difficult to maintain first-order constraints, and also in general the aberrations of the system behave in a strongly nonlinear fashion as functions of these variables.

An appropiate non-linear transformation to more suitable variables would lead to an improvement in the operation of an automatic design program. Fortunately, such a transformation is possible with the use of the y-$\bar{y}$ diagram introduced by Delano (1963), in which the variables replacing curvatures and thicknesses are the paraxial heights and of the marginal and chief rays, traced through the optical system.

The use of y and $\bar{y}$ or their equivalents $n, \bar{n}$ (see Chapter 2), allows the first-order constraints to be easily maintained; and with respect to these variables, the aberrations behave more linearly, permitting a better control of the design program.

Delano introduced the y-$\bar{y}$ diagram as a two-dimensional representation of the first order properties of an optical system in the December 1963 issue of Applied Optics dedicated to the topic of Optical Design. He was inspired by previous work by T. Smith (see references in Delano's article) on the theory of periscopes. The treatment given by Delano is extremely concise, and this may have contributed to the fact that it has not attracted the attention that it deserves in the optical community. Only a handful of papers describing its use have appeared in the literature.

Due to its graphical representation, the y-$\bar{y}$ diagram is an excellent analysis tool. It is possible to "see" all the first-order characteristics of an optical system in a single graph as a set of dots connected by lines. Constraints and limitations imposed on the system are particularly obvious.

It is also possible to see at a glance what changes may be made on the points in order to improve the design without affecting other parts of the system. This makes possible the use of the diagram as a design tool. This dual role of analysis and design is the basic fact that makes the y-$\bar{y}$ diagram so attractive. This tool may well revolutionize the field of optical design in the near future.

This graphical representation has another virtue not less important than the above, and that is that one may actually learn the characteristics and properties of different optical systems by

representing them in this two-dimensional plot. In other words the y-$\bar{y}$ diagram is also an outstanding teaching tool. As such, it has been used at the Optical Sciences Center since 1967 by Dr. Shack in the course on Geometrical Optics. Many students have been motivated by this tool to try their hand at designing simple optical systems at an early stage. Some of them have had some previous experience in optical design and they have found that it is usually much easier to arrive at a solution to first-order problems by using this tool rather than the conventional methods.

One may ask, then, why this tool which seems to be highly advantageous for optical design, at least in the early stages, has not after nearly ten years had the diffusion and acceptance that seemingly deserves. There is of course the natural inertia of the well-proven old methods used by optical designers, now very well assisted by computers, but I believe that the main reason this tool has not caught on is the fact that, except for Delano's original article, there has not been available in the literature a thorough presentation of the properties and possibilities of the y-$\bar{y}$ diagram, and, as mentioned before, the conciseness of Delano's presentation has caused many readers to simply set it aside for "when I have more time...."; one has to read it carefully several times to really appreciate the elegance and power of the approach.

Just before starting on this dissertation I was given the opportunity of spending five weeks (July-August 1968) at the Digigraphics Laboratory of Control Data Corporation in Burlington, Massachusetts. Due to the courtesy of CDC and a travel grant given by Perkin-Elmer Corporation, both of which I wish to aknowledge with thanks, I was able to write a preliminary program of analysis based on the paper by Delano, for the purpose of graphical display using a Digigraphics interactive terminal attached to a CDC 3300 computer. The results were quite successful as far as they went, but they were limited by the shortness of the time available and my relatively rudimentary understanding of the technique. Nevertheless, the experience was especially valuable in indicating the road to follow.

For example, when I was faced with the project of writing a computer program using y and $\bar{y}$ variables, capable of being used in design as well as analysis of optical systems, it became clear that an analytic basis had to be developed. All the properties and characteristics of the y-$\bar{y}$ diagram, which are so beautifully seen in geometric terms had to be expressed in algebraic form before an effective program could be written. As one would expect, analytic geometry provides the basis for the algebraic expression of the properties of the diagram.

The present work is the result of this algebraization and its main purpose is to establish the analytic basis of the y-$\bar{y}$ diagram,, spelling out in as much detail as possible all of its properties and, with this basis, to develop a computer

program which may be used not only for a detailed analysis but, to a limited extent, also for the design of optical systems. A short description of the contents follows.

Chapter 2 describes the qualitative properties of the y-$\bar{y}$ diagram and its relation to its dual counterpart, the u-$\bar{u}$ diagram.

Chapter 3 begins the algebraization process. All the points in the diagram may be treated as vectors, and this representation leads to a very elegant and powerful derivation of all the properties of the diagram. Likewise, the lines connecting these points may be considered as vectors. The same set of points and lines in the plane may be treated as complex numbers, an approach which offers distinct advantages from the computational point of view. Finally, these two representations are compared with the matrix approach developed by Brouwer (1964) and discussed in many recent books on optics.

In Chapter 4 we seek the representation of all first-order properties of an optical system in the y-$\bar{y}$ diagram, in order to be able to recognize them later when analyzing or designing a system. Magnifications, conjugate planes, cardinal points, location of pupils and images, shifts of the stop or the image, and vignetting, are considered.

Chapter 5 deals with a normalization of the diagram that has been found particularly useful when comparing different systems of the same general type, but of quite different individual characteristics.

Chapter 6 is a direct application of the algebraic method to the analytical study of the properties of a single physical element: the thick lens. This is important, not only for the insight obtained, but because the thick lens is the fundamental component of all refractive systems, and its relationship to its equivalent thin lens, a well known and very useful abstraction, is thoroughly developed. A byproduct of this analysis is the analytic solution of an old problem, the bending and/or thickening of a single element without affecting the first-order properties of the rest of the system of which it is a part. This is described in the form of a programmable algorithm in Chapter 7.

Finally Chapter 8 describes the program YYRANCH which permits the user to analyze and design an optical system in the first- and third-order approximations.

This work does not pretend to be exhaustive, but rather it is intended to supply the ground work necessary for more ambitious projects.

One of these projects, already begun, is the analytical study of the third-order aberrations of the system in terms of the properties of the y-$\bar{y}$ diagram. Another investigation of some interest is the study of certain types of inhomogeneous media in the y-$\bar{y}$ diagram. In such media the ray paths are curvilinear rather than straight line segments in the y-$\bar{y}$ diagram. A third project is the development of a much more

sophisticated design program in which the system is accurately evaluated by real ray tracing in the conventional manner, but the controlling design variables are those of the y-$\bar{y}$ diagram rather than thicknesses and curvatures. Such a program would be capable of the complete design of the system through the final optimization. An obvious advantage is the ease with which first-order constraints are maintained.

As it might be expected in a topic as young as this is, the bibliography available is quite limited. Following the article by Delano (1963), we may mention a rather uninformative report on the application of the technique by Pegis et al. (1967), a short description of the properties of the diagram by Powell (1970), and a better and more complete one by Shack (1972).

Parts of the present work have been presented at meetings of the Optical Society of America, López-López (1970b; 1971b,-c; 1972a,-c), and other parts have been published in the form of articles or notes: the normalization of the diagram (López-López 1970a), the vector representation (1971d), and the treatment of the thick lens (1972b).

CHAPTER 2

THE y-$\bar{y}$ AND Ω-$\bar{\Omega}$ DIAGRAMS

We shall restrict ourselves at the outset to the paraxial or first-order approximation of Geometrical Optics. It is well known that under this approximation, the ray tracing equations for a rotationally symmetric optical system are only two and that they are linear. This means that only two paraxial rays, the marginal ray and the chief ray, need to be traced through the system to determine its first-order properties. Note the reciprocity between the roles of these two rays: the marginal ray determines the position of the image and the size of the size of the aperture, whereas the chief ray defines the size of the image and the position of the aperture; this reciprocity is the core of the duality properties between the y-$\bar{y}$ and Ω-$\bar{\Omega}$ diagrams. We shall denote all quantities belonging to the chief ray by a bar above the quantity; see Appendix A for notation.

It has been shown by Delano that a single skew ray may be traced through the system in the following manner. Assume a coordinate system as in Fig. 1. The z-axis coincides with the optical axis of the system; the origin may be arbitrarily chosen, somewhere along the optical axis. As the marginal and chief rays are meridional rays, we may trace the marginal ray in the y-z plane and the chief ray in the x-z plane without any loss of generality. Then the skew ray referred to by Delano is such

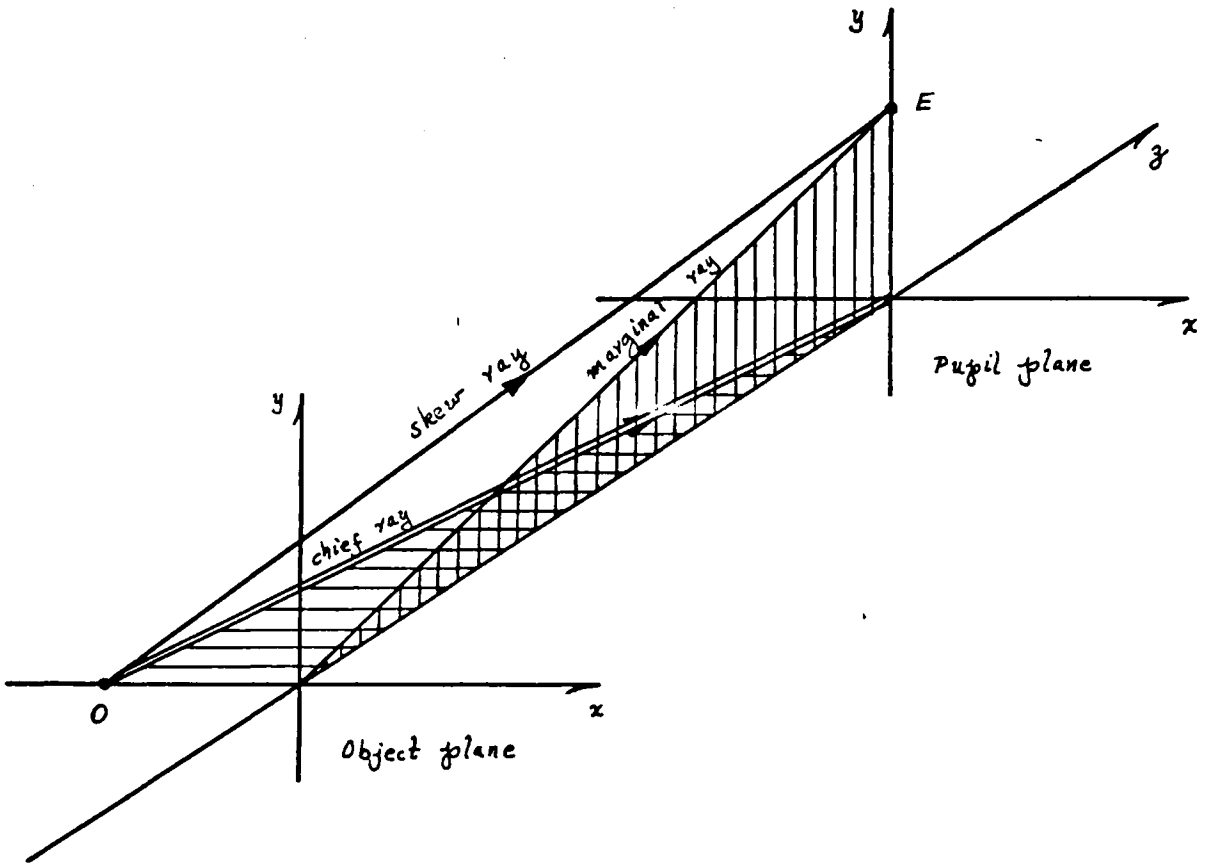

Fig. 1 Skew ray from object plane to pupil plane
with the marginal and chief rays as orthogonal projections

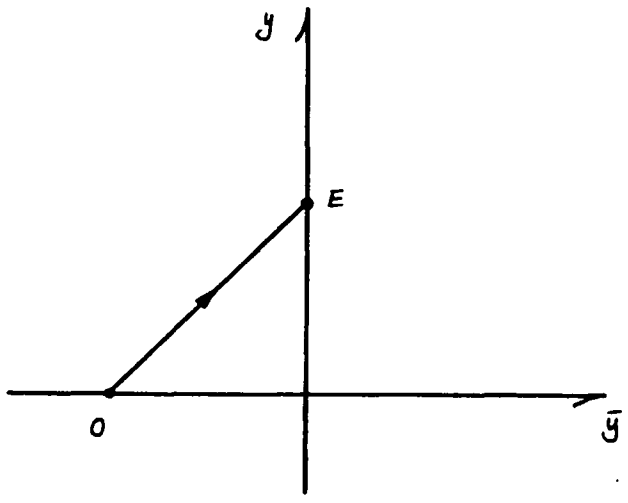

Fig. 2 $y-\bar{y}$ diagram corresponding to Fig. 1

that its projections on the x-z and y-z planes are the chief and marginal rays, respectively. Delano then obtains the y-$\bar{y}$ diagram as the projection of this skew ray onto the x-y plane of Fig. 1, resulting in the diagram of Fig. 2; it is assumed that one is viewing the system in the negative z-direction. We shall label the x-axis the $\bar{y}$-axis, as it contains the heights of the chief ray.

Note that the skew ray describing the system is uniquely defined. The great advantage of this approach is that the projection of this single skew ray onto the y-$\bar{y}$ diagram is sufficient to describe all the first-order properties of the system, provided that we specify the indices of refraction and the Lagrange invariant for the two rays. As noted by Delano, the optical system is represented in this diagram (y-$\bar{y}$) by a set of points and lines connecting these points; and the system is essentially described by the coordinates of these points; from these every other characteristic of the system may be derived. As Delano shows, there are two possible choices for these coordinates: one is to specify the three actual coordinates of the point $(\bar{y}, y, z)$, and the other is to restrict ourselves to the two coordinates $(\bar{y}, y)$ on the diagram, and specify separately the indices of refraction of the homogeneous spaces comprising the system. We shall adopt the latter alternative in this work.

As already noted in the Introduction our aim is to express all the geometrical features described by Delano in analytic or

algebraic form, suitable for numerical computation and quantitatively useful for actual design and analysis work. The main tool will be the use of two-dimensional vectors in the y-$\bar{y}$ diagram, but that will be deferred to the next chapter. In the rest of this chapter we shall discuss the qualitative features of the y-$\bar{y}$ diagram, as well as its dual relationship to the yet to be defined Ω-$\bar{\Omega}$ diagram.

The Lagrange Invariant

The concept of the single ray described above is so fruitful and elegant that we should proceed to give an analytic expression for it and derive the properties of the system from it. However, this three-dimensional description is not necesary in this context, due to the fact that we are only interested in the projections of this skew ray in the three coordinate planes. However such three-dimensional description is necessary when we are dealing with an inhomogeneous medium, in which case the skew ray is no longer a series of broken straight lines, but a twisted curve; this case is beyond the scope of this work, althought it is being investigated as a separate contribution.

Returning to our single skew ray, we may see that its projection onto the x-z plane of Fig. 1 is simply the ray-trace of the chief ray, which analytically will be given by the following two equations

$$\bar{y}_{i+1} = \bar{y}_i + \tau_{i+1}\,\bar{\omega}_{i+1}\,, \tag{2-1}$$

$$\bar{\omega}_{i+1} = \bar{\omega}_i - \varphi_i \bar{y}_i , \qquad (2\text{-}2)$$

where $\bar{\omega}_i \equiv n_i \bar{u}_i$, is the "reduced" chief ray angle;

$\tau_{i+1} \equiv t_{i+1}/n_{i+1}$, is the reduced axial separation along the y-axis between surfaces i and $i+1$;

$\varphi_i \equiv c_i(n_{i+1} - n_i)$, is the power at surface i, with c_i as the curvature of the surface; see Appendix A for notation.

Similarly, the projection of the skew ray onto the y-z plane is given by the ray-trace equations for the marginal ray:

$$y_{i+1} = y_i + \tau_{i+1} \omega_{i+1} , \qquad (2\text{-}3)$$

$$\omega_{i+1} = \omega_i - \varphi_i y_i , \qquad (2\text{-}4)$$

using the same nomenclature as above.

If we restrict ourselves to a single space of index of refraction n_i, we may easily show that the projection of the skew ray onto the y-$\bar{y}$ plane is given by:

$$\bar{\omega}_i y_i - \omega_i \bar{y}_i = \mathcal{H} = const , \qquad (2\text{-}5)$$

which may be recognized as the Lagrange invariant for the chief and marginal rays. We know that this is a numerical constant that applies to the entire system, and therefore it acts as a scaling factor in Eq. (2-5).[1] $\mathcal{H}$ can be either positive or

---

1. Moreover we may remember that the flux of energy through the system is proportional to $\mathcal{H}^2$.

negative; we assume a positive Lagrange invariant throughout this work. We may define new reduced angles by dividing by $\mathcal{H}$, $\Omega \equiv \omega/\mathcal{H}$. Then Eq. (2-5) takes the form

$$\bar{\Omega}_i y_i - \Omega_i \bar{y}_i = 1, \tag{2-6}$$

being the equation of a straight line in the y-$\bar{y}$ diagram.

We should note at this point that Eq. (2-5) may be derived on purely analytic grounds without recourse to the geometric picture given by Delano. Eq. (2-5) may be obtained by eliminating τ_{i+1} from Eqs. (2-1), (2-3) or by eliminating φ_i from Eqs. (2-2), (2-4). Then proceeding to Eq. (2-6) we see that this is a straight line in a two-dimensional diagram with $(\bar{y}, y)$ as coordinates and $(\bar{\Omega}, \Omega)$ as parameters.

Both pictures, the geometric and the analytic complement each other beautifully. The geometric picture affords the insight that any figure provides (one picture is worth one thousand words, says the Chinese adage). The analytic approach affords the accuracy that the geometric picture may lack. From these considerations it is seen that the best vehicle for a treatment of the y-$\bar{y}$ diagram is analytic geometry.

The y-$\bar{y}$ Diagram

If in the equation

$$\bar{\Omega} y - \Omega \bar{y} = 1 \tag{2-7}$$

we fix the values of $\bar{\Omega}$ and Ω, which for most applications

implies a fixed value for the index of refraction n, we obtain in the y-$\bar{y}$ diagram, a straight line with intercepts

$$\begin{aligned} \bar{y}^* &= -1/\Omega \equiv \bar{y}_I, \\ y^* &= +1/\bar{\Omega} \equiv y_E, \end{aligned} \tag{2-8}$$

as illustrated in Fig. 3. Three points are marked along this line: an image point $I(y=0)$, a pupil point $E(\bar{y}=0)$ and an arbitrary point $P(\bar{y}, y)$; the line itself is characterized by the index of refraction n, and completely determined by the two intercepts, Eqs. (2-8) or conversely by the values $(\bar{\Omega},\Omega)$. Any point on the $\bar{y}$-axis locates an image, and any point along the y-axis locates a pupil.

The graph in Fig. 3 contains all the information pertaining to the two paraxial rays, the marginal ray and the chief ray, related by the Lagrange invariant (2-5), and imbedded in the space of index of refraction n. The more conventional representation, the lay-out of the system, is given in Fig. 4, and it is the complete analog of Fig. 3 in the sense that both contain the same information. In the lay-out of the system we shall represent the marginal ray by a single line and the chief ray by a double line, as shown in Fig. 4.

We may appreciate from these two graphs that a line in the y-$\bar{y}$ diagram represents a whole space of index of refraction n, and points along this line represent planes perpendicular to the optical axis of the system, the coordinates of each point being the heights of the chief ray ($\bar{y}$) and marginal ray (y)

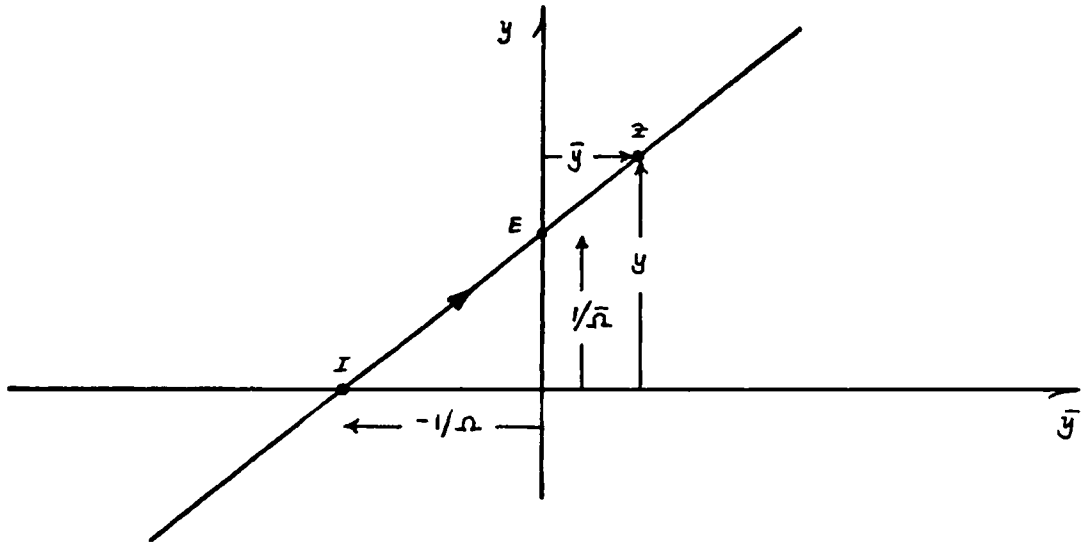

Fig. 3 Single line in the $y-\bar{y}$ diagram

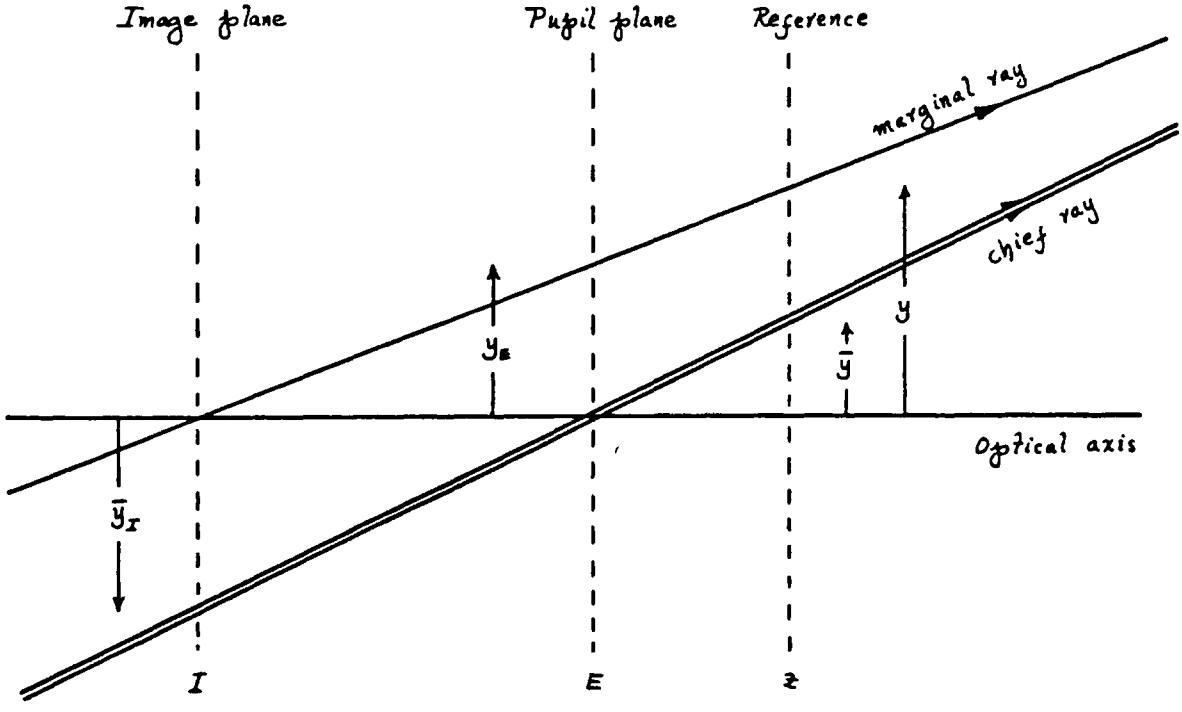

Fig. 4 Lay-out corresponding to diagram in Fig. 3

passing through this plane. Note that the line continues indefinitely, meaning that the space it represents exists throughout.

As an optical system consists of several spaces superimposed on each other, we now will consider the representation of this multitude of spaces in the diagram, each space being represented by a straight line, each characterized by an index of refraction n.

Before we combine two spaces of different index of refraction, let us look at the situation depicted in Fig. 5, of two reference points along the same line of index of refraction n. This case simply corresponds to a change in reference plane within the space of index of refraction n, or in other words, corresponds to a transfer from surface z_1 to surface z_2, operation under which the values of the ray angles remain unchanged and only the heights change.

It is clear that only the segment comprised between the two points z_1 and z_2, corresponds to the segment of space of index n in which the light is actually travelling, but of course both the space and the line it is represented by extend indefinitely in both directions; we shall call such a segment a "light-segment", and by extension a "light-ray" will denote the line in which it is contained. We see that the light-segment corresponds to the "real" part of the skew ray, and the rest of the line corresponds to the "virtual" part of the skew ray. In other words, when the light-segment crosses the $\bar{y}$-axis, it locates the position and size of a real image of the object; when the

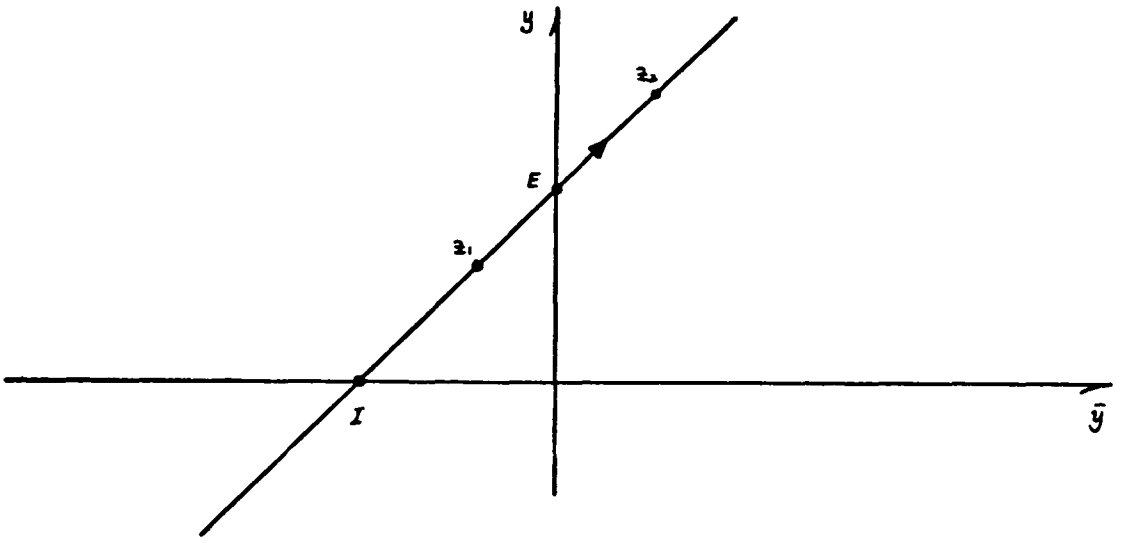

Fig. 5 Transfer from plane z_1 to plane z_2

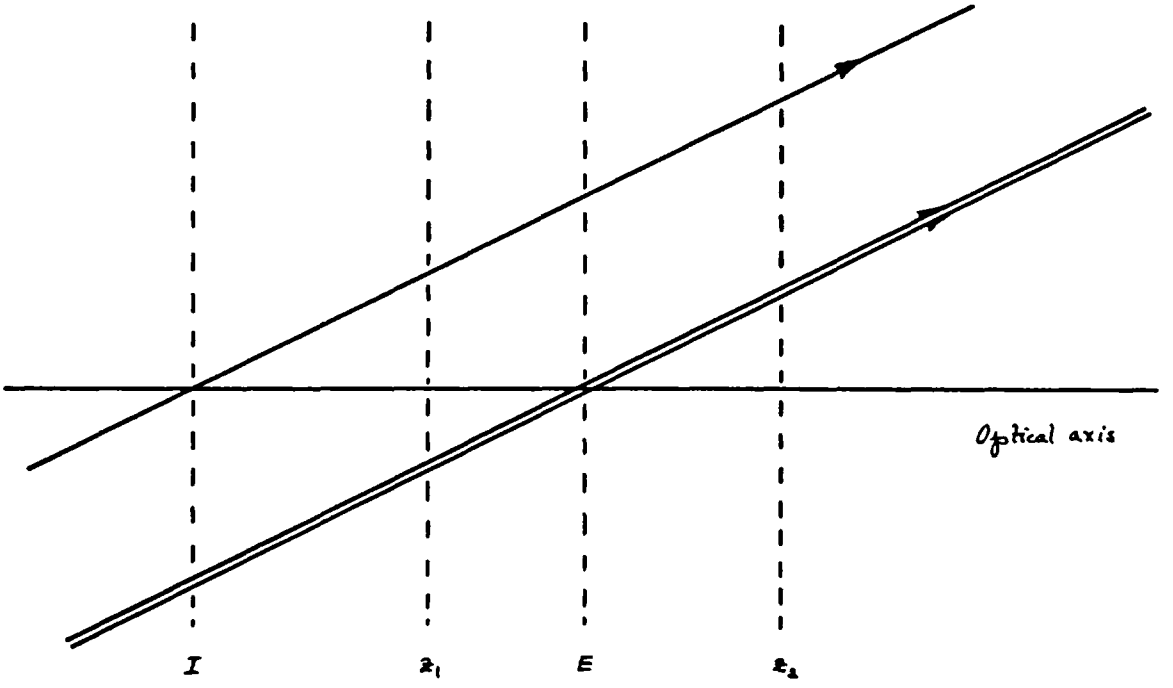

Fig. 6 Lay-out corresponding to diagram in Fig. 5

virtual part of the ray crosses the axis we obtain a virtual image. Similarly, when the light-segment crosses the y-axis we locate a real image of the stop; otherwise we have a virtual image of the same. It is also clear that the light-ray cannot pass through the origin of the y-$\bar{y}$ diagram, as this would imply that for that space, the image and the pupil coincide, which is impossible. As an illustration, in Fig. 5 the pupil is real and the image is virtual if we assume that the light-segment is $\overline{z_1 z_2}$. In the next chapter we shall give a quantitative criterion to find real images or pupils.

We now consider the case when we allow the two reference points to coincide but let there be two lines with different indices of refraction ($n \neq n'$), passing through this common point, as illustrated in Fig. 7. This situation obviously corresponds to a refraction of the two rays at the common reference surface z, where the ray angles change but the heights do not.

This is also the simplest imaging system; it relates planes in one space to planes in another space in a one-to-one correspondence. If we assume that the light goes from the plane I to the plane z where it is refracted towards the plane I', then the first light-segment from I to z, characterized by the index n, is the object ray and represents the physical object space of the same index; and the light-segment from z to I', with index n', is the image ray and represents the physical image space. We see from the figure that both images are real in this case, and the stop of the system is located in object space

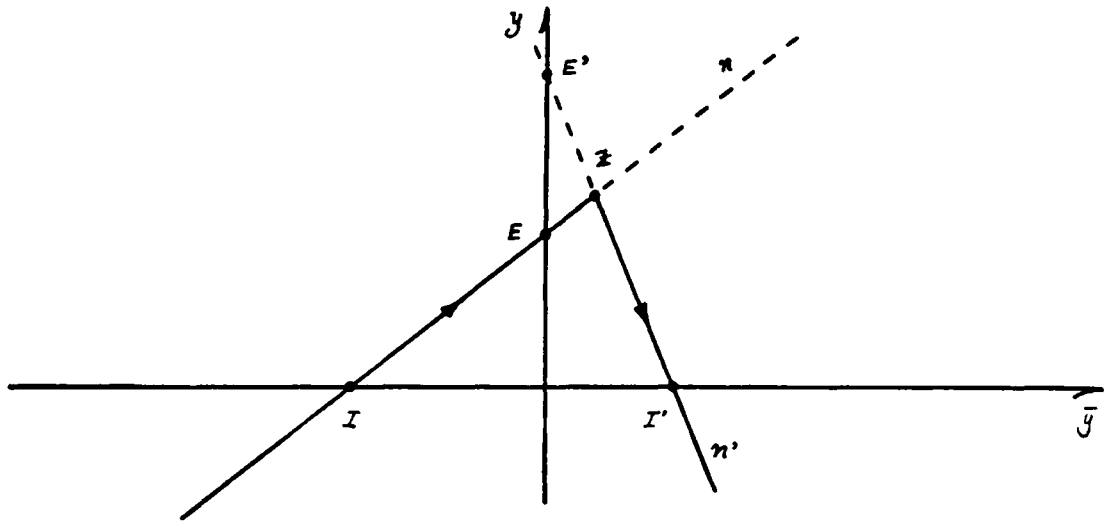

Fig. 7 Refraction at surface z

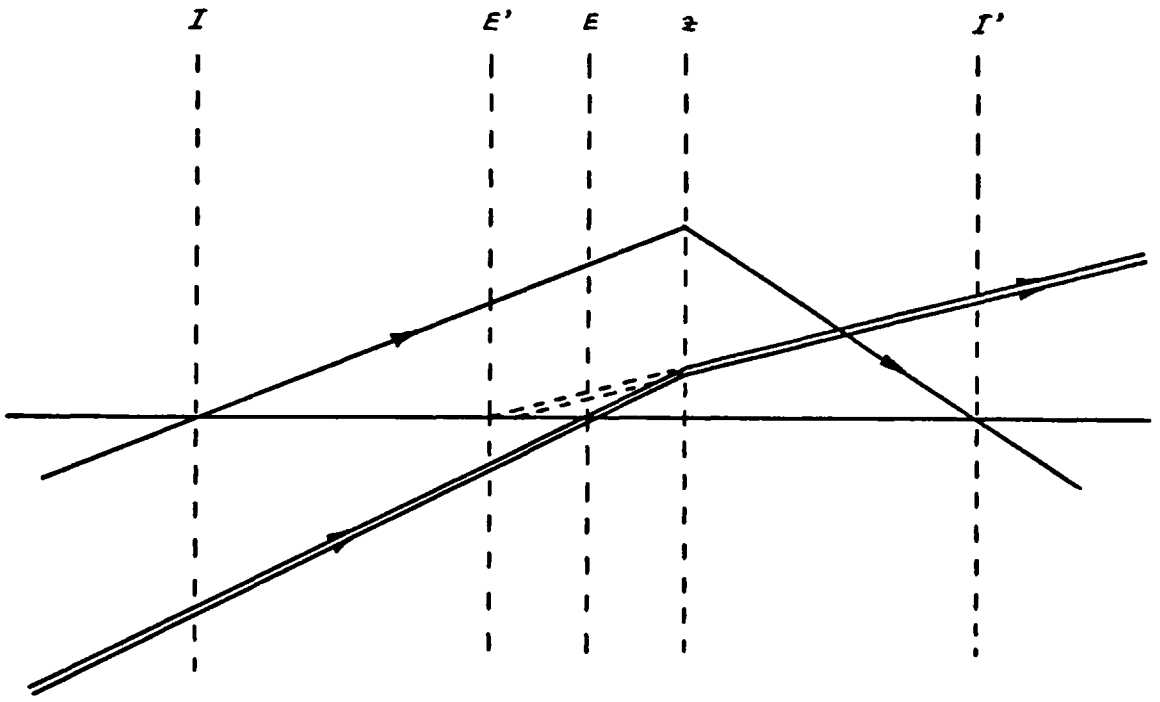

Fig. 8 Lay-out corresponding to diagram in Fig. 7

at E, coinciding with the pupil of the object line, identified with the entrance pupil of the system; the pupil of the image line, in this case virtual, is identified with the exit pupil of the system and is located at E'.

As depicted in Fig. 7, the point z represents a refracting surface dividing the two spaces of indices n, n', and imaging an object of height $\bar{y}_I$ into another of height $\bar{y}_I'$. It also may represent a thin lens doing the same thing between object and image spaces if we assume that $n = n'$, or even a mirror if we assume $n' = -n$. This ambiguity results from the fact that the y-$\bar{y}$ diagram deals only with "reduced" quantities, such as $\omega \equiv nu$, and $\tau \equiv t/n$; and in order to derive the real angles that the rays make with the optical axis or the axial separations between the surfaces, we must specify the indices of refraction associated with each space represented by a line in the diagram. This apparent drawback is indeed an asset because it gives the y-$\bar{y}$ diagram a great flexibility to represent simple as well as very complicated systems by a set of points and lines connecting them.

In the refraction situation depicted in Fig. 7, Delano has shown that if we assume a positive value for the Lagrange invariant, a light-line at the point of refraction will turn clockwise, towards the origin, for a surface having a positive power; and counterclockwise, away from the origin, for a negative power surface (Fig. 9). (We shall give a demonstration other than Delano's in the next chapter.) Therefore, each refraction will

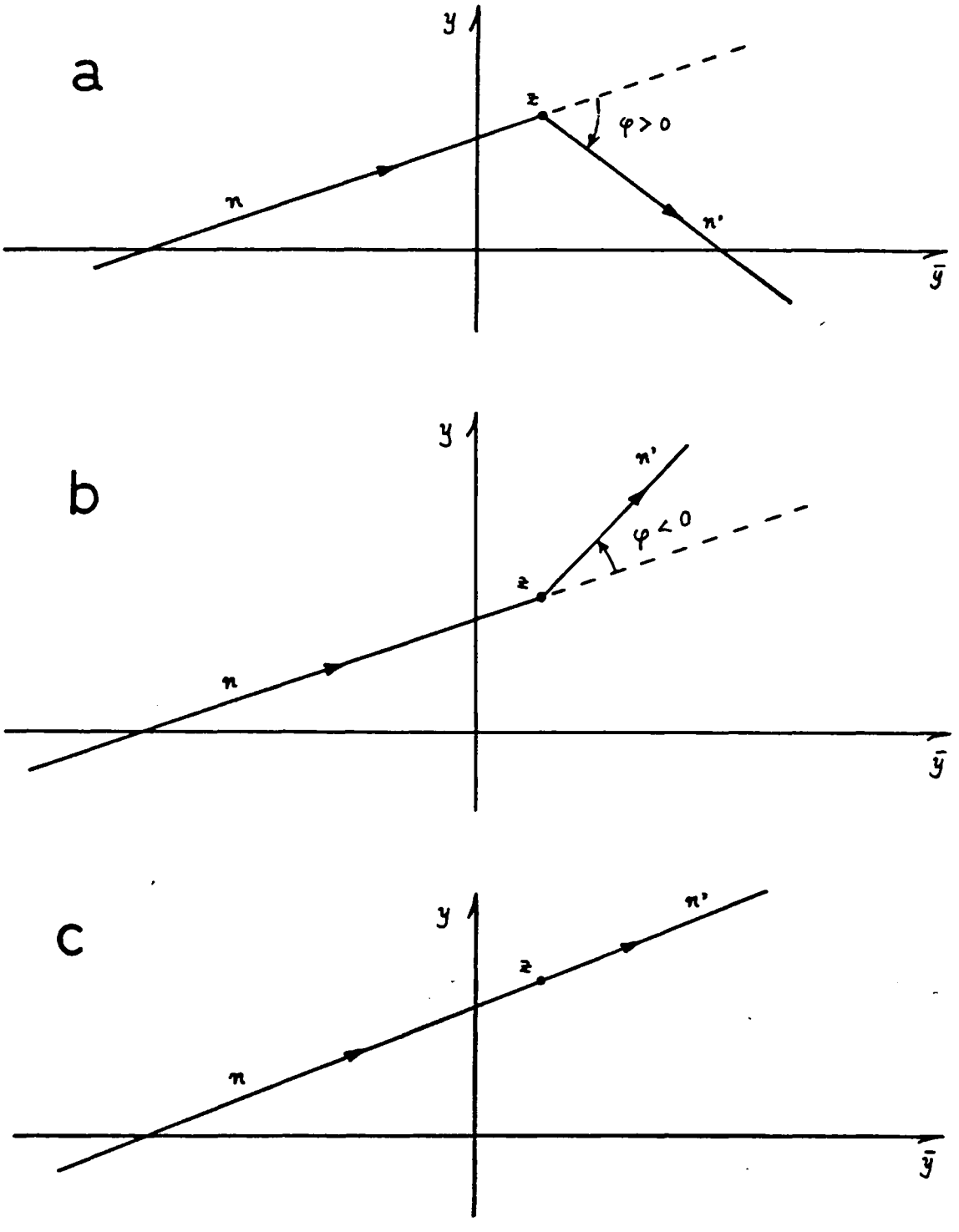

Fig. 9 a) Positive power surface
b) Negative power surface
c) Plane surface

be represented in the y-$\bar{y}$ diagram by a bending of the light-segment at the point representing the surface or lens, except when such a surface is a plane one (zero power). There is no bending for the zero-power surface because there is no change in the value of the reduced angles at such a surface, although the actual ray angles do change. This is represented in the diagram by a change in the index attached to the light-ray (see Fig. 9).

As any optical system consists of a finite number of surfaces and separating spaces of different indices of refraction, we may conclude from figures 5 and 7 that such an optical system will be represented in the y-$\bar{y}$ diagram by a set of points connected by light-segments. For example a thick-lens Taylor triplet would be represented as in Fig. 10, where points 3, 4

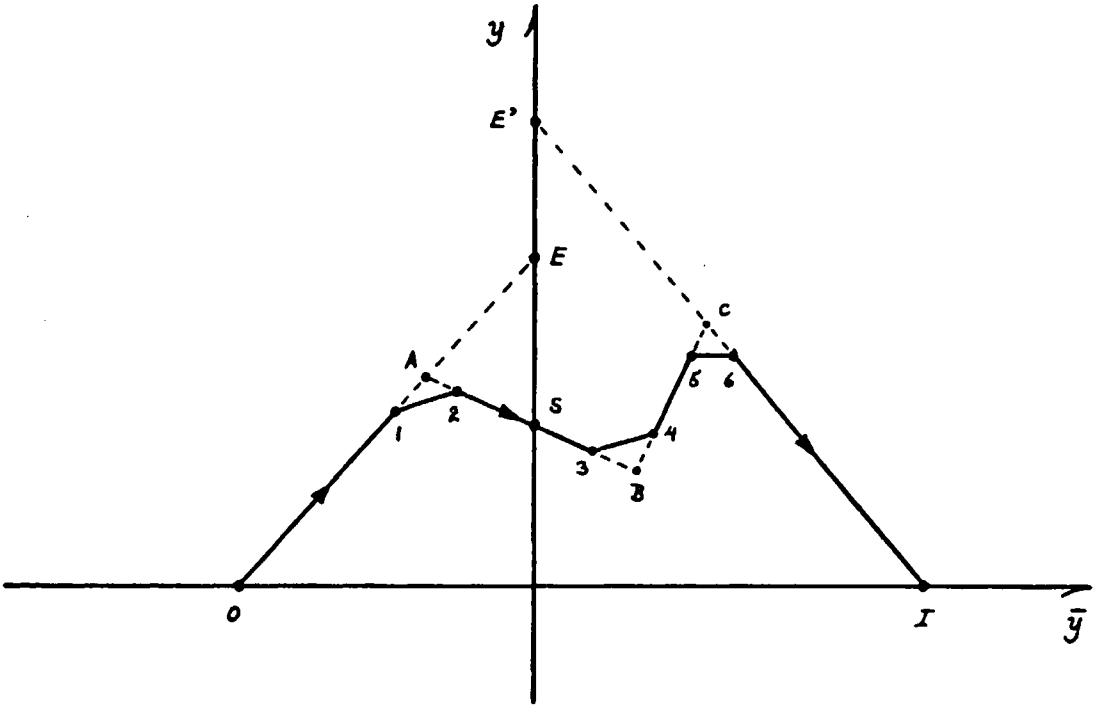

Fig. 10 Diagram of a thick-lens triplet

represent the surfaces of the middle, negative element, and points 1, 2 and 5, 6 represent the surfaces of the surrounding positive elements. The height of the object is represented in this case by O and that of the image by I. The object ray is the one connecting the points O, 1, and the entrance pupil is represented by the point E; similarly, the image ray is that passing through the points $6, I$ and the point E' represents the exit pupil. We may also see from the diagram that the actual stop of the system, represented by S is located slightly before surface 3. The points joining the dotted lines passing through the surfaces of the thick lenses, represent the thin-lens equivalents of these thick lenses. As far as the first-order properties of the system are concerned those three thin lenses (A, B, C) would do exactly as well as the group of surfaces (1 through 6).

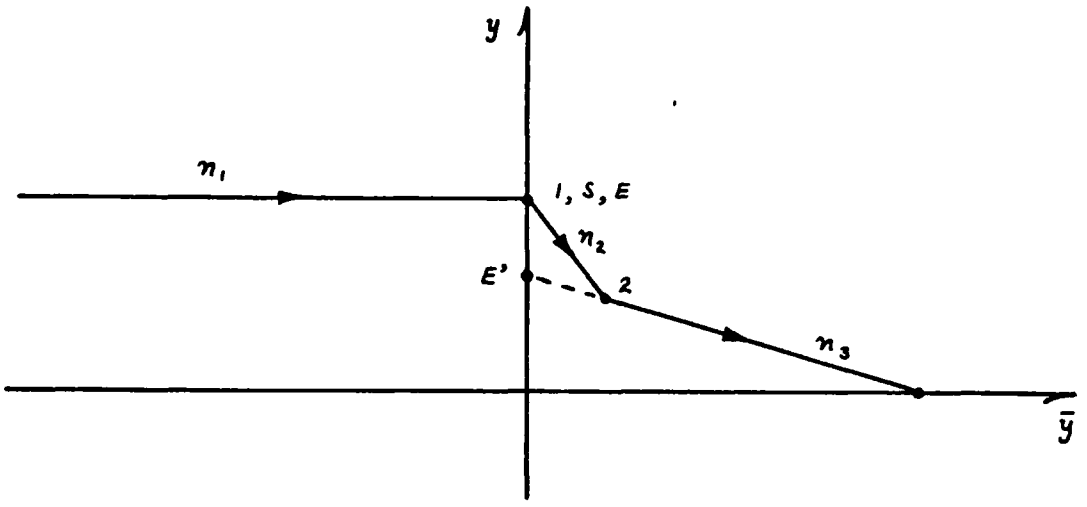

Fig. 11. Diagram of a two-element system

As another example, consider the diagram of Fig. 11. The first thing to notice is that the object line is parallel to the $\bar{y}$-axis, and therefore, the intersection of this line and the axis occurs at infinity; in other words, the object of this system is located at infinity. Secondly, the first element of the system coincides with the stop and the entrance pupil.

Depending on the choice of the indices of refraction n_1, n_2, n_3, this diagram will correspond to completely different lay-outs. Fig. 12 illustrates three different choices. In a) we have set $n_1 = n_2 = n_3 = 1$, thereby assuming that points 1 and 2 represent a positive and a negative lens respectively; in other words, a telephoto system. In b) we have set $n_1 = n_3 = 1$, but $n_2 = -1$, and the resulting system consists of mirrors and is a cassegrain objective. In c) we choose $n_1 = n_3 = 1$, $n_2 > 1$, and the resulting system is a thick lens element immersed in air.

At first glance, without being already familiar with Gaussian Optics, one would hardly suspect that the three systems illustrated on Fig. 12 are equivalent; however, this equivalence is clearly shown by the y-$\bar{y}$ diagram which gives the same representation to all of them, implying that as far as the first-order properties are concerned, the three systems are completely equivalent. The formulae derived from the diagram on Fig. 11 will apply to each of the systems of Fig. 12, when the proper indices of refraction are inserted.

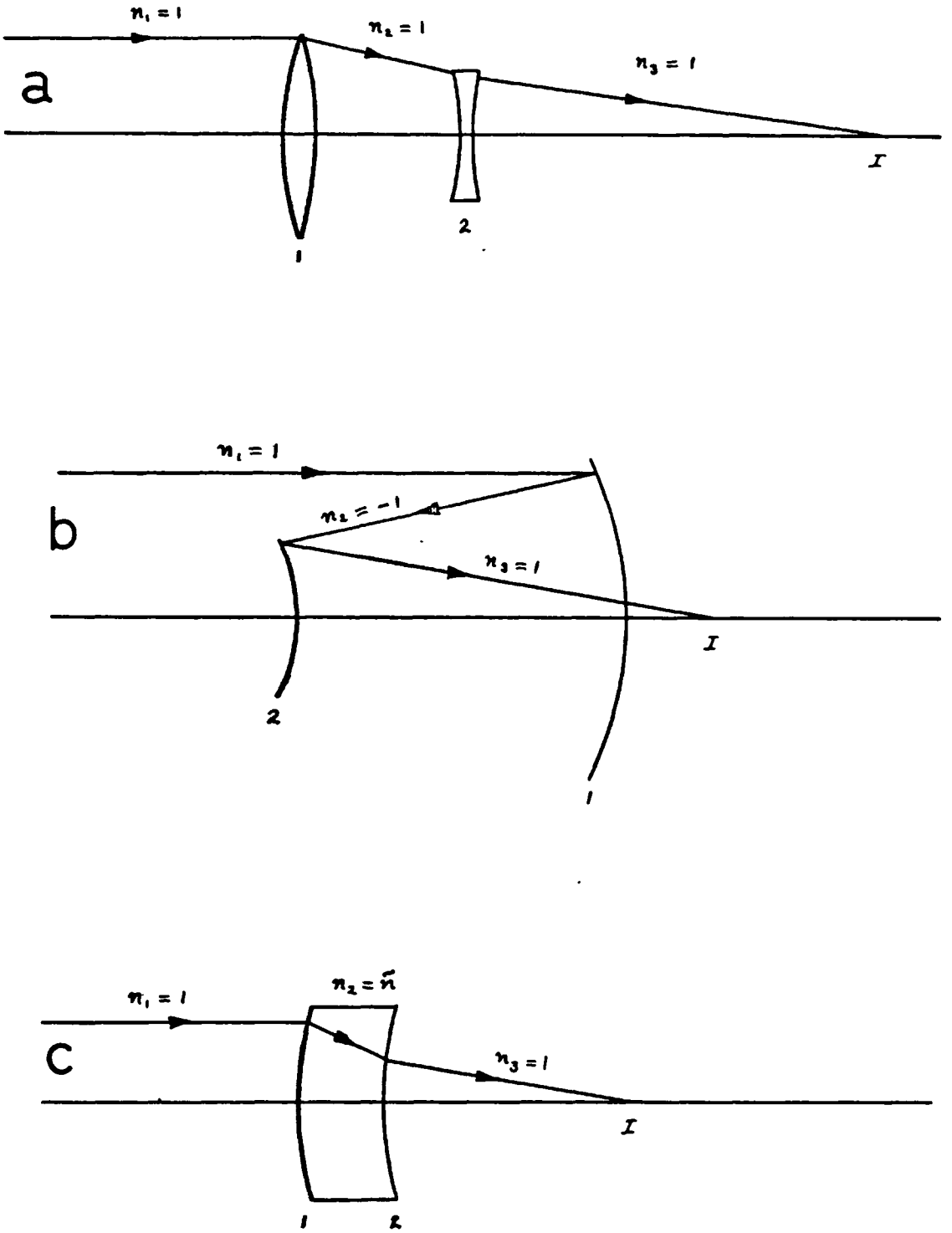

Fig. 12 a) A telephoto thin-lens system
b) A Cassegrain objective
c) A thick lens

The Ω-$\bar{\Omega}$ Diagram and Duality

Returning to the expression for the Lagrange invariant in the form of Eq. (2-7), we may rewrite it as follows

$$\Omega\,\bar{y} - \bar{\Omega}\,y + 1 = 0. \tag{2-9}$$

We recognize this as a "bilinear form" extensively studied in Projective Geometry, where they are expressed in terms of homogeneous coordinates (Gans, 1969, p. 280) as follows

$$x_1 u_1 + x_2 u_2 + x_3 u_3 = 0.$$

The x_i are called point coordinates because one set uniquely defines a point; similarly, the u_i are the line coordinates, and they uniquely define a line. Note that written in this form both set of coordinates are indistinguishable from each other. Non-homogeneous or cartesian coordinates are chosen as ratios; in our particular case:

$$x_1/x_3 \equiv \bar{y}\,, \qquad x_2/x_3 \equiv y \tag{2-10}$$

$$u_1/u_3 \equiv \Omega, \qquad u_2/u_3 \equiv -\bar{\Omega} \tag{2-11}$$

From these general remarks we see that there are two possible cartesian representations of the bilinear form (2-9); one is to use $(\bar{y}, y)$ from Eq. (2-10) as coordinates and $(\bar{\Omega}, \Omega)$ as parameters: this is the y-$\bar{y}$ diagram introduced by Delano and already discussed in the previous section. Another possibility

consists of taking ($\bar{\Omega}$, Ω) as coordinates and consider ($\bar{y}$, y) as coefficients: this is the Ω-$\bar{\Omega}$ diagram.

The two diagrams are "dual" to each other in the Projective Geometry sense; in other words, a point in the y-$\bar{y}$ diagram is represented by its "dual", a line, in the Ω-$\bar{\Omega}$ diagram, and vice versa. This duality has been extensively studied in the literature (Coxeter, 1969, p. 248; Maxwell, 1963, p. 11).

In the Ω-$\bar{\Omega}$ diagram, an optical system is also represented by a set of points and connecting lines, except that in this case, the points represent the spaces and the segments represent the refracting surfaces.

The dual relationship alluded above allows us to draw an Ω-$\bar{\Omega}$ diagram from a y-$\bar{y}$ diagram in a straighforward manner. As noted above, each point in the y-$\bar{y}$ diagram is transformed into a line in the Ω-$\bar{\Omega}$ diagram, and each line in the y-$\bar{y}$ diagram goes into a point in the Ω-$\bar{\Omega}$ diagram. This type of transformation is known in Projective Geometry as a "correlation" (Gans, 1969, p. 280). Figure 13 illustrates the Ω-$\bar{\Omega}$ diagrams corresponding to some y-$\bar{y}$ diagrams previously described: a single space of index n with a reference surface z; the case of a transfer between two surfaces z_1, z_2; and the refraction at a surface z from a space of index n to one of index n'.

One diagram may be geometrically constructed from the other by noting that the dotted lines of one diagram are parallel to the solid lines of the other. This is not an accident, but a consequence of the duality relation connecting the two diagrams.

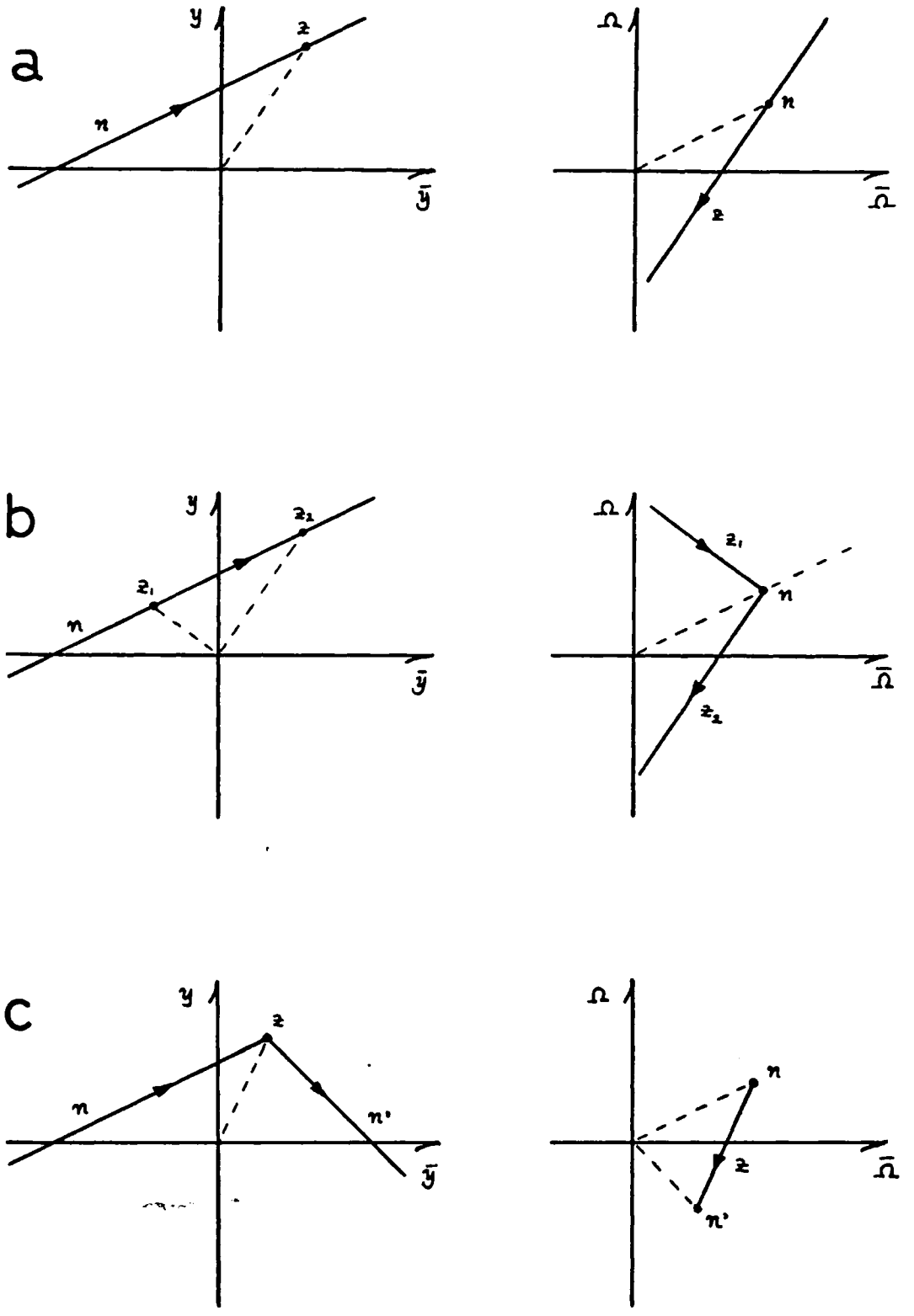

Fig. 13 a) Single space.
b) Transfer from z_1 to z_2. c) Refraction at z

Although the Ω-$\bar{\Omega}$ diagram is less easily visualized than the y-$\bar{y}$ diagram, it will prove nevertheless, extremely useful in several important instances when the analysis on the y-$\bar{y}$ diagram proves to be very cumbersome and, by contrast, much more tractable in terms of $\bar{\Omega}$ and Ω. For example, we shall see in a later chapter (Ch. 6) that certain properties of optical systems result, in the y-$\bar{y}$ diagram, in a series of lines whose envelope is the curve of interest for the study of such properties. Curves in a plane are difficult to analyze when they are defined by their tangents alone. However, if we translate this figure to the Ω-$\bar{\Omega}$ diagram, each of the tangents will go into a point and the curve will be easier to analyze as a series of points. Once we have completed the analysis of this curve in the Ω-$\bar{\Omega}$ diagram, we can calculate in turn its tangents in this diagram which will transform into points on the y-$\bar{y}$ diagram, giving us the desired curve in the usual point form.

In addition, as has already been pointed out by Pegis et al. (1967), the variables $\bar{\Omega}$, Ω are better suited to the control of the aberrations of the system.

Another advantage of the duality relation between the two sets of variables ($\bar{y}$, y) and ($\bar{\Omega}$, Ω) is that it permits us to treat lines as single entities, on the same footing as we treat the points. We shall see in the next chapter that in the same manner that we may represent a point by a single vector, we may also represent a line by a single vector and treat it in the same

way as any other vector. These vectors in turn may be considered as complex numbers in the plane, which offers a great computational advantage as both points and lines may be manipulated numerically as single entities by already available complex-number routines in most computers.

CHAPTER 3

VECTORIAL REPRESENTATION OF THE y-$\bar{y}$ DIAGRAM

In this chapter we shall develop the basic concepts and tools for an algebraic analysis of an optical system in the y-$\bar{y}$ diagram.

The geometric usefulness of the diagram may be made quantitative only by the application of the laws of analytic geometry to the two-dimensional projection of the single skew ray introduced by Delano (1963). In the last chapter we described some of the most elementary properties of the diagram in a very qualitative manner; in this chapter we substantiate quantitatively those assertions and give a more complete list of the properties of the diagram.

Inasmuch as the y-$\bar{y}$ diagram is a set of points and lines describing uniquely and completely the first-order properties of any rotationally symmetric optical system, we must deal with pairs of numbers such as $(\bar{y}, y)$ to represent the points, and $(\bar{n}, n)$ to represent the lines, and it will be convenient to find an expedient way of handling these ordered couples of numbers.

One such way is to think of these pairs of numbers as the cartesian components of appropiate vectors. Alternatively, they may be treated as the real and imaginary parts of corresponding complex numbers. The advantage of using vectors is the elegance

and simplicity of the formulae obtained and the insight derived from their graphical representation. The main advantage of using complex numbers lies in the numerical aspect of the computations: complex numbers are handled by most computers as single entities, and most of the operations carried out with them are made "on line," which constitutes a substantial saving in computation time. As the same point (or line) in the diagram may be represented both by a vector and by a complex number, we shall use them interchangeably to derive the properties of an optical system from the diagram. Also, the transformations to which these points are subjected are inherently linear and therefore may be expressed by means of matrices. These matrices turn out to be the same as those used by O'Neill (1963), and Brouwer (1964). We shall only mention them in this chapter to illustrate the unity and elegance of the y-$\bar{y}$ diagram approach; we also include the formulae for going from the vector-complex formulation to the matrix representation.

The formulae and concepts developed in this chapter will be used in subsequent chapters. In particular, in the next chapter they will be used to develop the representation of the most familiar concepts of Gaussian Optics in the y-$\bar{y}$ diagram.

Vectors and Complex Numbers

We now define the point vectors

$$\vec{z} \equiv (\bar{y}, y) \qquad (3\text{-}1)$$

at each surface of the optical system, and the line vectors

$$\vec{w} \equiv (\bar{\omega}, \omega) = (n\bar{u}, nu) \tag{3-2}$$

at each space of refractive index n. We also define the vector

$$\vec{W} \equiv (\bar{\Pi}, \Omega) = \vec{w}/\mathcal{H} \tag{3-3}$$

obtained from $\vec{w}$ by dividing by the Lagrange invariant as a scaling factor. In terms of the vectors $\vec{z}$ and $\vec{W}$, the paraxial ray trace equations, (2-1) through (2-4) become

$$\vec{z}_i = \vec{z}_{i-1} + T_i \vec{W}_i \quad , \text{ for transfer,} \tag{3-4}$$

$$\vec{W}_{i+1} = \vec{W}_i - \Phi_i \vec{z}_i \quad , \text{ for refraction;} \tag{3-5}$$

where now we have used the scaled quantities (see Appendix A),

$$\begin{aligned} T &\equiv \mathcal{H}\tau = \mathcal{H}t/n, \\ \Phi &\equiv \varphi/\mathcal{H}, \end{aligned} \tag{3-6}$$

as they are, together with the vector $\vec{W}$, directly derivable from the diagram.

By taking appropiate cross-products of Eqs. (3-4, 5) to eliminate either T_i, or Φ_i, we obtain the vectorial equation for the Lagrange invariant

$$\vec{z} \times \vec{W} = \hat{k} \tag{3-7}$$

where $\hat{k}$ is the unit vector along the y-direction; see Fig. 1. It may be easily verified, by carrying out the cross-product, that Eq. (3-7) goes directly into Eq. (2-7); in other words, this

equation represents a straight line in the y-$\bar{y}$ diagram, characterized by the vector $\vec{W}$. Note also that equation (3-7) may be written, when introducing the surface subscripts, in any of the equivalent forms,

$$\vec{z}_{i-1} \times \vec{W}_i = \vec{z}_i \times \vec{W}_i = \vec{z}_i \times \vec{W}_{i+1} = \vec{z}_{i+1} \times \vec{W}_{i+1} = \hat{k}. \qquad (3\text{-}8)$$

To corroborate the assertion that the heights $\bar{y}, y$ at each surface are sufficient to determine an optical system in the y-$\bar{y}$ diagram, we proceed now to express the vectors $\vec{W}$, the separations T, and the powers Φ all in terms of the vectors $\vec{z}$. However, to give the actual parameters for a real system, the angles $(\bar{u}, u)$, the axial separations t, and the curvatures of the surfaces c, we shall need to specify the values of the indices of refraction attached to each space as well as the value of the Lagrange invariant for the whole system. The Lagrange invariant in turn may be expressed in terms of the three parameters of the system as a whole: focal length, aperture and angular field of view. A different choice of the indices of refraction will give physically different systems as was illustrated in the example of Fig. 11. A different value of the Lagrange invariant, on the other hand, only changes the scaling of the system.

To obtain the value of the reduced separations T_i, we multiply vectorially Eq. (3-4) by $\vec{z}_i$, and by using Eq. (3-8) we get:

$$T_i = \hat{k} \cdot (\vec{z}_{i-1} \times \vec{z}_i). \qquad (3\text{-}9)$$

We may see from this expression that the reduced separation is equal to the numerical value of the cross product of two consecutive $\vec{z}$ vectors, i.e., to the area enclosed by the parallelogram formed by the two vectors. In other words, the reduced separation between two surfaces (scaled by the Lagrange invariant) is proportional to twice the area of the triangle formed by the two points representing the surfaces and the origin of the diagram. See Fig. 14.

Using Eq. (3-9) and the dot product, we may also write an expression for the angle formed by two $\vec{z}$ vectors,

$$\tan \vartheta_i = \tau_i / (\vec{z}_{i-1} \cdot \vec{z}_i). \tag{3-10}$$

Similarly, we may determine the value of the powers by multiplying vectorially Eq. (3-5) by $\vec{W}_i$, and using Eq. (3-8). We obtain

$$\Phi_i = \hat{k} \cdot (\vec{W}_i \times \vec{W}_{i+1}). \tag{3-11}$$

Therefore, Φ_i is represented <u>in the Ω-$\bar{\Omega}$ diagram</u> by an area in analogous fashion to the representation of τ_i in the y-$\bar{y}$ diagram; compare Figs. 13 b-c. Also, the angle between two consecutive $\vec{W}$ vectors is given by

$$\tan \psi_i = \Phi_i / (\vec{W}_i \cdot \vec{W}_{i+1}). \tag{3-12}$$

Remembering that the $\vec{W}$ vectors represent lines in the y-$\bar{y}$ diagram, we may see from Eq. (3-11), written in the form

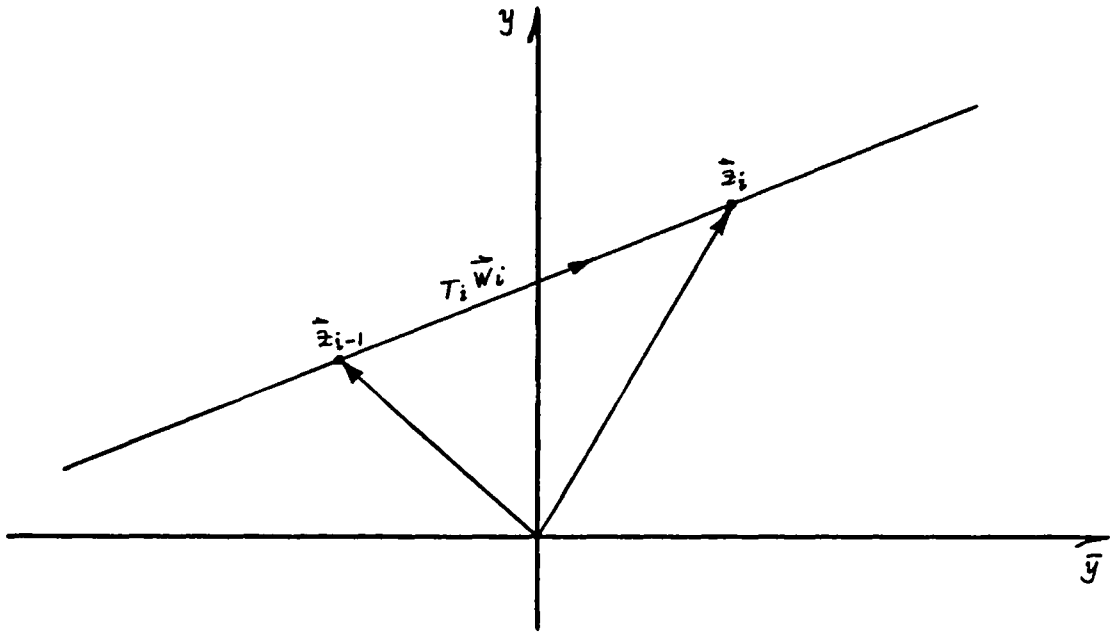

Fig. 14 The equation of transfer: $\vec{z}_i = \vec{z}_{i-1} + T_i \vec{W}_i$

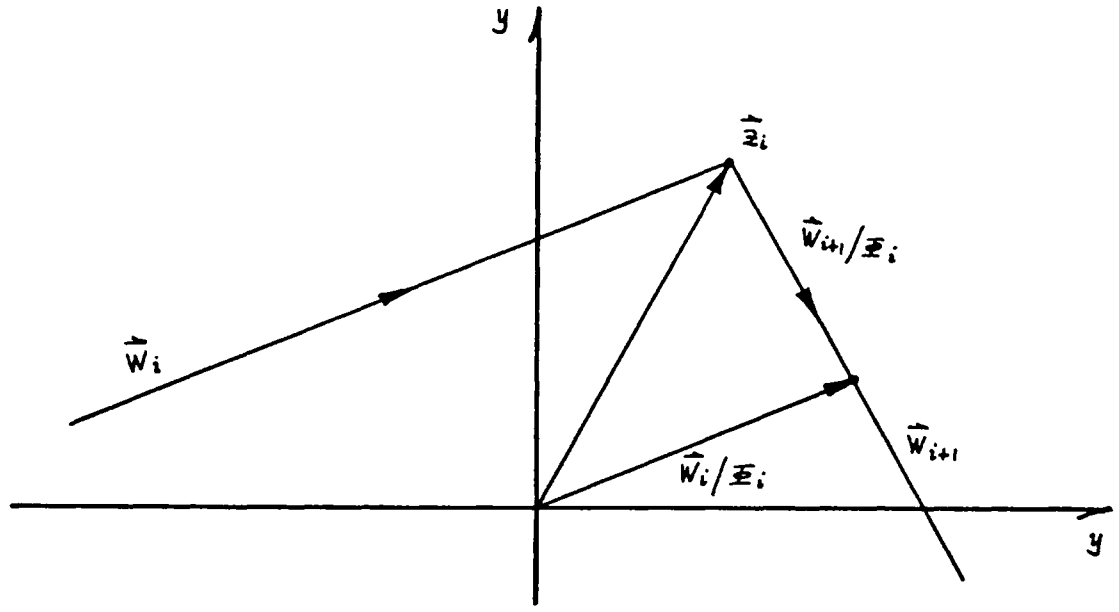

Fig. 15 The equation of refraction:
$\vec{W}_{i+1}/\vec{z}_i = \vec{W}_i/\vec{z}_i - \vec{z}_i$

$$\Phi_i \hat{k} = \vec{W}_i \times \vec{W}_{i+1},$$

that the power of a given surface is represented, in the y-$\bar{y}$ diagram, by the change in direction of the two $\vec{W}$ vectors defining the surface. When the power is positive, we see that the vector $\vec{W}_{i+1}$ lies clockwise to the $\vec{W}_i$ vector; when the power is negative we may write

$$-\Phi_i \hat{k} = \vec{W}_{i+1} \times \vec{W}_i,$$

and we see that in this case the $\vec{W}_{i+1}$ vector must lie counterclockwise to the $\vec{W}_i$ vector in order to preserve the proper sign for the unit vector $\hat{k}$. Finally, when the power is zero there is no deflection, and the two $\vec{W}$ vectors are parallel to each other. This is the case of an afocal system or of a plane interface.

The statements in the last paragraph may be shown algebraically as follows: consider the case of a single refracting surface (see Fig. 16), with an object line vector $\vec{W}$ changed into an image line vector $\vec{W}'$ by the refraction at surface $\vec{z}_p$.

The slope of the image line is given by

$$k' = \tan \gamma' = \frac{\Omega'}{\bar{\Omega}'} = \frac{\Omega - y_p \Phi}{\bar{\Omega} - \bar{y}_p \Phi}.$$

Solving for Φ, we get:

$$\Phi = \left(\frac{\bar{\Omega}}{\bar{y}_p}\right)\left(\frac{k' - k}{k' - k_p}\right),$$

where k and k_p are the slopes of the object line and the vector $\vec{z}_p$, respectively. But by using

$$y_E = 1/\bar{n} = \bar{y}_p (k_p - k),$$

we may express the power Φ as

$$\Phi = \frac{k' - k}{\bar{y}_p^2 (k_p - k)(k' - k_p)}. \qquad (3\text{-}13)$$

We see from this expression, as mentioned previously, that when $\Phi = 0$, we must have $k' = k$. Considering that both k and k_p are constant, let us differentiate Eq. (3-13) and solve for the change in slope dk' due to a change in the power $d\Phi$; the result is

$$dk' = - \bar{y}_p^2 (k' - k_p)^2 \, d\Phi.$$

This expression tells us that for a positive change in power, the slope of the image ray is less than the slope of the object line; in other words, a clockwise rotation is involved in going from an object ray to an image ray.

Equation (3-13) expresses another fact, a very important restriction on the relative positions of the object and image lines in the y-$\bar{y}$ diagram.

We see that if $k' = k_p$, the power becomes $\Phi = \pm\infty$ depending on the parallelism or antiparallelism of the image line and the vector $\vec{z}_p$; in other words, the whole range of powers is covered by positioning the image line in the region <u>to the right</u> of the vector $\vec{z}_p$ on Fig. 16; and the direction of

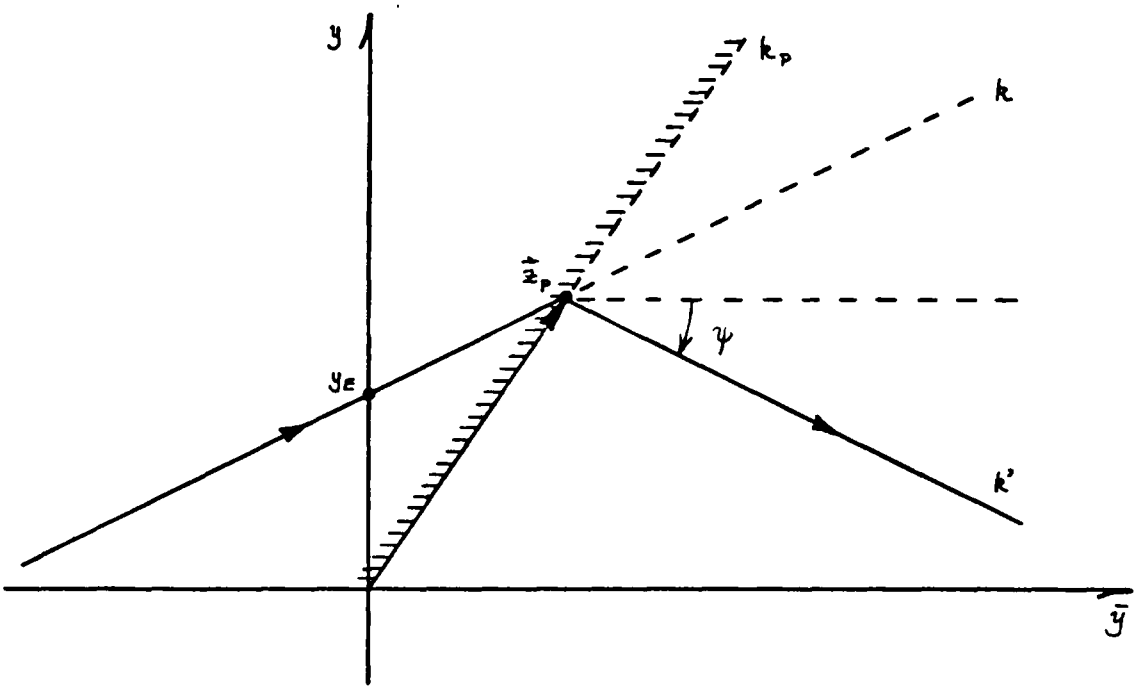

Fig. 16. Restriction on the relative positions of the object and image lines

the vector $\vec{z}_p$ as well as the region to the left are not allowable. We remember here briefly that no light-ray may pass through the origin of the $y-\bar{y}$ diagram, because this would imply that <u>both</u> $\bar{y}$ and y would be zero contrary to the assumption of the existence of the Lagrange invariant. However, Eq. (3-13) is still stronger, forbidding not only the passing of any light-ray through the origin, but also the location of the light-rays in certain regions that would imply a non-real value for the power. This restriction has to be kept in mind when drawing lines to create new-systems or modify existing ones. This restriction is also the basis for the statement made by Delano to the effect

that the projection of the skew ray on the y-$\bar{y}$ diagram winds about the origin in a clockwise direction, as the ray travels from surface to surface, for a positive choice of the Lagrange invariant.

To express now the $\vec{W}$ vectors in terms of the $\hat{z}$ vectors, we use the equation of transfer (3-4) together with Eq. (3-9) to obtain,

$$\vec{W}_i = \frac{\hat{z}_i - \hat{z}_{i-1}}{\hat{k}\cdot(\hat{z}_{i-1} \times \hat{z}_i)} . \qquad (3\text{-}14)$$

Similarly, using the equation of refraction (3-5) and Eq. (3-11) we obtain an expression for the vectors $\hat{z}$ in terms of the vectors $\vec{W}$,

$$\hat{z}_i = \frac{\vec{W}_{i+1} - \vec{W}_i}{-\hat{k}\cdot(\vec{W}_i \times \vec{W}_{i+1})} . \qquad (3\text{-}15)$$

Note the formal similarity of these two expressions. These two equations express analytically the principle of duality linking the y-$\bar{y}$ and the Ω-$\bar{\Omega}$ diagrams, that was discussed in the last chapter. In the y-$\bar{y}$ diagram the vectors $\hat{z}$ represent points, and clearly Eq. (3-14) is the vectorial equation of the straight line defined by two of these points. Therefore, the $\vec{W}$ vectors indeed represent lines. Similarly, in the Ω-$\bar{\Omega}$ diagram, the $\vec{W}$ vectors are the points and Eq. (3-15) tells us that the $\hat{z}$ vectors are the lines defined by such points. Any statement in terms of points $\hat{z}$ and lines $\vec{W}$ in the y-$\bar{y}$ diagram is true for points $\vec{W}$ and lines $\hat{z}$ in the Ω-$\bar{\Omega}$ diagram.

Because all vectors of interest in both the y-$\bar{y}$ and Ω-$\bar{\Omega}$ diagrams are plane vectors (the only exception being the constant unit vector $\hat{k}$), we may think of these planes as complex planes and identify each of the points and lines as complex numbers. In other words, we may write the vectors $\vec{z}$ and $\vec{W}$ in any of the equivalent forms

$$\vec{z} = (\bar{y}, y) = \bar{y}\,\hat{\imath} + y\,\hat{\jmath} = \bar{y} + iy,$$
$$\vec{W} = (\bar{\Omega}, \Omega) = \bar{\Omega}\,\hat{\imath} + \Omega\,\hat{\jmath} = \bar{\Omega} + i\Omega.$$

As most calculations involve the dot and cross products of combinations of these vectors, let us develop expressions for these. Assume we have two vectors $\vec{A}$ and $\vec{B}$, defined in analogous form to those above. The dot and cross products are given by

$$\vec{A} \cdot \vec{B} = A_x B_x + A_y B_y \tag{3-16}$$

$$\vec{A} \times \vec{B} = \hat{k} \begin{vmatrix} A_y & A_x \\ B_y & B_x \end{vmatrix}, \tag{3-17}$$

and the triple product used before, by

$$\hat{k} \cdot \vec{A} \times \vec{B} = \begin{vmatrix} A_y & A_x \\ B_y & B_x \end{vmatrix} = A_y B_x - A_x B_y. \tag{3-18}$$

Considering these same vectors as complex numbers, let us develop the complex product $\vec{A}\vec{B}^*$, where a star on a vector means its complex conjugate. We have

$$\vec{A}\vec{B}^* = (A_x B_x + A_y B_y) + i\,(A_y B_x - A_x B_y). \tag{3-19}$$

Comparing this expression with Eqs. (3-16) and (3-18), we see that

$$\vec{A}\cdot\vec{B} = Re\left(\vec{A}\,\vec{B}^*\right), \tag{3-20}$$

$$\hat{k}\cdot\vec{A}\times\vec{B} = Im\left(\vec{A}\,\vec{B}^*\right). \tag{3-21}$$

This result is of great numerical importance because a single complex product gives us the two vector products of interest: the dot product and the magnitude of the cross product (whose direction is always given by the unit vector $\hat{k}$).

Determinant Notation

The above comparison, Eq. (3-21) is also of algebraic importance because it allows us to devise a simple compact notation for the magnitude of the cross product. Consider

$$\hat{k}\cdot(\vec{A}\times\vec{B}) = Im(\vec{A}\vec{B}^*) = \frac{1}{2i}\begin{vmatrix}\vec{A} & \vec{A}^*\\ \vec{B} & \vec{B}^*\end{vmatrix}. \tag{3-22}$$

We introduce the following notation:

$$\left|\vec{A},\vec{B}\right| \equiv \frac{1}{2i}\begin{vmatrix}\vec{A} & \vec{A}^*\\ \vec{B} & \vec{B}^*\end{vmatrix} = \begin{vmatrix}A_y & A_x\\ B_y & B_x\end{vmatrix} = \begin{vmatrix}Im\,\vec{A} & Re\,\vec{A}\\ Im\,\vec{B} & Im\,\vec{A}\end{vmatrix}. \tag{3-23}$$

We may then write Eq. (3-21) as

$$\hat{k}\cdot(\vec{A}\times\vec{B}) = \left|\vec{A},\vec{B}\right| \tag{3-24}$$

This is just a plain 2 by 2 determinant, but written in the form of Eq. (3-23) it will simplify enormously the algebraic manipulations necessary to get powers and separations when using the y-$\bar{y}$ diagram. Among the properties of this determinant we summarize the most important for our purpose:

$$
\begin{aligned}
&|\vec{A},\vec{B}|^{*} = |\vec{A},\vec{B}|, \qquad \text{it is real}\\
&|\vec{A},\vec{A}| = |\vec{B},\vec{B}| = |\vec{A},0| = 0\\
&|\vec{A},\vec{B}| = -|\vec{B},\vec{A}|\\
&|a\vec{A},\vec{B}| = a|\vec{A},\vec{B}|\\
&|\vec{A}+\vec{C},\vec{B}| = |\vec{A},\vec{B}| + |\vec{C},\vec{B}|\\
&|\vec{A}+a\vec{B},\vec{B}| = |\vec{A},\vec{B}|
\end{aligned}
\tag{3-25}
$$

In the case of our vector $\vec{z}$ this notation takes the form

$$
|\vec{z}_j,\vec{z}_k| = \frac{1}{2i}\begin{vmatrix} \vec{z}_j & \vec{z}_j^{*} \\ \vec{z}_k & \vec{z}_k^{*} \end{vmatrix} = \begin{vmatrix} y_j & \bar{y}_j \\ y_k & \bar{y}_k \end{vmatrix} \equiv |y_j, y_k| \tag{3-26}
$$

Note that the last term in Eq. (3-26) is a shorthand notation of the preceding determinant in which the second column of the determinant has the barred quantities corresponding to the elements of the first column. The same holds true for determinants involving the $\vec{W}$ vector or the product between a $\vec{z}$ and a $\vec{W}$ vector, as is illustrated in the following important products that we have defined previously:

Lagrange invariant:

$$
\hat{k}\cdot(\vec{z}\times\vec{W}) = |\vec{z},\vec{W}| = |y,\Omega| = Im(\vec{z}\,\vec{W}^{*}) = 1. \tag{3-27}
$$

Separation:

$$
T_i = \hat{k}\cdot(\vec{z}_{i-1}\times\vec{z}_i) = |\vec{z}_{i-1},\vec{z}_i| = |y_{i-1},y_i| = Im(\vec{z}_{i-1}\vec{z}_i^{*}). \tag{3-28}
$$

Power:

$$
\mathcal{P}_i = \hat{k}\cdot(\vec{W}_i\times\vec{W}_{i+1}) = |W_i,W_{i+1}| = |\Omega_i,\Omega_{i+1}| = Im(\vec{W}_i\vec{W}_{i+1}^{*}). \tag{3-29}
$$

We shall have opportunity to use this notation extensively in subsequent paragraphs.

We note that, if we take the complex product $\hat{A}^*\hat{B}$ instead of $\tilde{A}\tilde{B}^*$, we get only a change of sign of the cross product, as these two products are complex conjugates of each other.

If at any time we wish to convert our vector equations into complex notation, we have only to make the substitutions implied by Eqs. (3-20) and (3-21). We prefer to use the vector notation for the algebraic calculations and the complex notation for the numerical calculations.

Matrix Representation

Considering the vectorial equations of refraction and transfer, Eqs. (3-4), (3-5), we see that they are linear in the vectors $\hat{z}$ and $\hat{W}$, and therefore they may be written in matrix form

$$\begin{pmatrix} \hat{z}_{i+1} \\ \hat{W}_{i+1} \end{pmatrix} = \begin{pmatrix} 1 & T_{i+1} \\ 0 & 1 \end{pmatrix} \begin{pmatrix} \hat{z}_i \\ \hat{W}_i \end{pmatrix} \quad , \text{ for transfer;}$$

$$\begin{pmatrix} \hat{z}_{i+1} \\ \hat{W}_{i+1} \end{pmatrix} = \begin{pmatrix} 1 & 0 \\ -\Phi_i & 1 \end{pmatrix} \begin{pmatrix} \hat{z}_i \\ \hat{W}_i \end{pmatrix} \quad , \text{ for refraction.}$$

These matrices are esentially those introduced by Brower (1964) and others, except for a slight difference in notation. The previous equations suggest that the general transformation between a point $\hat{z}$ and a line $\hat{W}$ in object space and the corresponding $\hat{z}'$ and $\hat{W}'$ in image space may be written in the form

$$\vec{z}' = a_{11}\vec{z} + a_{12}\vec{W}$$
$$\vec{W}' = a_{21}\vec{z} + a_{22}\vec{W}$$

By considering these vectors as complex numbers and taking their complex conjugates we may write the corresponding expressions

$$\vec{z}'^{*} = a_{11}\vec{z}^{*} + a_{12}\vec{W}^{*}$$
$$\vec{W}'^{*} = a_{21}\vec{z}^{*} + a_{22}\vec{W}^{*}$$

These four equations allow us to solve for the four unknown coefficients a_{ij}. The result is

$$\begin{aligned} a_{11} &= |\vec{z}', \vec{W}| \\ a_{12} &= |\vec{z}, \vec{z}'| \\ a_{21} &= |\vec{W}', \vec{W}| \\ a_{22} &= |\vec{z}, \vec{W}'| \end{aligned} \qquad (3\text{-}30)$$

where we have used the notation for determinants defined in the previous section, and the fact that $|\vec{z}, \vec{W}| = 1$. Note that the value of a_{21} is proportional to the power defined by the two vectors. We shall see in the next section that the other elements also have a simple interpretation in terms of the system as a whole.

Of course the particular matrices for refraction and transfer are special cases of the general matrix A whose elements are given by Eqs. (3-30); the matrix for transfer is

obtained when $\vec{W}' = \vec{W}$, and the matrix for refraction results when we set $\vec{z}' = \vec{z}$.

These matrices may be used interchangeably with the vector or complex number formulation when it is more convenient. It is encouraging to see how they arise here as a natural consequence of the linear relations inherent in the y-$\bar{y}$ diagram.

If we wish to know the matrix of a system for which the y-$\bar{y}$ diagram is known, we introduce the vectors of the first and last surfaces $\vec{z}_1$, $\vec{z}_k$ along with the object and image line vectors $\vec{W}_1$, $\vec{W}'_k = \vec{W}_{k+1}$, to obtain for the elements of the matrix A,

$$a_{11} = |\vec{z}_k, \vec{W}_1|$$

$$a_{12} = |\vec{z}_1, \vec{z}_k|$$

$$a_{21} = |\vec{W}_{k+1}, \vec{W}_k| = -\Phi$$

$$a_{22} = |\vec{z}_1, \vec{W}_{k+1}|$$

where Φ is the total power of the system..

CHAPTER 4

REPRESENTATION OF FIRST-ORDER CONCEPTS IN THE y-$\bar{y}$ DIAGRAM

In this Chapter we shall deal with the first-order properties of an optical system represented by a given set of points and lines in the y-$\bar{y}$ diagram. However, in order to carry out this type of analysis with the basic analytic tools described in the previous chapter, we must know in advance how familiar concepts of Gaussian Optics, such as magnifications, focal lengths, cardinal points, etc. are represented in the diagram. As the diagram is nothing more than the graphical representation of the basic equations of first-order optics, we anticipate that every concept and property defined in that discipline will have some sort of graphical counterpart in the diagram; once we become familiar with these geometric counterparts of the first-order optical concepts we shall be able to recognize them in a given diagram, and convert a given set of points into a set of constructable surfaces with definite curvatures and separations that will accomplish a predetermined function.

We shall see how the diagram can give us directly the relative positions of the different cardinal planes, the positions and sizes of the pupils, the powers and curvatures of the surfaces comprising the system, their separations, their

minimum sizes, etc. We shall also investigate in this chapter the effects on the points and the lines of the diagram, of a change in the position of the stop of the system, or of a change in the position of the object or the image; as well as the scaling effect on separations and curvatures, introduced by a change in the value of the Lagrange invariant.

We would like to make the comment at this point that, strictly speaking, Gaussian Optics does not consider the limitations on the bundle of rays going through the system, imposed by the finite apertures of diaphragms or the physical limits of the refracting surfaces, but only considers the imaging properties of the system between conjugate planes[1] in two determined spaces; in other words it applies the geometric laws of a collinear transformation, or "homography" to the planes tangent to the refracting surfaces at the points of intersection with the optical axis. The y-$\bar{y}$ diagram takes into account the effects of apertures right from the beginning, being incorporated in the definition of the marginal and chief rays.

We shall now proceed with the most important concepts of first-order optics.

The Magnification and the Conjugate Line

As defined in Gaussian optics, the transverse magnification (or simply the magnification), is the ratio of the heights of

---

1. Two points along the optical axis, and the perpendicular planes they define, are said to be conjugate when they obey a collinear transformation (Born and Wolf, 1970, p. 151).

a particular ray in two conjugate planes, one in object and the other in image space.

Accordingly, we define the magnification m_T, by the vector equation

$$\vec{z}' = m_T \vec{z} \tag{4-1}$$

and we say that the two points, $\vec{z}$ on line $\vec{W}$, and $\vec{z}'$ on line $\vec{W}'$ are conjugate to each other and related through the magnification m_T. Obviously, the two points are collinear with the origin of coordinates of the y-$\bar{y}$ diagram, and therefore the magnification m_T, is represented in the diagram by a line passing through the two points and through the origin. We call such a line the "conjugate" line of magnification m_T. This is illustrated in Fig. 17.

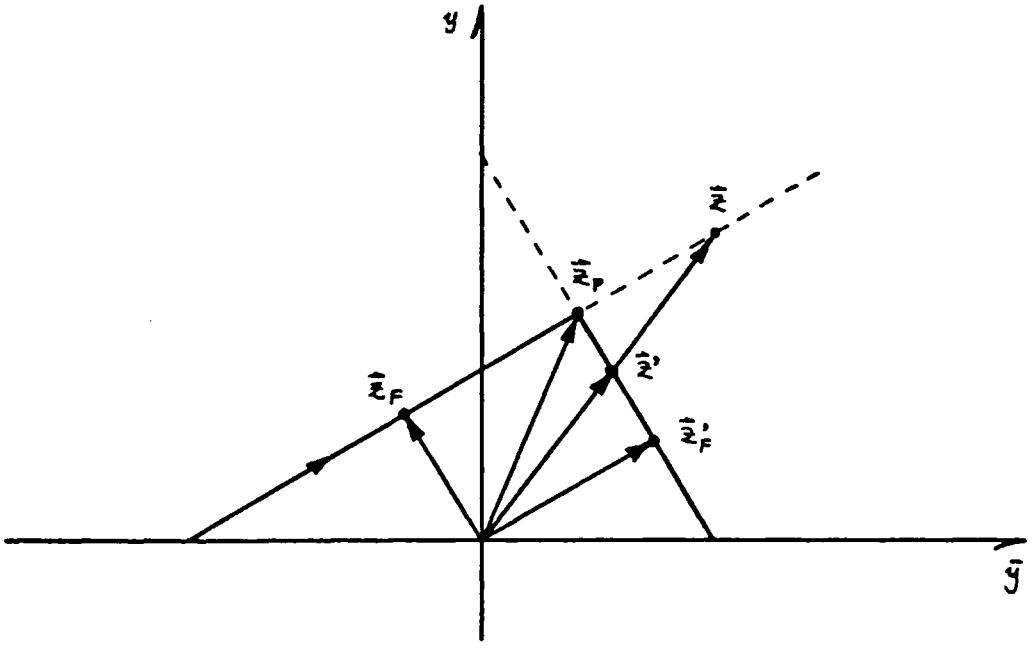

Fig. 17. Definition of conjugate points $\vec{z}$, $\vec{z}'$

We pointed out earlier that any line on the diagram representing a possible light path could not go through the origin. We see now that the lines going through the origin have a significance of their own, they identify conjugate planes for a given set of object and image rays, and they cut these object and image rays in proportion to the magnification associated with them.

We note that the magnification we have just defined refers to two specific spaces only. Therefore, when we refer to the magnification of the system, we are implicitly referring to the relation between the first and last spaces of the system (object and image space, respectively), represented in the diagram by the vectors $\vec{W}_1$ and $\vec{W}_k' = \vec{W}_{k+1}$. When we wish to talk about the magnification between any two other spaces, we shall explicitly say so.

For the moment then, we assume that the point $\hat{\vec{z}}$ is located on the line $\vec{W}$ (object line), and the point $\hat{\vec{z}}'$ is on the line $\vec{W}'$ (image line), and that these two lines are the only ones that constitute the system under consideration (see Fig. 17). In this case the vectors $\hat{\vec{z}}, \hat{\vec{z}}'$ satisfy Eq. (3-7),

$$\hat{\vec{z}} \times \vec{W} = \hat{\vec{z}}' \times \vec{W}' = \hat{k}$$

By appropiate cross products of Eq. (4-1) we have

$$\hat{k}\, m_T = \hat{\vec{z}}' \times \vec{W} \qquad (4\text{-}2)$$

$$\hat{k}/m_T = \hat{\vec{z}} \times \vec{W}' \qquad (4\text{-}3)$$

These expressions allow us to derive a relationship between the slope of a conjugate line and the magnification it represents. As the conjugate line goes through the origin, the only parameter needed to trace it is its slope, which is the same as that of the vectors $\hat{z}$, $\hat{z}'$ in Eq. (4-1). In other words, the slope of the conjugate line joining the points $\hat{z}$ and $\hat{z}'$ is given by

$$k_c = y/\bar{y} = y'/\bar{y}' \tag{4-4}$$

By using the determinant notation introduced in the last chapter, Eqs. (3-23), (3-24), we may write the expressions for the magnification, Eqs. (4-2), (4-3), in the form

$$m_T = |\hat{z}', \bar{W}| = y'\bar{\Omega} - \bar{y}'\Omega , \tag{4-5}$$

$$1/m_T = |\hat{z}, \bar{W}'| = y\bar{\Omega}' - \bar{y}\Omega'. \tag{4-6}$$

Solving for m_T in the two equations and using Eq. (4-1) we obtain

$$m_T = \frac{k_c\bar{\Omega} - \Omega}{k_c\bar{\Omega}' - \Omega'} ; \tag{4-7}$$

or solving for k_c ,

$$k_c = \frac{m_T\Omega' - \Omega}{m_T\bar{\Omega}' - \bar{\Omega}} . \tag{4-8}$$

The axes of the diagram, being lines through the origin, are themselves conjugate lines; the $\bar{y}$-axis is the image (or object) axis, and its associated magnification, the "image magnification" will be given by Eq. (4-7) when $k_c = 0$,

$$m_0 = \Omega/\Omega' ;$$

similarly, the y-axis is the pupil axis and the "pupil magnification" may be obtained from Eq. (4-7) by taking $k_c = \infty$,

$$m_E = \bar{\Omega}/\bar{\Omega}'.$$

From Eq. (4-8) we see that when $m_T = 0$,

$$k_c = \Omega/\bar{\Omega} = k,$$

which is the slope of line $\vec{W}$. Similarly, when $m_T = \infty$,

$$k_c = \Omega'/\bar{\Omega}' = k',$$

which is the slope of the line $\vec{W}'$. We see then, that every value of the magnification, from zero to ∞, is represented uniquely by a conjugate line in the diagram.

By noting that

$$\frac{m_o}{m_E} = \frac{k}{k'} \tag{4-9}$$

we may write the slope of the conjugate line of given magnification m_T in terms of the image and pupil magnifications as follows

$$k_c = \left(\frac{m_T - m_o}{m_T - m_E}\right) k' = \left(\frac{m_T - m_o}{m_T - m_E}\right) \frac{m_E}{m_o} k\,; \tag{4-10}$$

this expression has been found useful in some applications, specifically in dealing with image or pupil shifts.

We note in passing that Eq. (4-10) is the equation of a rectangular hyperbola in an m_T vs. k_c plot.

In Fig. 18a we have illustrated some of the magnifications associated with the same choice of image and pupil

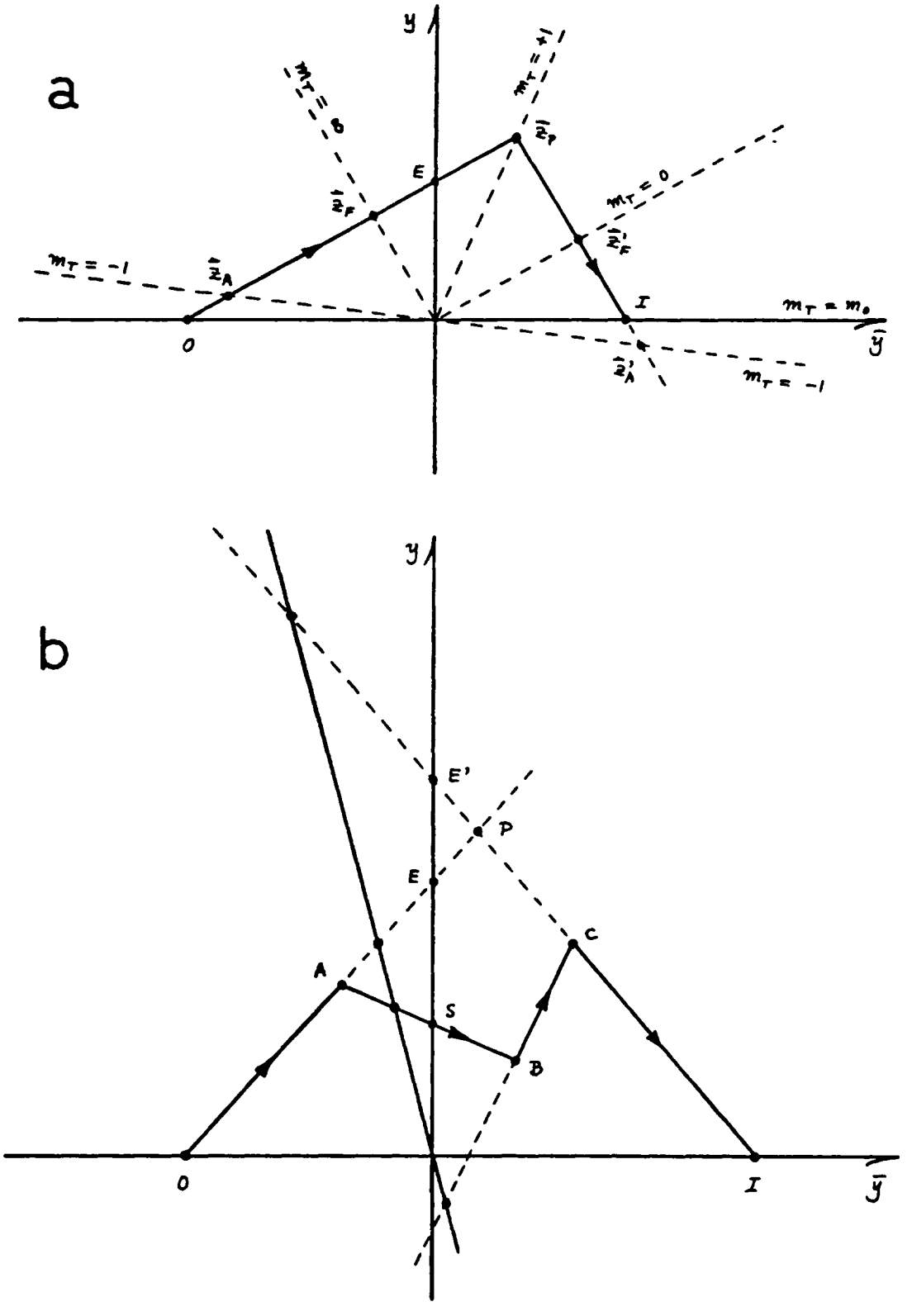

Fig. 18 a) Distribution of magnifications.
b) Conjugate line and associated conjugate points

magnifications as in Fig. 17. Figure 18b illustrates how a conjugate line defines the images of a given point in different spaces, each associated with one magnification.

From Eqs. (4-5), (4-6) we may derive the relationships between two points conjugate to each other. By substituting these values into Eq. (4-1) we obtain,

$$\vec{z} = \frac{\vec{z}'}{\hat{k}\cdot(\vec{z}' \times \vec{W})} = \frac{\vec{z}'}{|\vec{z}', \vec{W}|} , \tag{4-11}$$

or alternatively,

$$\vec{z}' = \frac{\vec{z}}{\hat{k}\cdot(\vec{z} \times \vec{W}')} = \frac{\vec{z}}{|\vec{z}, \vec{W}'|} . \tag{4-12}$$

These two expressions give the conjugate point of a given point as imaged into a given line.

The Cardinal Points

With the aid of these last two equations we may find the representation of the cardinal points.

The front focal point $\vec{z}_F$ is conjugate with the point at infinity in image space. In other words, we must have $\vec{z}' = \infty$ in Eq. (4-12); this implies that $\vec{z}_F \times \vec{W}' = 0$, i.e., $\vec{z}_F$ is parallel to $\vec{W}'$,

$$\vec{z}_F = a' \vec{W}'.$$

To determine the constant of proportionality a', we take the cross product of $\vec{W}$ with $\vec{z}_F$, and using Eq. (3-11), we obtain

$$\vec{z}_F = -\vec{W}'/\mathcal{D}. \tag{4-13}$$

Similarly the rear focal point $\hat{z}'_F$ is the conjugate of the point at infinity in object space. In order to have $\hat{z} = \infty$ in Eq. (4-11), we must have $\hat{z}'_F \times \vec{W} = 0$, i.e., $\hat{z}'_F$ must be parallel to $\vec{W}$,

$$\hat{z}'_F = a \vec{W}.$$

Taking the appropiate cross-product, we have

$$\hat{z}'_F = \vec{W} / \Sigma. \tag{4-14}$$

We see from these expressions that the focal point vectors are parallel to the object and image line vectors. On the other hand each vector lies in its corresponding line:

$$\hat{z}_F \times \vec{W} = \hat{z}'_F \times \vec{W}' = \hat{k},$$

and this provides us with the geometrical construction described by Delano: to locate the focal points of a system we draw a parallel line to the object and image lines through the origin; where these conjugate lines cross the object and image lines, they define the front and rear focal points respectively; see Fig. 17.

We may now use the two vectors $\hat{z}_F$ and $\hat{z}'_F$ as the basis for any other vector in object or image space. A vector on the object line may be thus expressed as

$$\hat{z} = a \hat{z}_F + b \hat{z}'_F = - a \vec{W}' / \Sigma + b \vec{W} / \Sigma.$$

Again, the constants of proportionality a, b may be calculated by appropiate cross-products, and by taking into account Eqs. (4-2), (4-3); the result is

$$\hat{z} = \hat{z}_F + (1/m_T)\,\hat{z}'_F , \tag{4-15}$$

and the conjugate of this vector in image space is given by

$$\hat{z}' = m_T\,\hat{z} = m_T\,\hat{z}_F + \hat{z}'_F . \tag{4-16}$$

We see then that, with the aid of the magnification, any vector or its conjugate may be expressed as a linear combination of the vectors $\hat{z}_F$, $\hat{z}_F'$.

The principal points are defined by $m_T = 1$,

$$\hat{z}_P = \hat{z}'_P = \hat{z}_F + \hat{z}'_F = \frac{\vec{W}' - \vec{W}}{-\Sigma} , \tag{4-17}$$

but this is the same point as the intersection of the lines $\vec{W}$, $\vec{W}'$, as may be seen by comparing the last member of Eq. (4-17) with Eq. (3-15). In other words, both principal points are represented by the point representing the surface of refraction but $\hat{z}_P$ is located on the object line and $\hat{z}'_P$ is located on the image line; see Fig. 17.

The other set of cardinal points, the nodal points $\hat{z}_N$, z'_N, is defined by $m_T = \mathcal{R} \equiv n/n'$ the ratio of the indices of refraction in object and image spaces. Thus

$$\hat{z}_N = \hat{z}_F + (n'/n)\,\hat{z}'_F$$

$$\hat{z}'_N = (n/n')\,\hat{z}_F + \hat{z}'_F$$

We shall also find use for the set of points defined by $m_T = -1$, which are called by some authors (e.g., Chrétien, 1958, p. 58) the "antiprincipal" points

$$\vec{z}_A = \vec{z}_F - \vec{z}'_F$$

$$\vec{z}'_A = -\vec{z}_F + \vec{z}'_F$$

These points become important when we wish to express the properties of the system independently of the choice of the positions of the stop or of the object. Fig. 19 shows the location of all these points for a single surface with $\mathcal{R} = 0.75$; the rest of the points and lines in this figure will be described shortly.

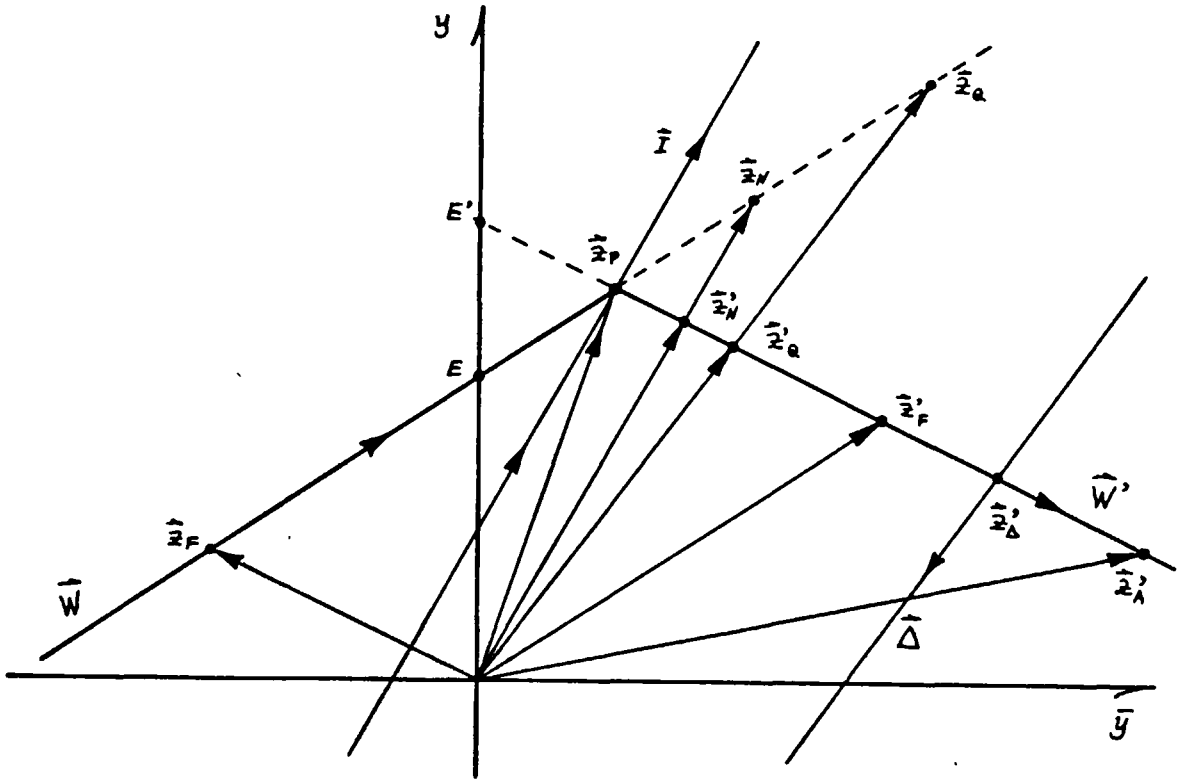

Fig. 19. Cardinal points and associated lines

When two lines are parallel to each other, say $\vec{W}' = \alpha \vec{W}$ we see from Eq. (3-11) that the power is zero and therefore, the focal points as well as the rest of the cardinal points no longer

have any meaning. The conjugate lines however, still exist and define conjugate planes, by cutting the parallel lines at the same angle. Therefore, the magnification remains finite, and by using Eq. (4-2) we may see that

$$m_T = 1/\alpha = \text{const};$$

this corresponds to an afocal system, and we see that in this case, the magnification remains constant throughout the diagram.

Conjugate Planes

Remembering that in the y-$\bar{y}$ diagram, reduced separations are represented by areas, and that these may be calculated more easily with the determinant notation introduced in the last chapter, we proceed now to calculate the distances between the principal planes and the conjugate planes defined by a given magnification m_T; these planes are represented by $\vec{z}_P$ and the conjugate points $\vec{z}, \vec{z}'$ given by Eqs. (4-17) and (4-15), (4-16), respectively. We have then, as a function of the magnifications, in object space:

$$T(m_T) = |\vec{z}_P, \vec{z}| = \frac{1 - m_T}{m_T \Phi}, \tag{4-18}$$

where we have used the expressions,

$$\begin{aligned} |\vec{z}_P, \vec{z}_F| &= -1/\Phi, \\ |\vec{z}_P, \vec{z}'_F| &= +1/\Phi, \end{aligned} \tag{4-19}$$

easily verified by direct substitution of Eqs. (4-13), (4-14) into Eq. (4-17).

Similarly, in image space the separation of point from the principal point is given by

$$T'(m_T) = |\bar{z}_F, \bar{z}'| = \frac{1 - m_T}{\Phi}. \qquad (4\text{-}20)$$

We may apply these expressions to calculate the relative distances between the cardinal points.

From Eqs. (4-15), (4-16), and (4-8), we see that the conjugate line for $m_T = \pm\infty$ passes through the front focal point $\bar{z}_F$, and the conjugate line for $m_T = 0$ goes through the rear focal point $\bar{z}'_F$. Therefore, the front focal length f may be obtained from Eq. (4-18) as

$$T(\infty) = \mathcal{H} f/n = -1/\Phi = -\mathcal{H}/\varphi;$$

and the rear focal length f', from Eq. (4-20) as

$$T'(0) = \mathcal{H} f'/n' = 1/\Phi = \mathcal{H}/\varphi;$$

in other words,

$$f = -n/\varphi,$$
$$f' = +n'/\varphi.$$

In a similar manner, the distances from the principal points to the nodal points ($m_T = R \equiv n/n'$) will be given by

$$\mathcal{H} l_N/n = T(R) = \mathcal{H}(n - n')f/n^2,$$
$$\mathcal{H} l'_N/n' = T'(R) = \mathcal{H}(n' - n)f'/nn';$$

or, in other words,

$$l_N = f + f'$$
$$l'_N = f + f'$$

The separations of the antiprincipal points, are likewise obtained when we set $m_T = -1$ in Eqs. (4-18), (4-20); the result is

$$\ell_A = 2f$$
$$\ell'_A = 2f'$$

Any other relation between conjugate planes, such as Newton's formula or the thin lens formula, for example, may be easily derived with the aid of the above or similar expressions. In Newton's expression, the conjugate planes are meassured from the focal planes, thus in this case:

$$\mathcal{H}\, x/n = |\vec{z}_F, \vec{z}| = 1/m_T \mathcal{F},$$
$$\mathcal{H}\, x'/n' = |\vec{z}'_F, \vec{z}'| = -m_T/\mathcal{F};$$

and multiplying these two expressions, we get Newton's formula:

$$\frac{\mathcal{H}^2 x x'}{n n'} = -1/\mathcal{F}^2 = \frac{\mathcal{H}^2 f f'}{n n'}.$$

Another useful problem we may solve with these concepts is the following. In the situation depicted in Fig. 20 we wish to find an expression for a point $\tilde{z}$ determined by the conjugate line of magnification m_T and any other line $\tilde{W}$. The resulting expression will be used in a later chapter.

We see from the figure that

$$\tilde{z} = \alpha \vec{z}' = \alpha m_T \vec{z}. \qquad (4\text{-}21)$$

where α is a proportionality factor to be determined. Remembering Eq. (4-16) we may write

$$\tilde{z} = \alpha m_T \vec{z}_F + \alpha \vec{z}'_F.$$

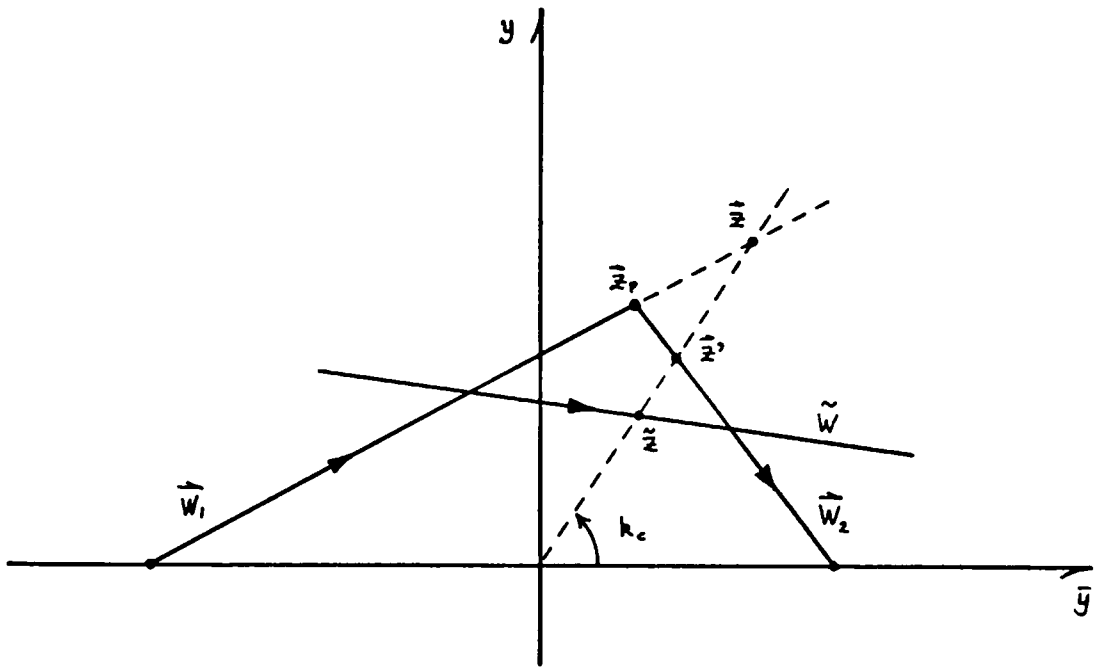

Fig. 20. Intersection of
a conjugate line and an arbitrary line

Taking the cross product with the line $\tilde{W}$,

$$\vec{z} \times \vec{W} = \frac{-\alpha\, m_T\, (\vec{W}_2 \times \tilde{W})}{\Xi} + \frac{\alpha\, (\vec{W}_1 \times \vec{W}_2)}{\Xi} = \hat{k}$$

and evaluating the cross products we get for the proportionality factor

$$\alpha = \frac{\Xi}{|\vec{W}_1, \tilde{W}| + m_T\, |\tilde{W}, \vec{W}_2|}; \qquad (4\text{-}22)$$

on the other hand,

$$\vec{\tilde{z}}' = m_T \vec{\tilde{z}}_F + \vec{\tilde{z}}'_F = \frac{-m_T \vec{W}_2 + \vec{W}_1}{\Phi} . \qquad (4\text{-}23)$$

Substituting Eqs. (4-22), (4-23) into Eq. (4-21) we finally get

$$\tilde{z} = \frac{\vec{W}_1 - m_T \vec{W}_2}{|\vec{W}_1, \tilde{W}| - m_T |\vec{W}_2, \tilde{W}|} . \qquad (4\text{-}24)$$

Angle of Incidence at a Surface

In the most general case, the situation depicted in Fig. 19 represents a single refracting surface when $n \neq n'$. As remarked earlier, different systems will result according to the choice of the indices of refraction. When $n = n'$, Fig. 19 represents a thin lens, for example. Even in the most general case we can think of Fig. 19 as representing a whole system of many elements, but restricting our attention only to the first and last spaces, the object and image space, respectively. In this case then, we may think of the whole system as an "equivalent" surface or thin lens.

In the general case of a surface we wish now to find the representation of the reduced angle of incidence, which by Snell's law we know is an invariant upon refraction; its value, for both the marginal and chief rays, will be needed to evaluate the third order aberration coefficients in a subsequent chapter. From the equation of refraction (3-5), and remembering the definition of the power Φ, we may write,

$$\vec{W}' = \vec{W} + nc\vec{\tilde{z}}/\mathcal{H} - n'c\vec{\tilde{z}}/\mathcal{H},$$

where C is the curvature of the surface in question. From here we see that the quantity

$$\vec{I} \equiv \vec{W}' + cn'\vec{z}/\mathcal{H} = \vec{W} + cn\vec{z}/\mathcal{H},$$

is an invariant on refraction and represents the reduced angle of incidence appropiately scaled by the Lagrange invariant:

$$\vec{I} \equiv (n\bar{i}/\mathcal{H}, ni/\mathcal{H}) \tag{4-25}$$

By introducing $\mathcal{R} \equiv n/n'$, the ratio of the refractive indices, also called the "refractance," and using again the definition of $\mathcal{E}$ (Appendix A) and the equation of refraction (3-5), we may express the refraction invariant as

$$\vec{I} = \frac{\mathcal{R}\vec{W}' - \vec{W}}{\mathcal{R}-1}. \tag{4-26}$$

This vector, being a linear combination of $\vec{W}$ vectors, will be represented by a line in the y-$\bar{y}$ diagram and by a point in the Ω-$\bar{\Omega}$ diagram.

The cross products of this line vector with the focal vectors are

$$\vec{z}_F \times \vec{I} = -\hat{k}/(\mathcal{R}-1)$$
$$\vec{z}'_F \times \vec{I} = \hat{k}\mathcal{R}/(\mathcal{R}-1)$$

which appropiately combined give

$$(\mathcal{R}\vec{z}_F + \vec{z}'_F) \times \vec{I} = \vec{z}'_N \times \vec{I} = 0.$$

On the other hand

$$(\vec{z}_F + \vec{z}'_F) \times \vec{I} = \vec{z}_P \times \vec{I} = \hat{k}.$$

In other words, the line representing $\hat{I}$ passes through the point of refraction $\hat{z}_P$ and is parallel to the conjugate line defining the nodal points of the surface. See Fig. 19.

We see that, if the line $\hat{I}$ is parallel to the y-axis, the pupils coincide with the nodal points, and because the component of $\hat{I}$ vanishes, the chief ray does not get refracted. The power for such a surface is given by

$$\varphi = \left(\frac{\mathcal{R}-1}{\mathcal{R}}\right)\frac{\bar{\omega}}{\bar{y}},$$

which leads to a radius of curvature $r = -\bar{y}/\bar{u}$. This surface has its center of curvature located at the stop.

The contribution of this type of surface to the coefficients of coma, astigmatism, distortion, and transverse chromatic aberration is zero.

When $\hat{I}$ is parallel to the $\bar{y}$-axis, the nodal points coincide with the object and image, both located at the center of curvature of the surface of refraction; the marginal ray does not get deviated in this case, and the power of such a surface is given by

$$\varphi = \left(\frac{\mathcal{R}-1}{\mathcal{R}}\right)\frac{\omega}{y},$$

which gives a radius of curvature $r = -y/u$.

And for this type of surface, the contributions to the coefficients of spherical aberration, coma, and longitudinal chromatic aberration, vanish.

Aplanatic Points of a Surface

Another quantity necessary for the computation of third order aberration coefficients is the vector whose components are given by

$$\Delta\left(\frac{\bar{u}}{n}\right) \equiv \frac{\bar{u}'}{n'} - \frac{\bar{u}}{n} = \frac{\bar{\omega}'}{n'^2} - \frac{\bar{\omega}}{n^2},$$

$$\Delta\left(\frac{u}{n}\right) \equiv \frac{u'}{n'} - \frac{u}{n} = \frac{\omega'}{n'^2} - \frac{\omega}{n^2}.$$

Accordingly, we define the line vector

$$\vec{\Delta} \equiv \frac{\vec{W}'}{n'^2} - \frac{\vec{W}}{n^2} = \frac{\mathcal{R}^2\vec{W}' - \vec{W}}{n^2} \qquad (4\text{-}27)$$

which we call the "aplanatic line," and which is represented by a line in the y-$\bar{y}$ diagram and by a point in the Ω-$\bar{\Omega}$ diagram.

By taking the cross product of this line with the focal vectors we get

$$\vec{z}_F \times \vec{\Delta} = -\hat{k}/n^2,$$
$$\vec{z}'_F \times \vec{\Delta} = \hat{k}\,\mathcal{R}/n^2.$$

By combining these two expressions we see that

$$\left(\mathcal{R}^2\vec{z}_F + \vec{z}'_F\right) \times \vec{\Delta} = 0.$$

In other words, the vector $\vec{\Delta}$ is represented by a line parallel to the conjugate line of magnification $m_T = \mathcal{R}^2$.

The two conjugate points $\vec{z}_a$, $\vec{z}'_a$, defined by the conjugate line of magnification $m_T = \mathcal{R}^2$ and the object and image lines, respectively, are the aplanatic points of the surface. Their values are given by

$$\vec{z}_Q = \vec{z}_F + (1/\mathcal{R}^2)\,\vec{z}'_F$$
$$\vec{z}'_Q = \mathcal{R}^2\,\vec{z}_F + \vec{z}'_F \qquad (4\text{-}28)$$

The aplanatic points are separated from the principal points by

$$|\vec{z}_P, \vec{z}_Q| = \frac{\mathcal{H}}{n}\left(1 + \frac{n'}{n}\right)\gamma,$$

$$|\vec{z}_P, \vec{z}'_Q| = \frac{\mathcal{H}}{n'}\left(1 + \frac{n}{n'}\right)\gamma;$$

where γ, is the radius of curvature of the surface.

The aplanatic line crosses the object and image lines at the points

$$\vec{z}_\Delta = \frac{\vec{W} - \vec{\Delta}}{|\vec{W}, \vec{\Delta}|} = \vec{z}_F + \left(1/\mathcal{R}^2 + n'^2\right)\vec{z}'_F$$

$$\vec{z}'_\Delta = \frac{\vec{\Delta} - \vec{W}'}{|\vec{\Delta}, \vec{W}'|} = \left(\mathcal{R}^2 - n^2\right)\vec{z}_F + \vec{z}'_F$$

which are <u>not</u> conjugate to each other. The separation of these points from the aplanatic points are given by

$$|\vec{z}_Q, \vec{z}_\Delta| = -\mathcal{H}n'^2 f/n,$$

$$|\vec{z}'_Q, \vec{z}'_\Delta| = +\mathcal{H}n^2 f'/n'.$$

The position of this line and points is illustrated in Fig. 19.

When $\vec{\Delta}$ is parallel to the $\bar{y}$-axis, the object and image coincide with the aplanatic points; in such a case the surface is called "aplanatic," and it is free of spherical aberration, coma and astigmatism. The power of such a surface is given by

$$\varphi = \frac{R^2 - 1}{R^2} \frac{\omega}{y},$$

which gives a radius of curvature

$$r = \frac{-Ry}{(1+R)u} = \frac{-y}{(1+R)u'}.$$

Location of Real Pupils and Real Images

We shall give now an analytical criterion to decide if a given line when crossing either of the two coordinate axes produces a real or a virtual image or pupil. We know that every time a segment of a $\vec{W}$ line comprised between two successive $\vec{z}$ points (what we have previously defined as a light-segment), crosses the y-axis, the chief ray is crossing the optical axis; in other words, we have a physical stop or a real image of it located between the two surfaces represented by the $\vec{z}$ vectors. When it is the extension of the light-segment that crosses the y-axis we have a "virtual" stop or pupil, a conjugate to the actual physical aperture.

Similarly, if the light-segment crosses the $\bar{y}$-axis we know that the marginal ray is crossing the optical axis and we have a real image, in the sense that we can actually put a screen there. If on the other hand, it is the extension of the light-segment that crosses the $\bar{y}$-axis, we have a virtual image, which is conjugate to the real image.

Geometrically, we can see by inspection of the diagram where these crossings occur, and the problem of determining the location of stops or real images is trivial. Numerically, however, this problem is not trivial: When we try to do this in a computer program without recourse to the graph, for example, it is not obvious what sort of decision we must make, based on the values of the coordinates of the points, to say with precision that we have stops between surfaces 2 and 3, and between 4 and 5, (see Fig. 21); or that we have a real image between surfaces 3 and 4 as well as at O and O'.

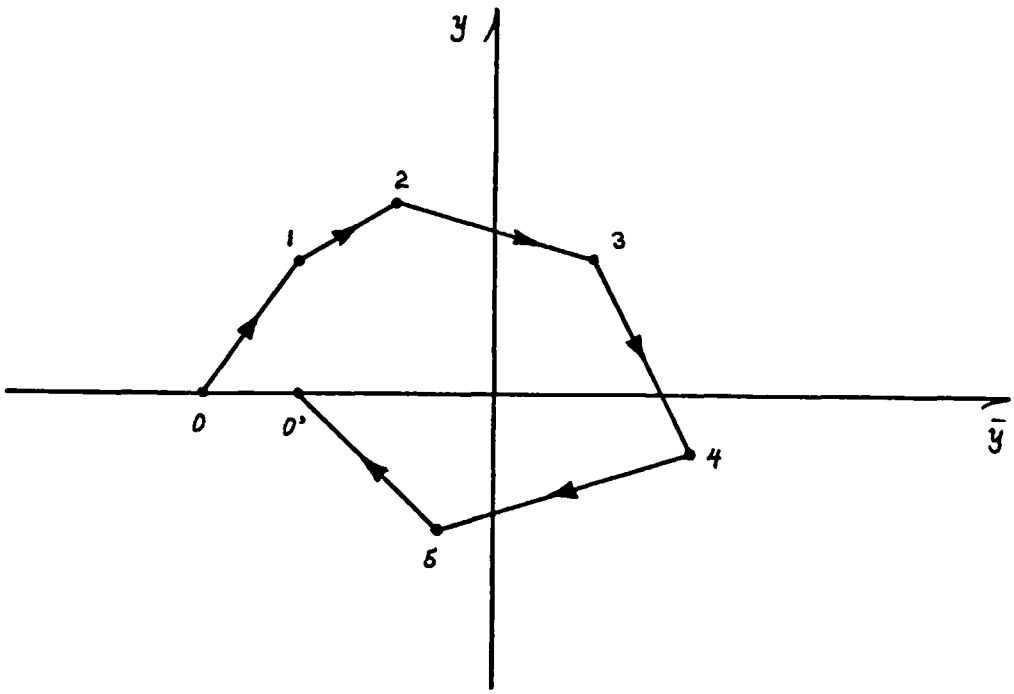

Fig. 21. Location of real pupils and images

For cases such as this it is convenient to express the vectors $\vec{e}$ in some parametric form that will show unmistakably

that such a point lies within a light-segment or outside. The following representation (Zwikker, 1950, p. 33), has been found useful. Consider the line defined by the vectors $\vec{z}_{i-1}$, $\vec{z}_i$; then any other vector along that line may be represented as a function of a parameter s_i by the equation

$$\vec{z} = \frac{\vec{z}_{i-1} + s_i \vec{z}_i}{1 + s_i} . \tag{4-29}$$

When $s_i = 0$, then $\vec{z} = \vec{z}_{i-1}$, and when $s_i = \infty$, then $\vec{z} = \vec{z}_i$. We see then that only non-negative values of s_i represent points located within the light-segment defined by $\vec{z}_{i-1}$ and $\vec{z}_i$. This is a very useful parametric representation for our purposes, since only the values of $\vec{z}$ within the light-segment have a physical meaning in the $y-\bar{y}$ diagram.

Applying this formula to the location of the stops of the system, we see that we have a stop or a real image of it every time $\bar{y} = 0$; this leads to the following criterion to test whether a stop exists between surfaces $\vec{z}_{i-1}$ and $\vec{z}_i$:

$$s_i = -\bar{y}_{i-1} / \bar{y}_i \geq 0 \tag{4-30}$$

and the size of such an aperture is given by

$$y_s = \frac{y_{i-1} + s_i y_i}{1 + s_i} . \tag{4-31}$$

The distances of this stop from surfaces $\vec{z}_{i-1}$ and $\vec{z}_i$ are given by

$$T_{i-1,s} = |y_{i-1}, y_s| = -y_s \bar{y}_{i-1} ,$$

$$T_{s,i} = |y_s, y_i| = y_s \bar{y}_i ,$$

respectively. We may use this test for each of the spaces in turn to find the location and size of the stop and its real images (pupils), if any; if the test fails we have a virtual pupil. Of course, if either $\bar{y}_{i-1} = 0$ or $\bar{y}_i = 0$, the test is unnecessary as the answer is obvious.

Similarly, the same parametric form, Eq. (4-29), may be used to test whether a real or a virtual image is formed between two given surfaces. In this case, as $y = 0$ for an image, a real image will be located between surfaces $\vec{z}_{i-1}$ and $\vec{z}_i$ if

$$s_i = -y_{i-1}/y_i \geqslant 0 \qquad (4\text{-}32)$$

and its size will be given by

$$\bar{y}_I = \frac{\bar{y}_{i-1} + s_i \bar{y}_i}{1 + s_i} \qquad (4\text{-}33)$$

The reduced distances of this image from surfaces $\vec{z}_{i-1}$ and $\vec{z}_i$ will be given by

$$T_{i-1,I} = |y_{i-1}, y_I| = y_{i-1} \bar{y}_I ,$$
$$T_{I,i} = |y_I, y_i| = -y_i \bar{y}_I ,$$

respectively. If the test fails, we have a virtual image instead.

Shifts of the Stop or the Object

Delano in his paper shows that a shift of the stop of the system or a change of the position of the object, reflects itself as a shear of all the points and lines of the diagram with

respect to one of the coordinate axes. We derive the same result in this section in a different manner which will yield us the transformation to be applied to the vectors in the diagram to accomplish a given shift. We base our derivation on the idea that a shift means essentially a change in the magnification either of the pupils or of the conjugates. We recognize that these shifts must be made in such a manner that the Lagrange invariant is conserved in value.

By looking back at Fig. 18, we see that the stop of that system is located on the line $\vec{W}$ and therefore it coincides with the entrance pupil. The magnification between the pupils is given by m_E, which corresponds to the slope of the y-axis. It is clear that if we change the position of the stop we are in effect choosing another magnification for the pupils without otherwise altering the diagram. But if we choose another value of m_E, this is the same as changing the slope of the y-axis without altering the role of the $\bar{y}$-axis. For example, if we choose as the new value of the pupil magnification $m_E' = 1.086$, say, instead of the value adopted in Fig. 18, the new y'-axis, i.e., the conjugate line with the new magnification m_E', will be inclined 75° with respect to the $\bar{y}$-axis instead of being perpendicular to it. The $\bar{y}$-axis itself has not changed at all, as the magnification associated with it is independent of this change. However, as may be appreciated in the Fig. 22, the new diagram is identical to that in Fig. 18 <u>except</u> that now it is referred to an oblique set of axes instead of the original orthogonal one.

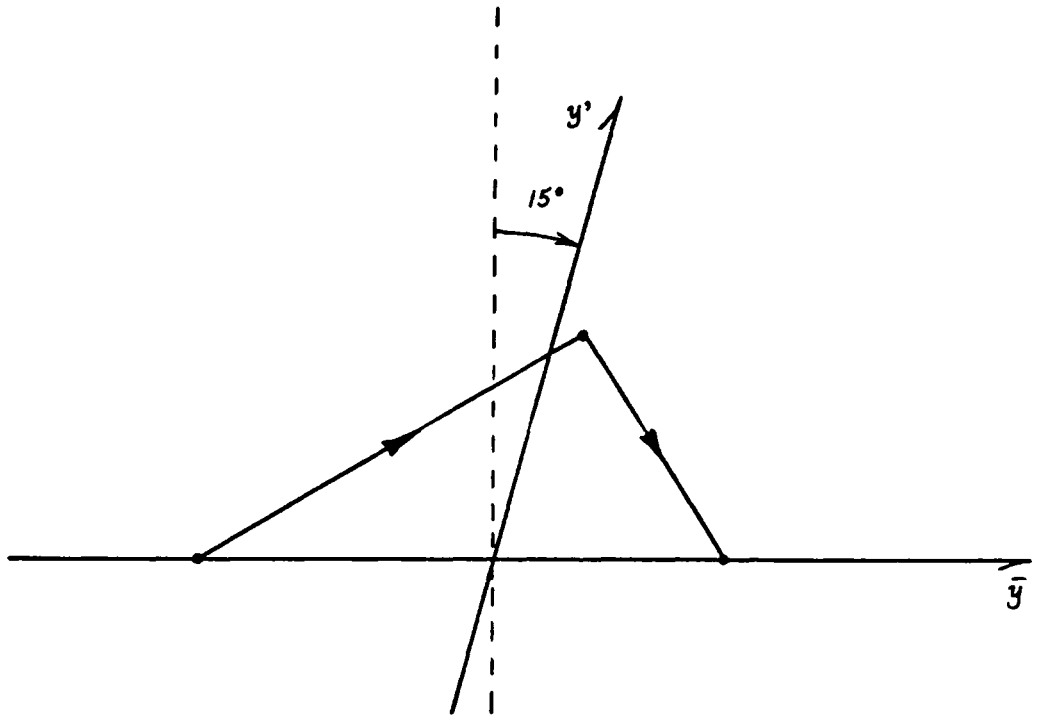

Fig. 22 Choice of a new pupil magnification

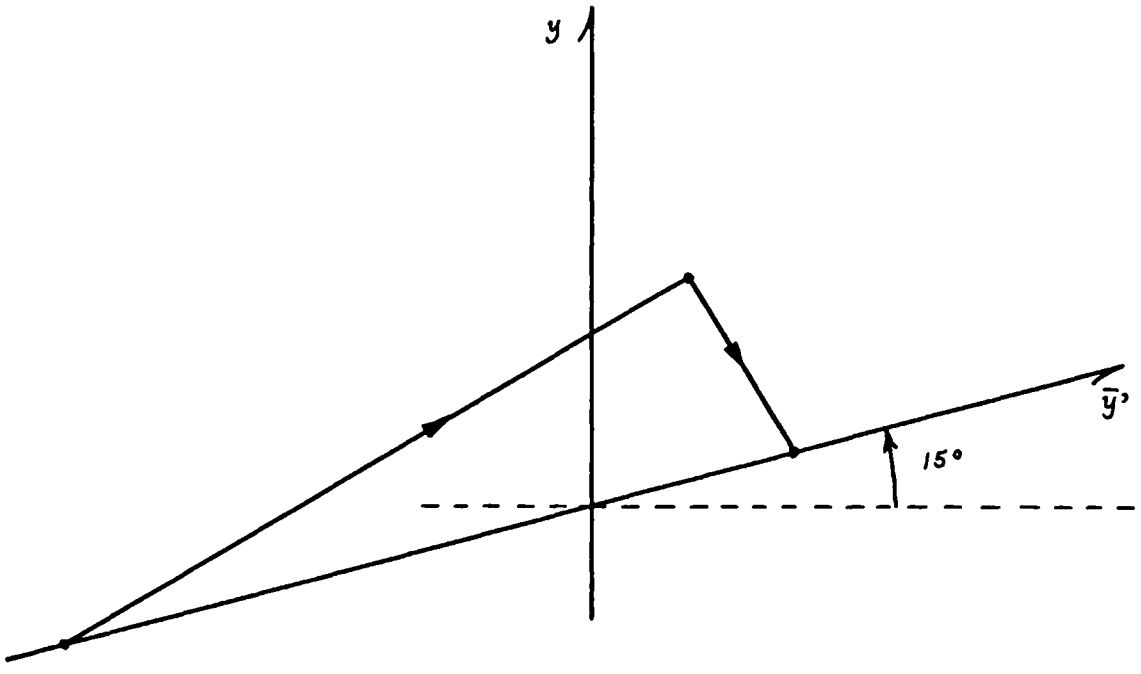

Fig. 23 Choice of a new object magnification

In order to reorthogonalize the axes we have to "shear" the whole set of points and lines, in this case to the left, which means that we are going to change by this operation, only the $\bar{y}$ values, the marginal heights remaining the same as before. This makes sense, because after all, we are only changing the heights of the chief ray that must now cross the optical axis at the position of the new stop.

An entirely similar situation occurs if we decide to change the position of the image (or object); this implies a different choice for the object magnification, and therefore the choice of a new conjugate line for the $\bar{y}$-axis. Again the new system would be referred to an oblique set of axes, as pictured in Fig. 23, which represents a change from the original diagram in Fig. 18. To reorthogonalize the set of axes we shear the whole diagram downwards, which only affects the y heights as the chief ray heights remain the same; we have only changed the origin of the marginal ray, and the chief ray continues to define the position of the stop that has been left unchanged by this operation.

In either case, the size of the stop or of the image will change accordingly, in order to preserve the numerical value of the Lagrange invariant as we shall see shortly.

In order to derive the algebraic expressions for the shifts, note that the most general transformation between a point $\vec{z}$ on the light-ray $\vec{W}$ and a point $\vec{z}'$ on the line $\vec{W}'$, may be written as follows: from the equality,

$$\hat{z} \times \vec{W} = \hat{z}' \times \vec{W}' = \hat{k},$$

and by adding to both sides the product $\vec{W} \times \hat{z}'$, we may write

$$\vec{W} \times \Delta \hat{z} = \hat{z}' \times \Delta \vec{W} ; \qquad (4\text{-}34)$$

or in determinant form,

$$|W, \Delta \hat{z}| = |\hat{z}', \Delta \vec{W}|. \qquad (4\text{-}35)$$

This is the most general transformation from a plane in one space to another plane in a different space. The cases of refraction and transfer may be recognized as special cases: when $\Delta \hat{z} = 0$, we have a refraction, i.e., a change of value of the vector $\vec{W}$; when $\Delta \vec{W} = 0$, we have a transfer.

However, this equation is also satisfied when $\Delta \hat{z}$ and $\Delta \vec{W}$ are both real or both pure imaginary vectors, as may be easily verified by inserting $\Delta \hat{z}^* = \Delta \hat{z}$ and $\Delta \vec{W}^* = \Delta \vec{W}$, into Eq. (4-35).

Now, when $\Delta \hat{z}$ and $\Delta \vec{W}$ are real, this means that $\Delta \hat{z}$ is parallel to the $\bar{y}$-axis ($\Delta y = 0$), and $\Delta \vec{W}$ is parallel to the $\bar{\Omega}$-axis ($\Delta \Omega = 0$), in their respective diagrams; this obviously corresponds to a shift of the stop, according to our previous remarks at the beginning of this section. When this is the case, Eq. (4-35) reduces to

$$\Omega \, \Delta \bar{y} = y' \, \Delta \bar{\Omega}$$

or in other words:

$$\frac{\Delta \bar{y}}{y'} = \frac{\Delta \bar{\Omega}}{\Omega} = const. \qquad (4\text{-}36)$$

The value of the constant may be determined directly from Fig. 24,

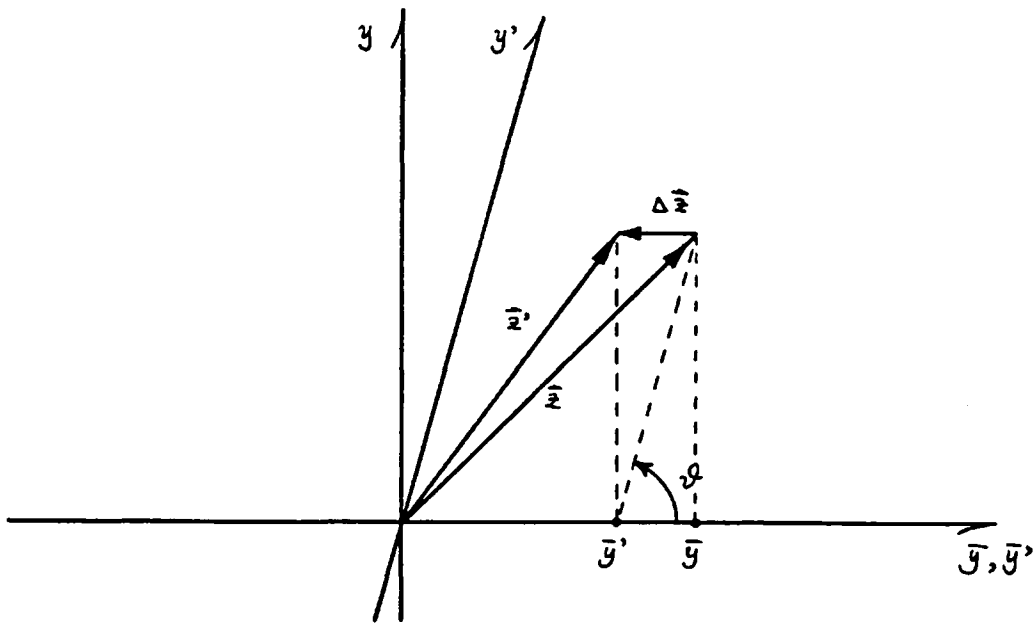

Fig. 24. Stop shift

$$k' = \tan \vartheta = y/\Delta \bar{y}$$

where k' is the slope of the new y-axis. Thus, Eq. (4-36) reads

$$\frac{\Delta \bar{y}}{y} = \frac{\Delta \bar{\Omega}}{\Omega} = 1/k'.$$

This transformation may be written in matrix form:

$$\hat{z}' \equiv \begin{pmatrix} \bar{y}' \\ y' \end{pmatrix} = \begin{pmatrix} 1 & -1/k' \\ 0 & 1 \end{pmatrix} \begin{pmatrix} \bar{y} \\ y \end{pmatrix} \equiv \mathcal{S}\, \hat{z} \,; \qquad (4\text{-}37)$$

and similarly for the $\vec{W}$ vectors,

$$\vec{W}' = \mathcal{S}\, \vec{W} \qquad (4\text{-}38)$$

Note that $|\mathcal{S}| = 1$, i.e., the matrix $\mathcal{S}$ is unimodular, and accordingly[1], the values of the cross-products between vectors $\hat{z}$ and/or $\vec{W}$ do not change under this transformation; in other words, the separations T and the powers Φ remain invariant under stop shift. The dot products, however, do change and therefore the angles between the lines will change.

As seen from the form of the matrix $\mathcal{S}$ the only parameter necessary to carry out the stop-shift transformation is the slope k' of the new y-axis; this may be specified in a variety of ways, we may want to pass the new y-axis through some given point or we may want it parallel to a certain line, or we may wish to have a specific new value of the pupil magnification in which case we obtain k' from Eq. (4-8). Or we may wish to place the stop before surface $\hat{z}_j$ in which case we must use as new y-axis the conjugate line passing throught the point defined by

$$\hat{z}_s = \hat{z}_j - T_s \vec{W}_j \,,$$

---

1. It may easily be proven that if two vectors $\hat{a}$, $\hat{b}$ obey the transformation $\hat{a}' = A\hat{a}$, $\hat{b}' = A\hat{b}$, where A is the transformation matrix, then $\hat{a}' \times \hat{b}' = |A|(\hat{a} \times \hat{b})$, where $|A|$ is the determinant of matrix A . (See Goldstein 1953, p. 130.)

where $\tau_s \equiv |\vec{z}_s, \vec{z}_j|$, is the distance between the desired stop and the surface $\vec{z}_j$. Similarly, if the stop is to be located at a distance τ_s after the surface $\vec{z}_j$, the corresponding equation for $\vec{z}_s$ is

$$\vec{z}_s = \vec{z}_j + \tau_s \vec{W}_{j+1}.$$

We wish to emphasize that although the matrix $\mathcal{S}$ is of the same type as the matrices for refraction and transfer, its role is quite different: while a refraction or a transfer matrix only involve two vectors at a time, the matrix $\mathcal{S}$ must be applied to <u>all</u> $\vec{z}$ and $\vec{W}$ vectors of the diagram when carrying out a stop-shift. In other words, it is a transformation for the whole plane.

It is instructive to see how a given line with a reference point on it is changed by a stop-shift transformation. We notice first of all that the change $\Delta\bar{y}$ is proportional to the y-height of the reference point in question; therefore, the points along the $\bar{y}$-axis, for which $y = 0$, do not change at all. Secondly, if we denote by k_w, k'_w the slopes of the line before and after shifting, it is easy to show that

$$1/k'_w = 1/k_w - 1/k'$$

where k' is again the slope of the new y-axis. Thirdly, the height of the new pupil will be given by

$$y'_E = (k'_w/k_w)\, y_E.$$

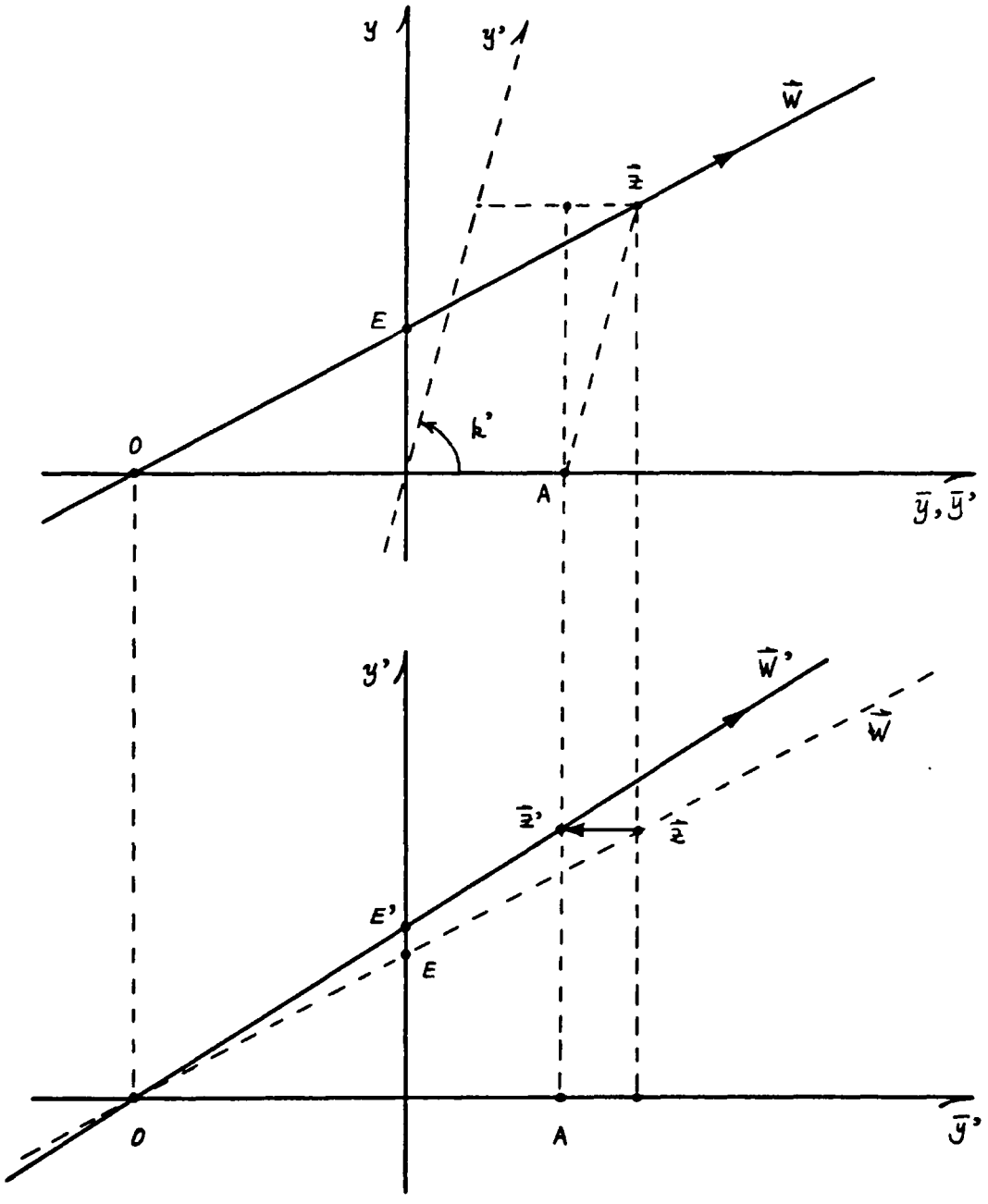

Fig. 25 Effect of a stop shift on a single line (Primes represent values after the shift).

As the line $\hat{W}'$, after transformation, must pass through the new point $\hat{z}'$ and through the same image point as before the shift, we may see that, after reorthogonalizing the axes, the net effect on the line is to tilt it using its intersection with the $\bar{y}$-axis as a pivot. This is illustrated in Fig. 25.

In a completely similar manner, when $\Delta\hat{z}$ and $\Delta\hat{W}$ in Eq. (4-34) are pure imaginary, means that they are parallel to the ordinate axis ($\Delta\bar{y} = \Delta\bar{\Omega} = 0$) in their respective diagrams; this then, corresponds to an object shift and in this case Eq. (4-35) reduces to

$$\bar{\Omega}\,\Delta y = \bar{y}'\Delta\Omega,$$

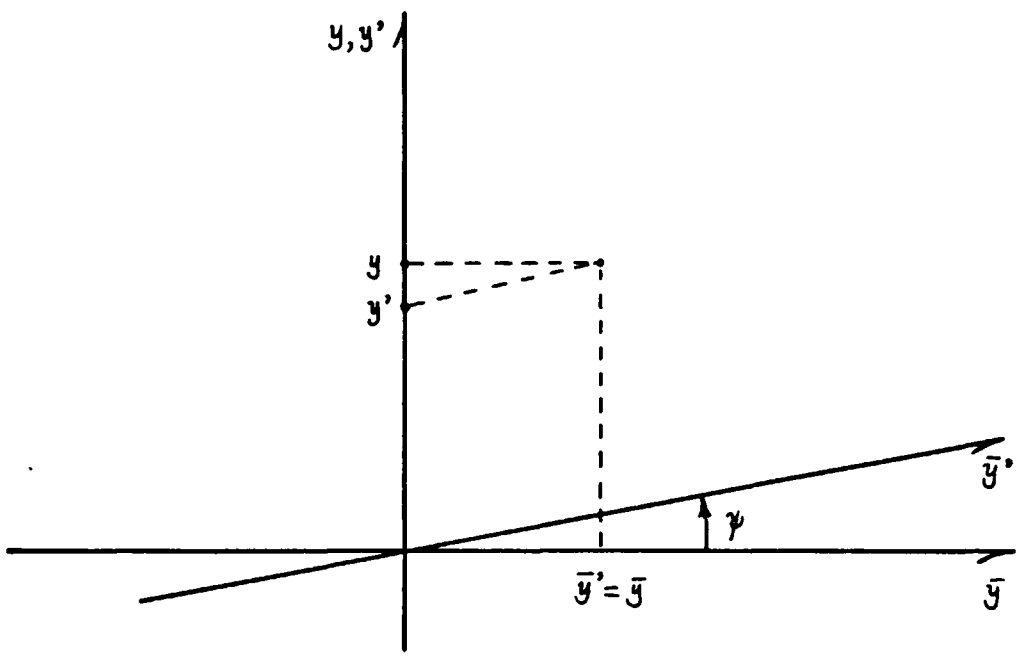

Fig. 26. Conjugate shift

which may be written as

$$\frac{\Delta y}{\bar{y}'} = \frac{\Delta \Omega}{\bar{\Omega}} = const.$$

Again, the value of the constant may be easily determined from Fig. 26,

$$\bar{k}' = \tan \psi = \frac{\Delta y}{\bar{y}},$$

where $\bar{k}'$ stands for the slope of the new $\bar{y}$-axis. This transformation may also be expressed in matrix form,

$$\hat{\bar{z}}' \equiv \begin{pmatrix} \bar{y}' \\ y' \end{pmatrix} = \begin{pmatrix} 1 & 0 \\ -\bar{k}' & 1 \end{pmatrix} \begin{pmatrix} \bar{y} \\ y \end{pmatrix} \equiv \bar{\mathcal{S}}\, \hat{\bar{z}}, \tag{4-39}$$

and

$$\vec{W}' = \bar{\mathcal{S}}\, \vec{W} \; ; \qquad |\bar{\mathcal{S}}| = 1. \tag{4-40}$$

The same remarks expressed about the matrix $\mathcal{S}$ apply to matrix $\bar{\mathcal{S}}$, and the same choices exist for the value of $\bar{k}'$ as was the case for k'. The separations T and the powers $\mathcal{P}$ remain invariant under this transformation also, and the matrix $\bar{\mathcal{S}}$ must be applied to <u>all</u> the $\hat{\bar{z}}$ and $\vec{W}$ vectors of the diagram to effect an object shift.

Regarding the transformation of a line due to an object shift, we note that the change Δy is proportional to the $\bar{y}$-height of the reference point on the line, and therefore, the points along the y-axis ($\bar{y} = 0$) do not change. In this case, the slope of the line after the shift is given by

$$k' = k_w - \bar{k}'$$

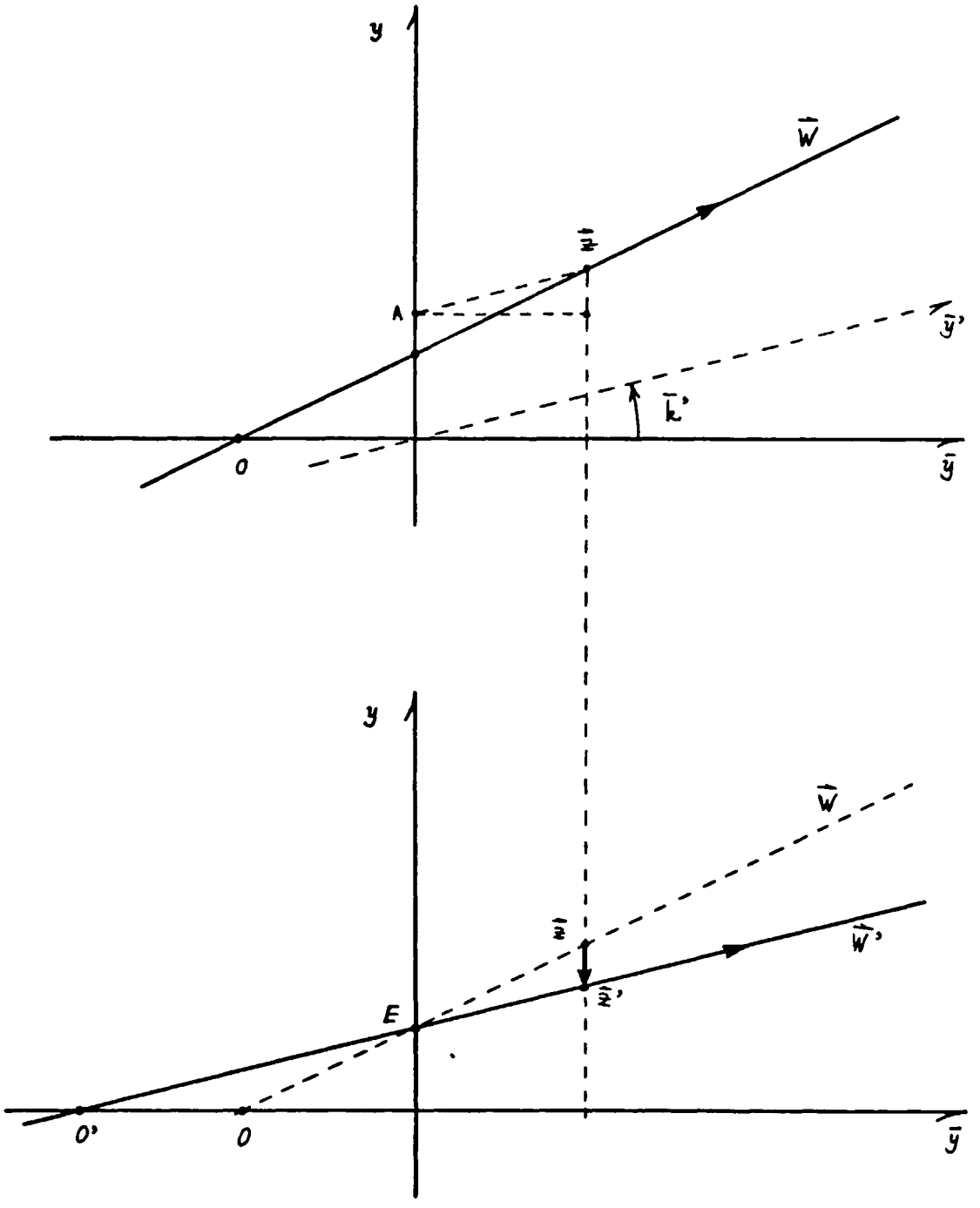

Fig. 27 Effect of a conjugate shift on a single line. (Primes represent values after the shift)

where $\bar{k}'$ is the slope of the new $\bar{y}$-axis. The object shift defines a new value for the object height, in order to preserve the numerical value of the Lagrange invariant, which is given by

$$\bar{y}'_o = (k_w / k'_w)\, \bar{y}_o .$$

We may conclude, as in the case of the stop shift, that the net effect of an object shift on a line after reorthogonalization of the axes is to tilt it using as a pivot its intersection with the y-axis, as illustrated in Fig. 27.

Both figures 25 and 27, suggest a geometrical construction to find the position of the new point $\hat{\bar{z}}'$ after either shift. Taking for example Fig. 25, we draw first the new y'-axis and a parallel to it though the point $\hat{\bar{z}}$; this line crosses the $\bar{y}$-axis at point A, and determines the new value $\bar{y}'$; we now trace a parallel line to the original y-axis through A, and where this line crosses a corresponding parallel line to the fixed $\bar{y}$-axis, through the original point $\hat{\bar{z}}$, defines the new point $\hat{\bar{z}}'$. A similar construction on Fig. 27 yields the new point $\hat{\bar{z}}'$ after an object shift.

We may of course carry out the two shifts at the same time, by application of the two transformations in succession,

$$\hat{\bar{z}}' = \bar{S} S \hat{\bar{z}}$$
$$\hat{\bar{W}}' = \bar{S} S \hat{\bar{W}}$$

but note that the two operations are not commutative, as obviously

$$\bar{S} S \neq S \bar{S} .$$

This is also clear from the fact that once one of the shifts is made, all the points are different (sheared from their original positions) and any conjugate line to be chosen as new axis for the next shift will be determined by these new points rather than by the original ones.

However, it would be interesting to know under what circumstances the product $\bar{S}S$ is indeed commutative. To that effect we may compute the quantity $S\bar{S} - \bar{S}S$, and see under what conditions it vanishes. We get

$$S\bar{S} - \bar{S}S = \begin{pmatrix} \bar{k}'/k' & 0 \\ 0 & -\bar{k}'/k' \end{pmatrix}.$$

We see from this expression that in order for S and $\bar{S}$ to be commutative, we must have $\bar{k}'/k' = 0$. This is fulfilled by three cases: (a) $\bar{k}' = 0$, $k' \neq 0$, i.e., stop shift alone; (b) $\bar{k}'$, arbitrary, $k' = \infty$, i.e., conjugate shift alone; and (c) $\bar{k}' = 0$, $k' = \infty$, i.e., no shifts at all.

In other words, for non-trivial cases, the product of S and $\bar{S}$ is <u>always</u> noncommutative. Therefore, when carrying out two shifts simultaneously, we must be careful of the order followed because, depending on this order, two entirely different systems will be obtained after two two shifts.

<u>Vignetting</u>

As mentioned by Delano in his paper, the $y-\bar{y}$ diagram seems to be ideally suited to portray the effects of constraints

on the system in a very clear manner. The vignetting, or limitation of the bundle of rays going through the system, imposed by any other aperture than the stop is a good example. Vignetting diminishes the amount of energy eventually reaching the image plane, and most of the time is caused by the lenses having a smaller diameter than required to pass all the rays coming from the object and limited in a prescribed manner by the stop of the system.

To avoid vignetting, every surface contained in the system must have a minimum radius given by

$$\rho_j \geq |\bar{y}_j| + |y_j|. \tag{4-41}$$

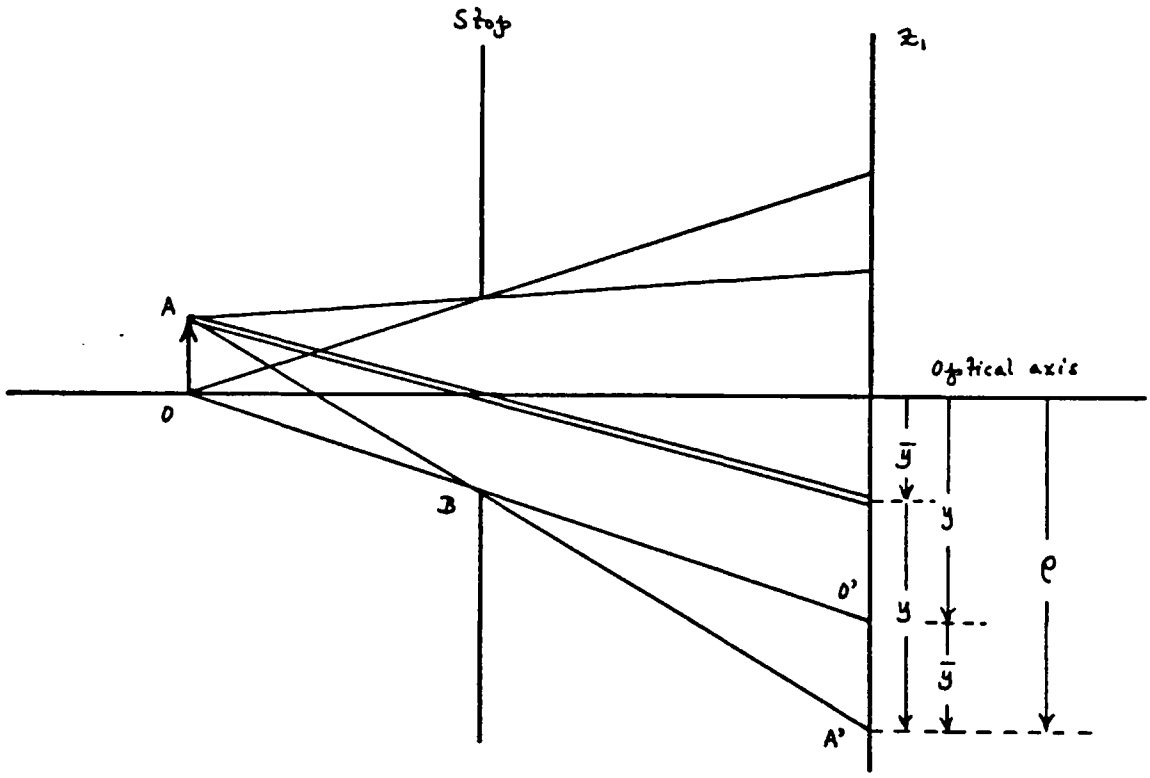

Fig. 28. Derivation of the minimum clear aperture of a surface

This may be seen clearly from Fig. 28, where we have restricted ourselves to the case of the bundle of rays coming from an object O and striking the first surface. Obviously the two triangles $\Delta\, OAB$ and $\Delta\, O'A'B$ are similar and $\overline{O'A'} = \bar{y}$, leading to a minimum value of ρ as the sum of y and $\bar{y}$ at the surface; as this holds true for negative values of $\bar{y}$, y (as in the figure), as well as for positive ones, we must use the absolute values as indicated by Eq. (4-41).

The representation of this equation in the y-$\bar{y}$ diagram, as may be seen in Fig. 29, consists of a 45° straight line in each of the four quadrants; in general, the value of ρ will be different for each quadrant (as shown) and will be given by the particular set of $(\bar{y}, y)$ chosen to define it.

Taking in general the case of the first quadrant, we see that a line passing throught the point $\hat{z}$, and with slope $k_\rho = -1$, represents the minimum radius that the corresponding surface must have in order to avoid vignetting. This, what we may call "construction" radius, determining the clear aperture of the surface, should not be confused with the radius of curvature of the same surface. If a system of several surfaces (or lenses) must be mounted inside a tube of a given diameter $\mathcal{D}$, as is the case of a relay system, then the ρ values in all quadrants must be the same and the graph showing this constraint is a quadrangle as illustrated in Fig. 30. This means that any point (representing a possible surface) located outside the quadrangle will produce vignetting, as its minimum radius ρ

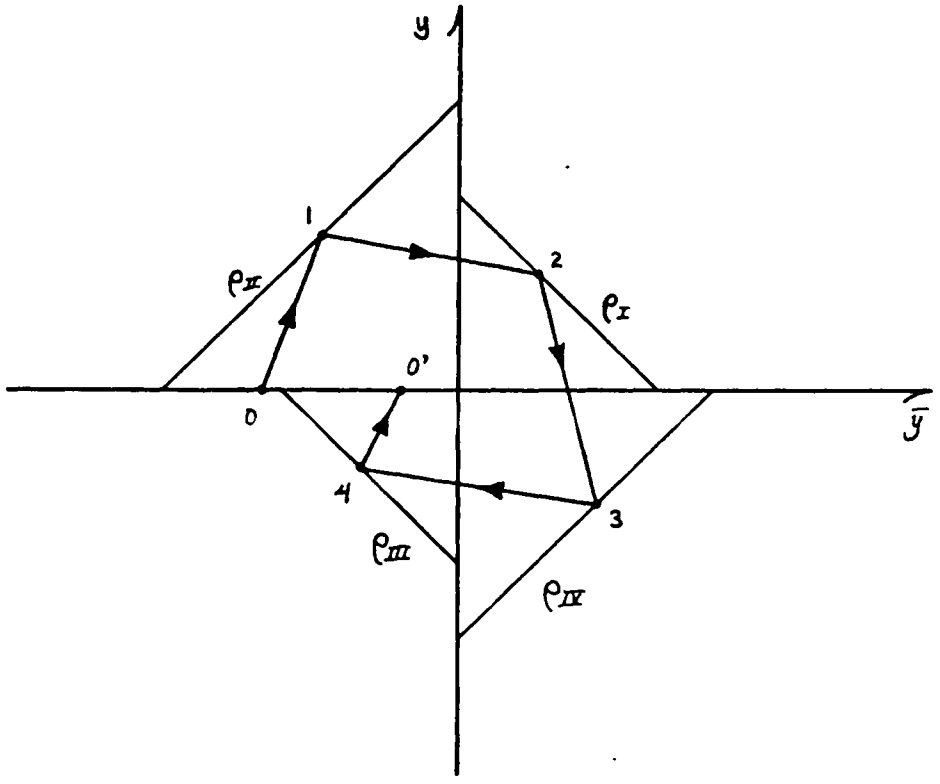

Fig. 29 Geometrical representation of the relation $\rho = |\bar{y}| + |y|$ in each quadrant

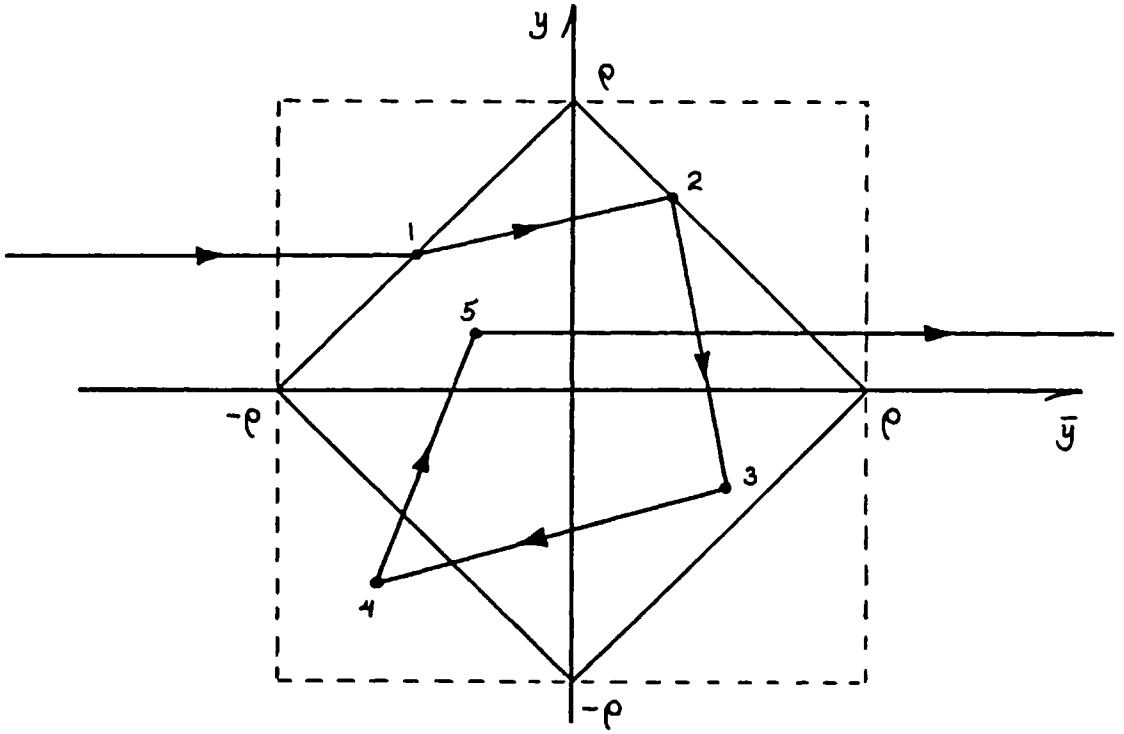

Fig. 30 Example of a relay system enclosed in a tube of diameter $\mathfrak{D} = 2\rho$

for the clear aperture exceeds the value given by the tube. For example in Fig. 30, surface No. 4 will introduce vignetting as $\rho_4 = |\bar{y}_4| + |y_4| > \rho$.

The more relaxed conditions

$$\rho \geqslant |\bar{y}| \geqslant |y|, \qquad \rho \geqslant |y| \geqslant |\bar{y}|, \tag{4-42}$$

which indicate that some vignetting is allowable, to the extent that both marginal and chief rays barely get through, is depicted in Fig. 30 by dotted lines.

The actual vignetting diagram, in other words, the shape of the beam of light that passes through the optical system from an object point off the axis, may be contructed directly with data from the y-$\bar{y}$ diagram. The vignetting diagram is shown on Fig. 32, but to arrive at it geometrically, we draw first an auxiliary diagram shown on Fig. 31. This auxiliary diagram is the actual lay-out of the system in either object or image space; we have chosen object space for Fig. 31. We first continue the object light-segment and locate on the object line the images of all other points in the diagram by appropiate conjugate lines; in Fig. 31 we have located E, the image of the stop and B' the image of point B. Analytically, the coordinates of the image of any point $\vec{z}$ on the line $\vec{W}_i$ (object line) are given by Eq. (4-12) which takes the form

$$\vec{z}' = \frac{\vec{z}}{\hat{k}\cdot(\vec{z}\times\vec{W}_i)} = \frac{\vec{z}}{|\vec{z},\vec{W}_i|}. \tag{4-43}$$

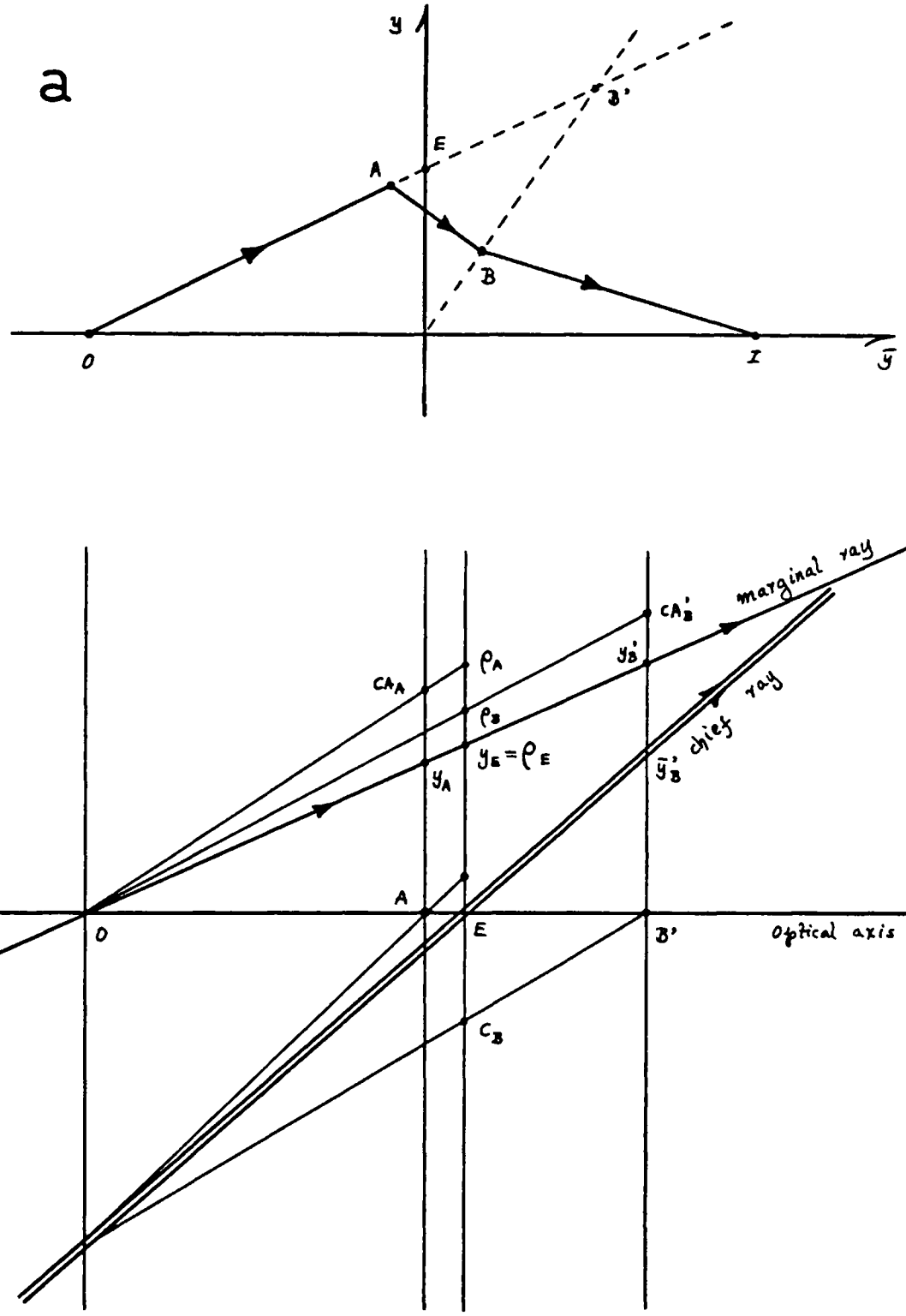

Fig. 31 a) Two-element system. b) Auxiliary diagram for the construction of vignetting diagram

We now begin to trace our auxiliary diagram by noting that the actual separations of the planes along the optical axis, are proportional to the separations of the points along the $\bar{W}_1$ line in the y-$\bar{y}$ diagram; we may actually draw them equal without loss of generality. We now trace in the auxiliary diagram (Fig. 31-b) the marginal and chief rays, in the usual manner. The chief ray crosses the planes A and B' at $\bar{y}_A$, $\bar{y}_{B'}$, respectively; and the marginal ray crosses the same planes at y_A, $y_{B'}$.

We now project the points A and B' into the entrance pupil, using as projection center the point $\bar{y}_0$; this produces the points C_A, C_B which represent the locations of the images of the centers of surfaces A, B in the entrance pupil plane. If we take $C_E = 0$, C_A and C_B are the actual displacements of these centers. We now mark off on the planes A, B' the actual clear apertures of the surfaces A, B', which we shall denote by CA_A, $CA_{B'}$. Note that we must use the size of these apertures in <u>object</u> space, in other words, they will be given, in terms of the physical size by an expression similar to Eq. (4-43); for example:

$$CA'_B = \frac{CA_B}{|\bar{z}_B, \bar{W}_1|} . \qquad (4\text{-}44)$$

We then project the points (CA_A, $CA_{B'}$) onto the entrance pupil plane, using as center of projection the point 0; this produces the points R_A, R_B, which are the actual radii of the surfaces projected on the entrance pupil plane.

We may now draw the vignetting diagram as shown in Fig. 32. We first choose a center C_E and draw a circle with radius

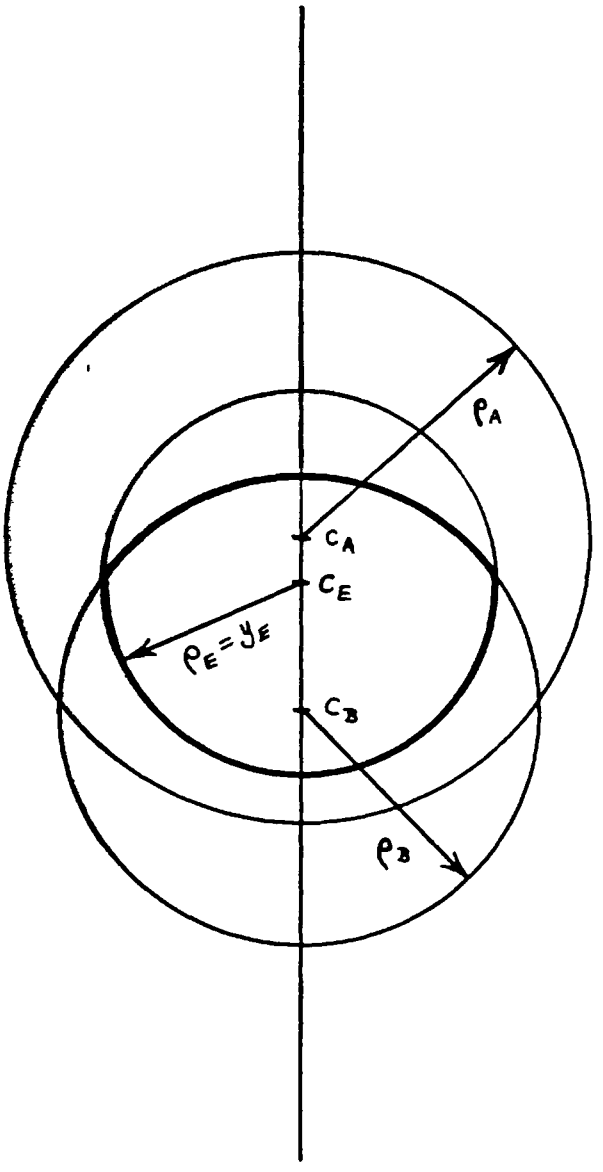

Fig. 32 Vignetting diagram

$R_E = y_E$; we then mark the centers C_A , C_B as obtained on Fig. 31-b and with these centers draw circles of radii R_A , R_B , respectively. The resulting clear part of the original circle of radius R_E is the unobstructed part of the entrance pupil through which light is entering into the system.

From the geometry of Fig. 31-b we may deduce expressions for the location of the center and the radius of the circle of any surface as projected on the entrance pupil plane. Using the point A as an example, and by using the triangles $\Delta(A, E, C_A)$ and $\Delta(0, A, \bar{y}_0)$, we may see that

$$C_A = (-\bar{y}_0 / T_A)\, T_E = -(\bar{y}_A / y_A)\, y_E ,$$

where

$$T_A = |y_0, y_A| = -\bar{y}_0 y_A ,$$

$$T_E = |y_E, y_E| = -\bar{y}_A y_E .$$

By using the triangles $\Delta(0, CA_A, A)$ and $\Delta(0, E, R_A)$, we may see that

$$R_A = \frac{CA_A}{|y_A|} |y_E| .$$

If we have done it with point B' we would have used primed quantities to emphasize that we are dealing with images of the surfaces in object space, but using Eqs. (4-43), (4-44) we see that

$$R_B = \frac{CA_B'}{|y_B'|} |y_E| = \frac{CA_B}{|y_B|} |y_E| ,$$

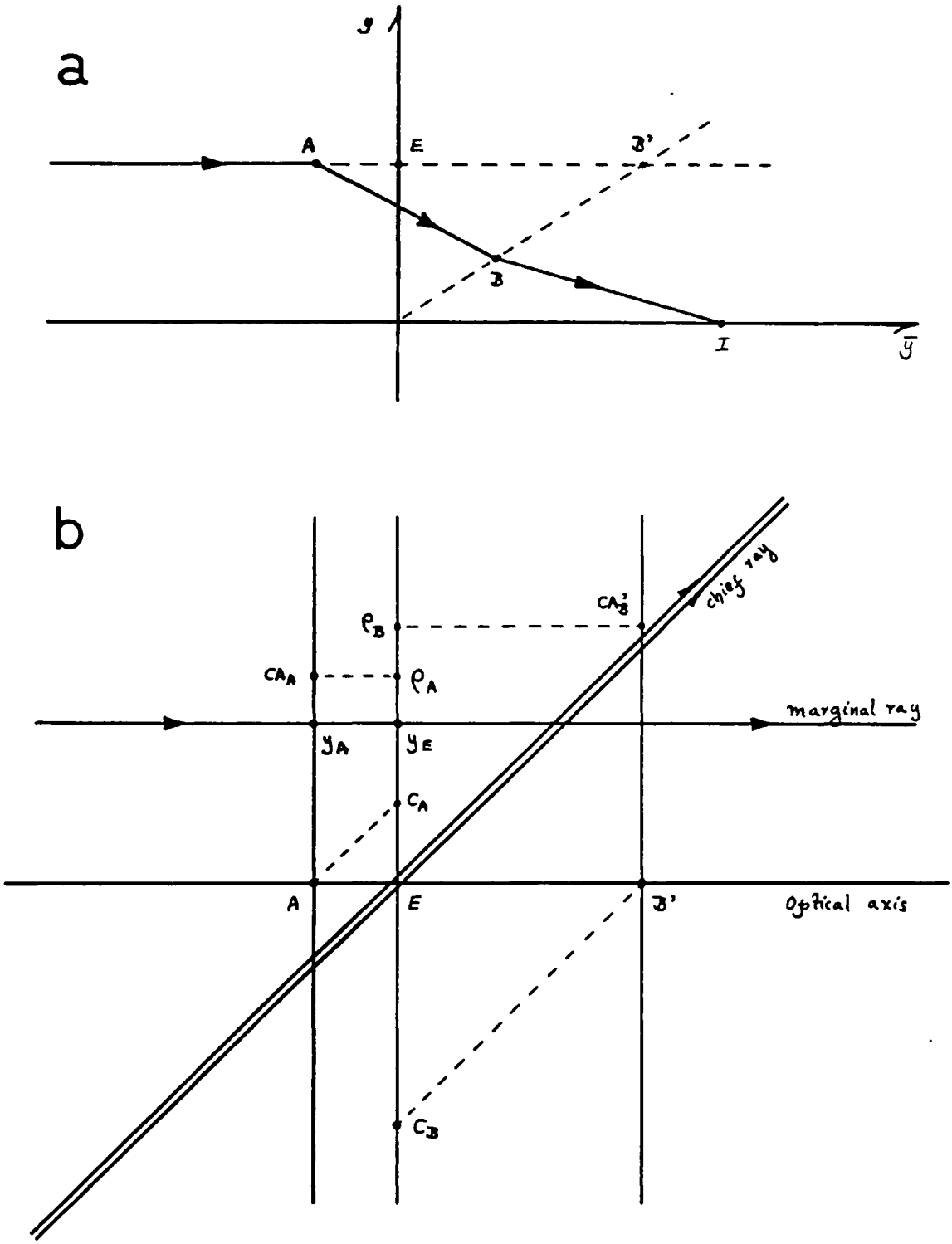

Fig. 33 a) Case of the object at infinity. b) Corresponding auxiliary diagram

because the factor $|\vec{z}_B , \vec{W}_i|$ is common to both. Therefore, we may use the original heights and clear apertures of the system to obtain C_B, $\mathcal{R}_B$ in order to trace the vignetting diagram.

Summarizing, from the y-$\bar{y}$ diagram we derive the radius of the pupil,

$$\mathcal{R}_E = |y_E| = |1/\bar{\Omega}_1| ;$$

and for each surface $\vec{z}_j$, we locate the center above (or below) C_E, by

$$C_j = -(\bar{y}_j/y_j)\, y_E ;$$

and the radius of the circle by

$$\mathcal{R}_j = \left| \frac{CA_j}{y_j}\, y_E \right| ,$$

where CA_j is the actual radius of the surface $\vec{z}_j$.

In the special case of the object located at infinity, the auxiliary diagram is simpler, as shown in Fig. 33.

Conclusion

We conclude this chapter by pointing out that to derive the properties of an optical system represented in the diagram by a set of points, it is convenient to set up the reduction in some tabular form that will facilitate the numerical computations and at the same time will be easy to check. Such a scheme is described by Shack (1972). It replaces the conventional ray-tracing tables described for example by Hopkins and Hanau (1962).

CHAPTER 5

NORMALIZATION OF THE y-$\bar{y}$ DIAGRAM

In many practical applications of this diagram it is convenient to work with normalized quantities of some sort. A normalized diagram permits a separation of specific properties from general ones. It is independent of the entrance pupil and image heights (which might be quite dissimilar, as in Cassegrain systems), producing a diagram that is easier to work with. It also facilitates the analytical treatment of the diagram. The results obtained by using a normalized diagram are applicable to a greater number of optical systems by simply changing the normalization factors. A normalized diagram also allows a fair comparison of several systems of widely different parameters.

This chapter presents a particular normalization that has been found very useful in practice. The normalization factors for separations, powers, and "reduced" angles are derived, and they are expressed in terms of such system parameters as focal length field angle, and f-number. In addition, the effects of refractions and transfers are investigated as well as of conjugate and stop shifts on an already normalized system.

The Normalization Factors

We shall use as normalization quantities the entrance pupil height and the height of the image. See Fig. 34.

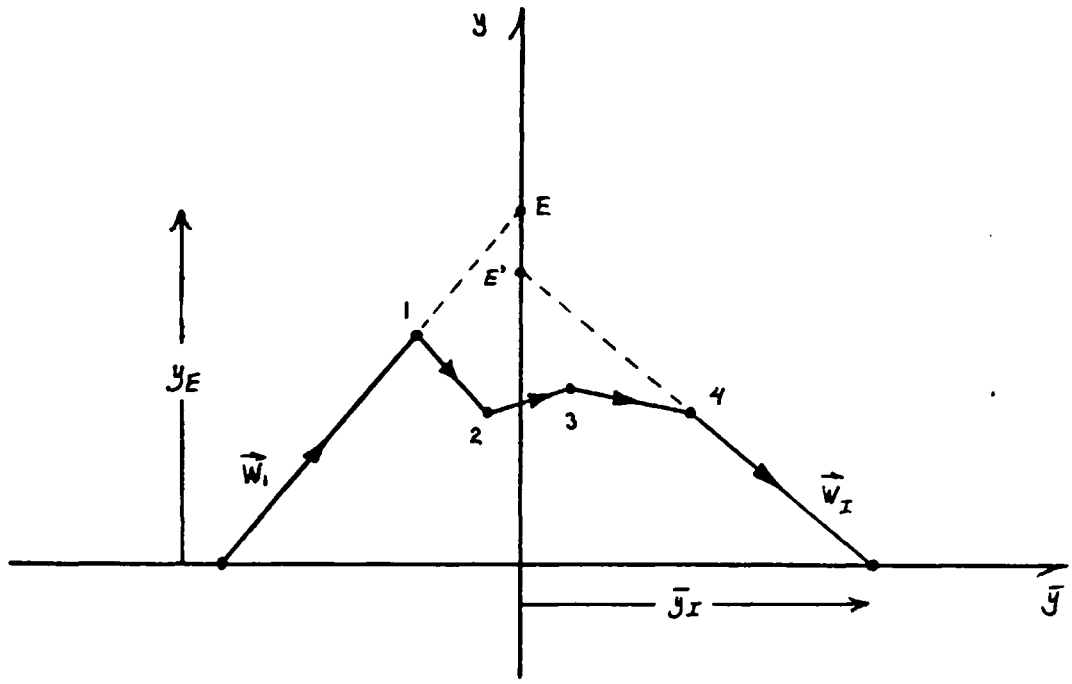

Fig. 34. Definition of normalization variables

Specifically, we divide all marginal ray heights by the entrance pupil height y_E, and divide all the chief ray heights by the image height $\bar{y}_I$.

As a result of this normalization, we shall see that the reduced distances are divided by a quantity proportional to the focal length of the system, the reduced angles for the marginal ray by the numerical aperture, the reduced angle for the chief ray by the field angle, and the powers of the components by the power of the system. In other words, the normalization is complete.

Using a circumflex (^) over a letter to denote its normalized value, we may write:

$$\hat{y} \equiv y/y_E, \qquad \hat{\bar{y}} \equiv \bar{y}/\bar{y}_I, \tag{5-1}$$

and by definition

$$\hat{y}_E = \hat{\bar{y}}_I = 1. \tag{5-2}$$

If we substitute the values (5-1) in the equations for the quantities derivable from the y-$\bar{y}$ diagram, (Appendix A), we get the normalization factors as follows:

For the reduced distances

$$T_i = \hat{T}_i\, y_E\, \bar{y}_I. \tag{5-3}$$

For the reduced angles

$$\Omega_i = \hat{\Omega}_i/\bar{y}_I, \tag{5-4}$$

$$\bar{\Omega}_i = \hat{\bar{\Omega}}_i/y_E. \tag{5-5}$$

And for the powers

$$\Phi_i = \hat{\Phi}_i/(y_E\,\bar{y}_I). \tag{5-6}$$

It may also be noted that the Lagrange invariant relation does not change in form:

$$\hat{y}\,\hat{\bar{\Omega}} - \hat{\bar{y}}\,\hat{\Omega} = 1. \tag{5-7}$$

Although in many instances it is quite possible to specify the values of the normalizing quantities (the entrance pupil height and the height of the image) and the Lagrange

invariant, often it is more convenient to express the normalization factors in terms of certain system parameters commonly used to specify a given optical system. Such parameters are the power (or focal length) of the system, its f-number, and the field angle. We shall use the following nomenclature:

φ = power of the system

f' = n_I / φ , focal length

N = f-number or f-ratio of system

ϑ = $2\bar{u}_1$, field angle

$\hat{\mathcal{F}}$ = correction factor derivable from the normalized diagram

We proceed to establish the values of the normalizing factors in terms of these system parameters.

From the expression of the power at each surface, we may see that the total power of the system is given by

$$\mathcal{F} = \hat{\mathcal{F}} / (y_E \bar{y}_I), \tag{5-8}$$

where

$$\hat{\mathcal{F}} = 1 + \hat{\Omega}_1 \hat{\Omega}_I , \tag{5-9}$$

because $\hat{\Omega}_1 = 1$, $\hat{\Omega}_I = -1$, as may be seen from the value of the Lagrange invariant, Eq. (5-7), at the entrance pupil and at the image, respectively. We see also that this factor, which acts as a correction factor, and whose value may be derived directly from the normalized diagram, will be unity when the object is located at infinity ($\hat{\Omega}_1 = 0$), or when the system is telecentric in image space ($\hat{\Omega}_I = 0$).

Since $\mathfrak{E}$ is given by Eq. (5-8), the normalization factor for powers is

$$1/(y_E \bar{y}_I) = \mathfrak{E}/\hat{\mathfrak{E}}, \tag{5-10}$$

that is, proportional to the power of the system; and the normalization factor for reduced distances is

$$y_E/\bar{y}_I = \hat{\mathfrak{E}}/\mathfrak{E} = \mathcal{H}\hat{\mathfrak{E}} f'/n_I, \tag{5-11}$$

that is, proportional to the focal length of the system.

From the value of the Lagrange invariant at the entrance pupil, we see that

$$1/y_E = \bar{\Omega}_1 = \bar{\omega}_1/\mathcal{H} = n_1 \vartheta/2\mathcal{H}, \tag{5-12}$$

or the normalization factor for the chief ray angles is proportional to the field angle.

Similarly, from the value of the Lagrange invariant at the image, we have

$$1/\bar{y}_I = -\Omega_I = -\omega_I/\mathcal{H}, \tag{5-13}$$

which is the numerical aperture of the system ($\omega_I = n_I u_I$). This last normalization factor for the marginal ray angles may be expressed in terms of the f-number of the system.

Let us define the f-number as

$$N \equiv \frac{f'}{2y_E} = \frac{n_I}{2y_E \varphi} = \frac{n_I}{2y_E \mathcal{H}\mathfrak{E}};$$

or equivalently

$$y_E = \frac{n_I}{2N\mathcal{H}\mathfrak{E}}. \tag{5-14}$$

From Eq. (5-10) we have, by using Eq. (5-14),

$$1/\bar{y}_I = y_E \frac{\bar{\Phi}}{\hat{\Phi}} = \frac{n_I}{2\mathcal{H}\hat{\Phi}N}; \qquad (5\text{-}15)$$

which is another expression for the numerical aperture, valid for finite conjugates. The minus sign in Eq. (5-13) is on account of the sign convention for angles adopted here, which is the same as in analytic geometry.

Besides these normalization factors, the ratio $\bar{y}_I/y_E$ is useful in calculations of clear apertures and obstructions. Its value is easily derived from the above expressions:

$$\bar{y}_I/y_E = (n_1/n_I)\,N\vartheta\hat{\Phi}. \qquad (5\text{-}16)$$

We may also express the Lagrange invariant as a function of the system parameters. By equating the values of from Eqs. (5-14) and (5-12), we obtain

$$\mathcal{H} = n_1\vartheta_f'/4N. \qquad (5\text{-}17)$$

Effects of Shifts on the Normalization

We may see by direct substitution of Eq. (5-1) in the equations of paraxial ray tracing, Eqs. (2-3), (2-4), that these expressions retain their form after the normalization. In other words,

$$\hat{\Omega}_{i+1} = \hat{\Omega}_i - \Phi_i\,\hat{y}_i, \qquad \text{for refraction,}$$

$$\hat{y}_{i+1} = \hat{y}_i + T_{i+1}\,\hat{\Omega}_{i+1}, \qquad \text{for transfer,}$$

and similar expressions for the chief ray. Therefore we conclude that the normalization of the diagram is not affected by any number of transfers and refractions that may occur between object and image points.

However, the normalization will be upset if we make either a stop shift (pupil shift) or a conjugate shift (object or image shift). A stop shift will change the scale of the marginal ray heights, defining a new entrance pupil height, and a conjugate shift will change the scale of the chief ray heights, defining a new image height.

A new normalization must be carried out with the new entrance pupil height or the new image height, according to which shift was made, in order to keep a normalized diagram. The normalizations factors will be changed accordingly.

Let us see first the effect of the stop or pupil shift. We denote with a prime the new values after the stop shift.

The equations for a stop shift are given by

$$\begin{aligned} \hat{\bar{y}}' &= \hat{\bar{y}} - \hat{y}/k', & \hat{\bar{\Omega}}' &= \hat{\bar{\Omega}} - \hat{\Omega}/k', \\ \hat{y}' &= \hat{y}, & \hat{\Omega}' &= \hat{\Omega}, \end{aligned} \tag{5-18}$$

where k' is the slope of the new y'-axis. Accordingly, the new entrance pupil height is given by

$$\hat{y}_E' = \frac{1}{\hat{\bar{\Omega}}_1'} = \frac{k'}{k' - \hat{\Omega}_1}. \tag{5-19}$$

We recognize this equation as the intersection between the new y'-axis and the line $\vec{W}_1$. We see from here that, if

$k' = \infty$, we have the trivial case of no stop shift. But if $\hat{\Omega}_1 = 0$, that is, when the object is at infinity, although there is a shift of all points in the diagram, the line $\vec{W}_1$ does not change, and there is no change in the normalization.

The equations for the conjugate shift are

$$\begin{aligned} \hat{\bar{y}}' &= \hat{\bar{y}}, & \hat{\bar{\Omega}}' &= \hat{\bar{\Omega}}, \\ \hat{y}' &= \hat{y} - \bar{k}'\hat{\bar{y}}', & \hat{\Omega}' &= \hat{\Omega} - \bar{k}'\hat{\bar{\Omega}}, \end{aligned} \tag{5-20}$$

where $\bar{k}'$ is the slope of the new $\bar{y}'$-axis. Then, the new height of the image is

$$\hat{\bar{y}}'_I = \frac{-1}{\hat{\Omega}'_I} = \frac{1}{\bar{k}'\hat{\bar{\Omega}}_I + 1}. \tag{5-21}$$

We recognize this equation as the intersection of the new $\bar{y}'$-axis with the line $\vec{W}_I$. We also see that, if $\bar{k}' = 0$, there will be no conjugate shift; but if $\hat{\bar{\Omega}}_I = 0$, that is, if the system is telecentric in image space, then although there will be a shift given by Eq. (5-10), the value of $\hat{\Omega}_I$ will not change, and therefore the normalization is not affected.

As a result of these operations, either Eq. (5-19) or Eq. (5-21) will be different from unity —or perhaps both will be, if a stop shift and a conjugate shift are performed simultaneously. Therefore, we have to perform a new normalization using as normalizing quantities the values in Eqs. (5-19) and (5-21).

If we carry out this second normalization in the same way as was done before, Eqs. (5-1) through (5-6), we get new

normalization factors that, expressed in terms of the original values, look like the following:

For reduced distances and powers: $(y_E \hat{y}'_E)(\bar{y}_I \hat{\bar{y}}'_I)$

For reduced angles: $1/(\bar{y}_I \hat{\bar{y}}'_I)$

$1/(y_E \hat{y}'_E)$

where y_E, $\bar{y}_I$ are the original normalizing quantities and $\hat{y}'_E$, $\hat{\bar{y}}'_I$ are given by Eqs. (5-19) and (5-21).

We may conclude by induction that, if several stop shifts are performed in succesion, the original entrance pupil has to be multiplied by corresponding factors to mantain a normalized diagram:

$$y_E \longrightarrow y_E \hat{y}'_E \hat{y}''_E \hat{y}'''_E \ldots,$$

and similarly for the conjugate shifts:

$$\bar{y}_I \longrightarrow \bar{y}_I \hat{\bar{y}}'_I \hat{\bar{y}}''_I \hat{\bar{y}}'''_I \ldots,$$

where each of the new factors has an expression equivalent to Eq. (5-19) or (5-21)

Summary

Summarizing, we see that by dividing all marginal ray heights by the entrance pupil height, and all chief ray heights by the image height, the resulting normalization factors for the quantities derivable from the diagram can be expressed in terms of the system parameters (power φ, or focal length f', f-number N, and field angle ϑ); these factors become

For reduced distances,

$$\tau_i / \hat{\tau}_i = y_E \bar{y}_I = \hat{\mathfrak{E}} f' / n_I,$$

which is seen to be proportional to the focal length of the system.

For chief ray reduced angles,

$$\bar{\omega}_i / \hat{\bar{\omega}}_i = 1 / y_E = \bar{\omega}_1 = n_1 \vartheta / 2,$$

which is proportional to the field angle.

For marginal ray reduced angles,

$$\omega_i / \hat{\omega}_i = 1 / \bar{y}_I = -\omega_I = (n_I / \hat{\mathfrak{E}})(1/2N),$$

which is proportional to the numerical aperture of the system.

For the powers,

$$\varphi_i / \hat{\varphi}_i = 1 / (y_E \bar{y}_I) = \varphi / \hat{\mathfrak{E}},$$

which is proportional to the power of the system.

The factor $\hat{\mathfrak{E}} = 1 + \hat{\Omega}_1 \hat{\bar{\Omega}}_I$ is derivable from the normalized diagram and will be equal to unity when the object is at infinity or when the system is telecentric in image space.

These normalization factors are unaffected by any number of refractions and transfers but have to be changed when a stop shift or a conjugate shift is performed in the already normalized diagram. Any shift and subsequent renormalization has the net effect of changing the original entrance pupil height or the height of the image, as the case may be, by

$$y_E \longrightarrow y_E \hat{y}'_E ,$$

$$\bar{y}_I \longrightarrow \bar{y}_I \hat{\bar{y}}'_I ,$$

where the expressions for $\hat{y}'_E$ and $\hat{\bar{y}}'_I$ are given by Eqs. (5-19) and (5-21).

CHAPTER 6

TREATMENT OF A SINGLE LENS ELEMENT IN THE $y-\bar{y}$ DIAGRAM

The simplest single element in the $y-\bar{y}$ diagram is a thin lens, or in a more general sense, a surface; by a thin lens we understand here a lens of strictly zero axial thickness. However, real optical systems do not consist of thin lenses, but of thick ones; or at best of what we shall call here "narrow" lenses, i.e., lenses with a thickness small compared to their focal length. In this context then, the thick lens is the simplest lens element that we have to deal with; there is an exception to this though, as mirrors may be considered as thin lenses.

Therefore, we shall look in this chapter at some of the properties of thick lenses. This approach has the advantage that narrow lenses, thin lenses, single surfaces, and mirrors may be considered as special cases of the thick lens, by the appropiate choice of thickness, shape factor and indices of refraction.

In the $y-\bar{y}$ diagram, a typical thick lens is represented by three lines, representing in turn the three spaces that the two surfaces of the thick lens delimit; or conversely, by two points representing the surfaces, connecting the object and image points. See Fig. 35; the shaded area represents the reduced thickness of the lens.

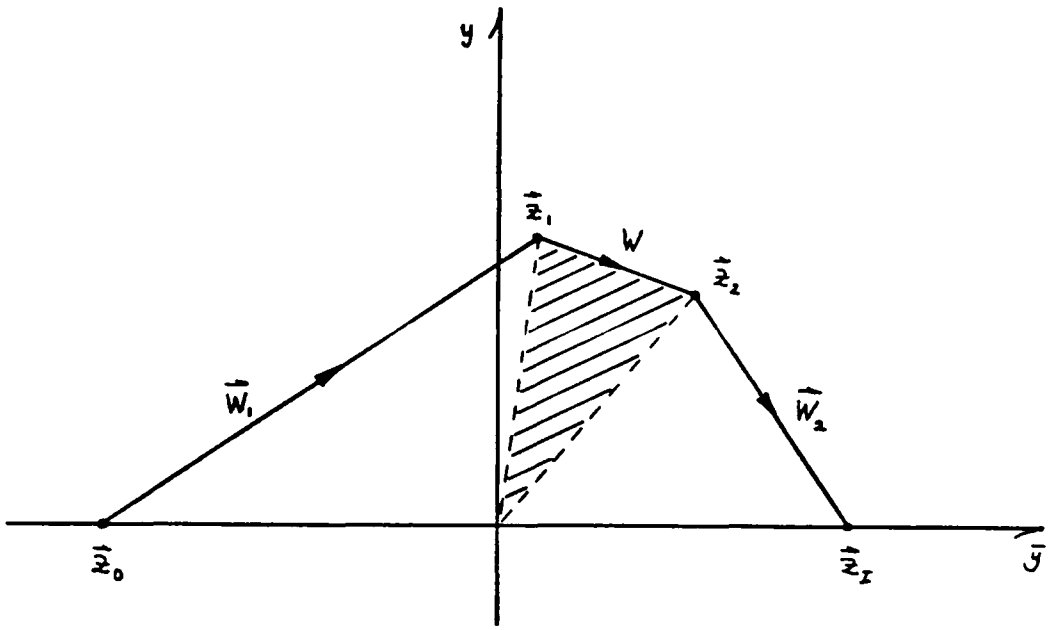

Fig. 35 A thick lens

It is clear that Fig. 35 does not uniquely represent a thick lens, for if we keep the object and image lines fixed we still have the freedom of choosing the position of the intermediate line $\vec{W}$. We shall show that if we move this line parallel to itself we shall have lenses of varying thicknesses but of constant ratio of the curvatures of the surfaces. This is illustrated in the diagrams of the left-hand side of Fig. 36. On the other hand, if we keep the thickness constant and vary the shape of the lens (bending) we get the series of diagrams shown on the right-hand side of Fig. 36. Of course, the most general change will be a combination of these two changes. In all cases illustrated on Fig. 36, although they represent different thick lenses,

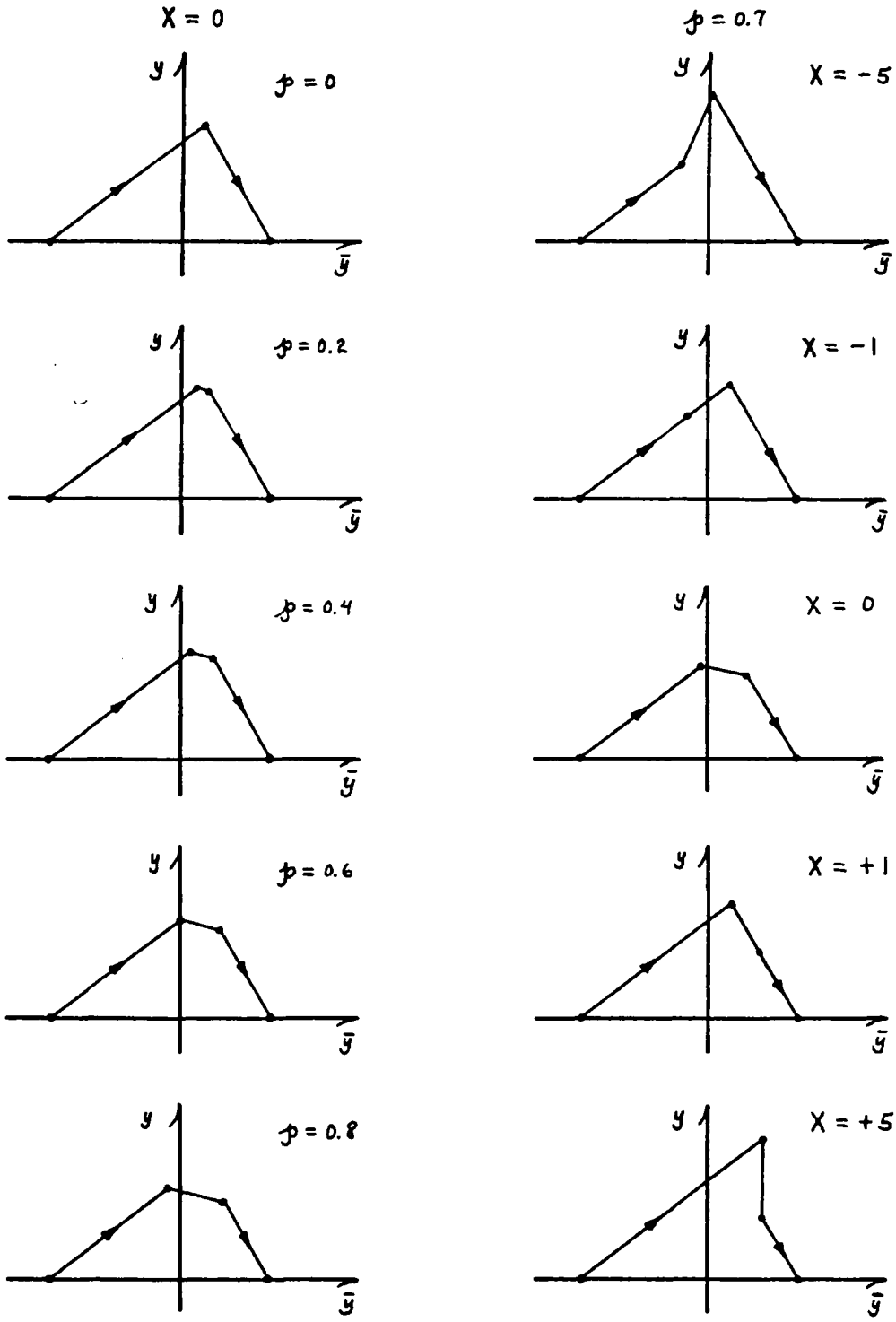

Fig. 36 Different thick lenses. On the left, different thicknesses, same shape factor. On the right, same thickness different shape factors

all of them have the same first-order imaging properties as the lens of Fig. 35; as these properties depend only on the relative positions of the object and image lines, which are the same in all cases.

From these considerations it is clear that it is possible to write down an expression for the vector $\vec{W}$ as a function of the thickness and shape of the lens, and from it and the two other line vectors we may derive the properties of the lens. These expressions also allow the derivation of an algorithm to change at will the thickness or the shape of a given lens; thus, we shall solve the problem of bending a lens and thickening a previously thin lens, for example. Because of its practical importance we shall describe this algorithm in a separate chapter.

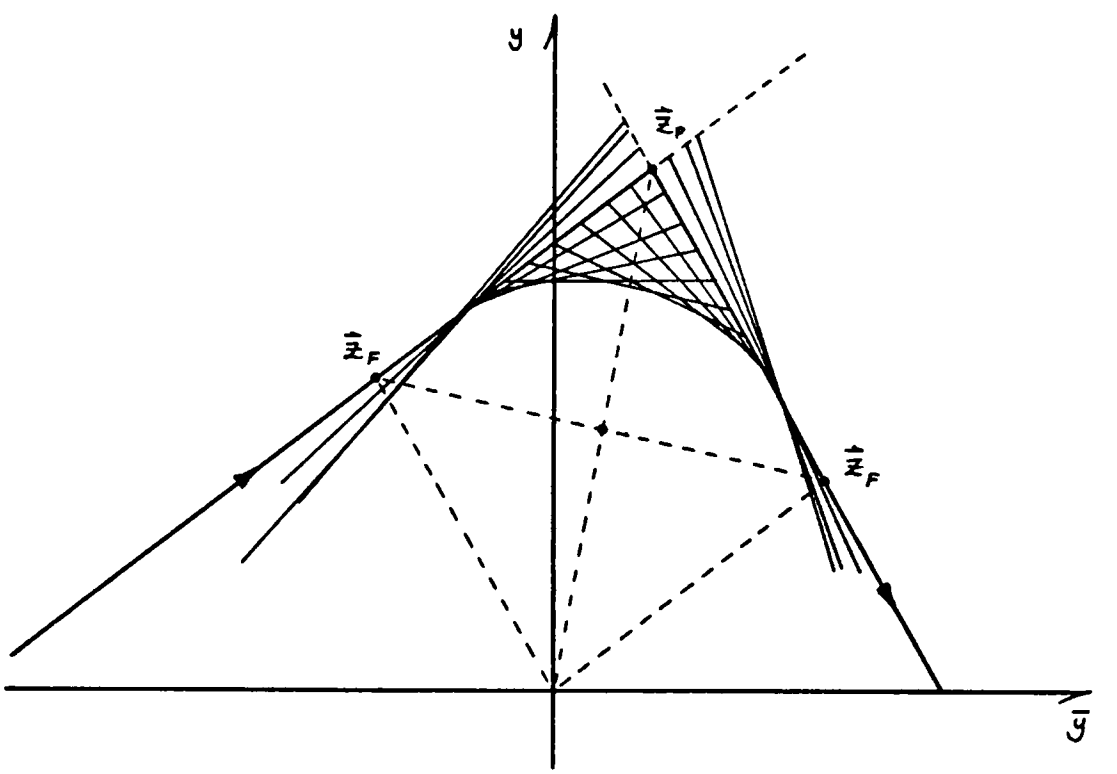

Fig. 37 Variation of the shape factor line for a fixed thickness

A very interesting property of the thick lens arises from this analysis as we shall see shortly: If we draw in the same diagram all the possible positions of the intermediate line for a thick lens of fixed thickness, we get the graph shown in Fig. 37. We may see that all these intermediate lines, each representing one possible space for the interior of the thick lens, envelope a curve; however, it is not immediately obvious what kind of curve this is, and its determination is complicated by the fact that it is defined by lines and not by points. This is a case in which the dual of the y-$\bar{y}$ diagram becomes useful, as in the Ω-$\bar{\Omega}$ diagram each line will be transformed into a point and the set of points will define a curve which is much easier to analyze. When we have completed the analysis in the Ω-$\bar{\Omega}$ diagram, we may return to the y-$\bar{y}$ diagram by computing the tangents of the point-curve in the Ω-$\bar{\Omega}$ diagram. These tangents will become points in the y-$\bar{y}$ diagram defining the desired curve.

It turns out that the curve in the y-$\bar{y}$ diagram is an ellipse. Each point of the ellipse represents a possible bending of the lens, and this ellipse is inscribed in the parallelogram defined by the focal vectors and its center is half way between the origin of coordinates and the vector representing the principal points of the lens as a whole. Another interesting feature is that if we change the thickness of the lens we define a new ellipse, but this new ellipse will also be inscribed in the same parallelogram and will have the same center. All this is true

for a lens with a positive power; if the power is negative, the resulting curve is one branch of a hyperbola, with the same center as before.

In the case of the Ω-$\bar{\Omega}$ diagram, the dual curve of that one in the y-$\bar{y}$ diagram is always a hyperbola.

We shall now proceed to prove these statements analytically.

The Thick Lens Equation

We shall depart slightly from the notation adopted in the previous chapters, for reasons that will become apparent presently. As noted in Fig. 35, the object and image vectors will be denoted by $\vec{W}_1$ and $\vec{W}_2$, respectively, and the object and image planes by $\vec{z}_0$, $\vec{z}_2$, respectively; the intermediate vector $\vec{W}$ will represent the space within the thick lens itself, of index of refraction $\tilde{n}$. The surfaces of the thick lens will be represented by $\vec{z}_1$ and $\vec{z}_2$.

We restrict ourselves in this chapter to the case in which the lines $\vec{W}_1$, $\vec{W}_2$ are constant, and therefore all the cardinal points will be fixed and the first-order properties of the lens as a whole are derived from them. This still leaves plenty of freedom, as the values of the surface vectors $\vec{z}_1$, $\vec{z}_2$ will change when we vary both the thickness of the lens and the curvatures of the surfaces.

One immediate consequence of the constancy of $\vec{W}_1$ and $\vec{W}_2$ is that the power of the thick lens is constant,

$$\Phi = \hat{k}\cdot(\vec{W}_1 \times \vec{W}_2) = |\vec{W}_1, \vec{W}_2|, \tag{6-1}$$

according to Eq. (3-11). We now wish to express this power in terms of the power of each component surface Φ_1, Φ_2, and the reduced thickness of the lens T. Using the definitions given in chapter 3, these quantities are given by

$$\Phi_1 = \hat{k}\cdot(\vec{W}_1 \times \vec{W}) = |\vec{W}_1, \vec{W}|, \tag{6-2}$$

$$\Phi_2 = \hat{k}\cdot(\vec{W} \times \vec{W}_2) = |\vec{W}, \vec{W}_2|, \tag{6-3}$$

$$T = \hat{k}\cdot(\vec{z}_1 \times \vec{z}_2) = |\vec{z}_1, \vec{z}_2|. \tag{6-4}$$

On the other hand, the surface vectors and the intermediate space vector $\vec{W}$ are given by

$$\vec{z}_1 = (\vec{W}_1 - \vec{W})/\Phi_1, \tag{6-5}$$

$$\vec{z}_2 = (\vec{W} - \vec{W}_2)/\Phi_2, \tag{6-6}$$

$$\vec{W} = (\vec{z}_2 - \vec{z}_1)/T. \tag{6-7}$$

Therefore, the set of lines $\vec{W}_1$, $\vec{W}_2$, $\vec{W}$ or the set of points $\vec{z}_0$, $\vec{z}_1$, $\vec{z}_2$, $\vec{z}_r$, uniquely determines the system.

By writing

$$\vec{W}_1 \times \vec{W}_2 = (\vec{W}_1 - \vec{W}) \times \vec{W}_2 + \vec{W} \times \vec{W}_2,$$

and using the above equations we may write Eq. (6-1) as

$$\hat{k}\Phi = \hat{k}\Phi_1 + \hat{k}\Phi_2 - \hat{k}T\Phi_1\Phi_2$$

which is the well known "thick-lens equation." By substituting the values of the powers as given by Eqs. (6-2), (6-3), we may write this equation in vectorial form as

$$\hat{k}\,T\,(\vec{W}_1 \times \vec{W}) \cdot (\vec{W}_2 \times \vec{W}) + \vec{W} \times (\vec{W}_2 - \vec{W}_1) - \hat{k}\,\Phi = 0. \tag{6-9}$$

By using now the cartesian components of the $\vec{W}$ vectors, e.g., $\vec{W} \equiv (\bar{\Omega}, \Omega)$, etc., we may develop the dot product in Eq. (6-9) and obtain the quadratic equation in $(\bar{\Omega}, \Omega)$,

$$A\Omega^2 + B\Omega(-\bar{\Omega}) + C\bar{\Omega}^2 + D\Omega + E(-\Omega) + F = 0, \tag{6-10}$$

where

$$\begin{aligned} A &= T\,\bar{\Omega}_1 \bar{\Omega}_2, \\ B &= T\,(\Omega_1 \bar{\Omega}_2 + \bar{\Omega}_1 \Omega_2), \\ C &= T\,\Omega_1 \Omega_2, \\ D &= \Delta\bar{\Omega} \equiv \bar{\Omega}_2 - \bar{\Omega}_1, \\ E &= \Delta\Omega \equiv \Omega_2 - \Omega_1, \\ F &= -\Phi \end{aligned} \tag{6-11}$$

This obviously represents a conic in the Ω-$\bar{\Omega}$ diagram, the dual of the y-$\bar{y}$ diagram.

We still have the problem of transforming this conic to the y-$\bar{y}$ diagram, but we know from the theory of algebraic curves that it will transform also into a conic, as conics are of both degree 2 and class 2. (The class of a curve being the number of tangents that can be drawn from an external point to the curve). The operation of "correlation" which is the point-line transformation between the y-$\bar{y}$ and Ω-$\bar{\Omega}$ diagrams exchanges the degree

and the class of a curve: For example, a curve of degree 4 and class 3 in one diagram will transform into one of degree 3 and class 4 in the other (see Zwikker, 1950, p. 76). Therefore, a conic, being of degree 2 and class 2, will remain a conic in going from one diagram to the other although the two conics will not necessarily be of the same type. Appendix B, gives the formulae to transform from the conic on one diagram to its dual in the other diagram.

Note that the equation of a line in either of the two diagrams is given by (Appendix B, Eq. B-19)

$$x\xi + y\eta + 1 = 0.$$

By comparing this expression with the Lagrange-Helmholtz invariant

$$\bar{y}\Omega - y\bar{\Omega} + 1 = 0,$$

we see that if we identify $(\bar{y}, y)$ with the point coordinates (x, y), we must choose the line coordinates as $(\xi, \eta) = (\Omega, -\bar{\Omega})$; see Eqs. (2-10), (2-11). This explains the way we wrote the quadratic expression in Eq. (6-10).

Before we investigate the form of the point-conic in the y-$\bar{y}$ diagram, let us describe the properties of the line-conic in the Ω-$\bar{\Omega}$ diagram. We shall use freely the expressions in Appendix B.

Using as coefficients the expressions in Eqs. (6-11), the minors of the determinant Δ of Appendix B, become

$$\Delta_A = -[\Omega_1^2 + \Omega_2^2 + 2\Omega_1\Omega_2(2p-1)]$$

$$\Delta_B = \bar{\Omega}_1\Omega_1 + \bar{\Omega}_2\Omega_2 + (\Omega_1\bar{\Omega}_2 + \bar{\Omega}_1\Omega_2)(2p-1)$$

$$\Delta_C = -[\bar{\Omega}_1^2 + \bar{\Omega}_2^2 + 2\bar{\Omega}_1\bar{\Omega}_2(2p-1)]$$

$$\Delta_D = -p(\Omega_1 + \Omega_2) \qquad (6\text{-}12)$$

$$\Delta_E = +p(\bar{\Omega}_1 + \bar{\Omega}_2)$$

$$\Delta_F = -p^2 < 0$$

where the quantity $p \equiv T\Phi = 2\varphi$, will be called the thickness factor and will prove to be a better parameter to characterize the thickness of the lens than T itself. The determinant is given by

$$\Delta = D\Delta_D + E\Delta_E + 2F\Delta_F = -2pq\Phi, \qquad (6\text{-}13)$$

where for convenience, we have introduced the quantity $q \equiv 1 - p$.

We see immediately that Δ_F is always less than zero. We are then dealing with a hyperbola that degenerates into its asymptotes when $p = 1$. From the invariant of the curve

$$I = A + C = T(\vec{W}_1 \cdot \vec{W}_2), \qquad (6\text{-}14)$$

we see that the hyperbola will be equilateral when $\vec{W}_1 \perp \vec{W}_2$.

The center of the hyperbola is given by the vector

$$\vec{W}_c = (\vec{W}_1 + \vec{W}_2)/p \qquad (6\text{-}15)$$

The equations of the asymptotes may be more easily computed by considering them as the locus of the degenerate hyperbola

when $\Delta = 0$ (i.e., when $\varphi = 1$); but $\varphi = T\mathfrak{F}$ may be expanded by using Eq. (6-8) into

$$T\mathfrak{F} = T\mathfrak{F}_1 + T\mathfrak{F}_2 - (T\mathfrak{F}_1)(T\mathfrak{F}_2) = 1.$$

This equation is fulfilled when $T\mathfrak{F}_1 = T\mathfrak{F}_2 = 1$, which become the equations sought when they are written as

$$\begin{aligned} T\mathfrak{F}_1 &= T|\vec{W}_1, \vec{W}| = T\Omega_1\bar{\Omega} - T\bar{\Omega}_1\Omega = 1, \\ T\mathfrak{F}_2 &= T|\vec{W}, \vec{W}_2| = T\Omega\bar{\Omega}_2 - T\bar{\Omega}\Omega_2 = 1. \end{aligned} \tag{6-16}$$

It may be seen from Eqs. (6-16) that the asymptotes are respectively parallel to the object and image vectors $\vec{W}_1$, $\vec{W}_2$, and therefore, are of fixed inclination. Because the excentricity of the curve depends on the angle between the asymptotes, we deduce that the eccentricity of the hyperbola is a constant independent of the thickness of the lens. In fact, if we denote by ψ the angle between the $\vec{W}_1$ and $\vec{W}_2$ vectors, whose value is given by

$$\cot\psi = (\vec{W}_1 \cdot \vec{W}_2)/\mathfrak{F},$$

the value of the eccentricity is

$$e = \begin{cases} \csc(\psi/2), & \text{if } \varphi < 1, \\ \sec(\psi/2), & \text{if } \varphi > 1. \end{cases} \tag{6-17}$$

Note that the two hyperbolas that have the eccentricities given by Eqs. (6-17) are conjugate to each other, i.e., have a common set of asymptotes.

We could also express the values of the semi-major and semi-minor axes as well as the semi-focal distance in terms of

this angle, which would permit us, with the rest of the parameters already calculated, to trace the curve on the Ω-$\bar{\Omega}$ diagram. However, in our particular context it is preferable to proceed differently.

The Shape Factor

The conic given by Eq. (6-10) defines, for a constant value of T, a point in the diagram for each value of $\bar{W}$, the space inside the thick lens. It proves more convenient to specify the two components of this vector as functions of a single parameter that may vary between the values $-\infty$ and $+\infty$ and that has some physical significance. We choose as such a parameter a "shape" factor that is related to the physical curvatures of the two surfaces composing the thick lens. We adopt the shape factor used by Hopkins (1950), but generalize it to the case in which all the media involved have different indices of refraction; thus we define as the shape factor the quantity

$$X \equiv (\mathcal{F}_1 - \mathcal{F}_2)/(\mathcal{F}_1 + \mathcal{F}_2), \tag{6-18}$$

where the powers of the surfaces $\mathcal{F}_1$, $\mathcal{F}_2$ are given by Eqs. (6-2) and (6-3). It may easily be shown that, when $n_1 = n_2$, this factor reduces to that defined by Hopkins, namely

$$X = \frac{c_1 + c_2}{c_1 - c_2}, \quad \text{for } n_1 = n_2,$$

where c_1, c_2 are the curvatures of the surfaces of the lens.

We now seek the representation of this shape factor in the Ω-$\bar{\Omega}$ diagram. By using Eqs. (6-2) and (6-3), we may expand the determinants to obtain the expression

$$\left| \Omega, \; X \, \Delta\Omega + \Sigma \Omega \right| = 0, \tag{6-19}$$

where we have abbreviated

$$\Delta\Omega = \Omega_2 - \Omega_1, \quad \text{etc.},$$

$$\Sigma\Omega = \Omega_2 + \Omega_1, \quad \text{etc.}$$

This may also be written as

$$(\Sigma\Omega + X\Delta\Omega)\,\bar{\Omega} = (\Sigma\bar{\Omega} + X\,\Delta\bar{\Omega})\,\Omega$$

which is the equation of a line passing through the origin of the Ω-$\bar{\Omega}$ diagram, and with slope

$$k_X = \frac{\Sigma\Omega + X\,\Delta\Omega}{\Sigma\bar{\Omega} + X\,\Delta\bar{\Omega}} =$$

$$= \frac{\Omega_2(X+1) - \Omega_1(X-1)}{\bar{\Omega}_2(X+1) - \bar{\Omega}_1(X-1)}.$$

Parametric Equation of the Conic in the Ω-$\bar{\Omega}$ Diagram

Once the parameter has been selected, the theory of algebraic curves shows that the parametric equation of the hyperbola may be obtained by finding the intersection of the line $\Omega = k_X \bar{\Omega}$ with the hyperbola of Eq. (6-10); with the appropriate substitution, this equation takes the form

$$(A k_x^2 - B k_x + C)\,\bar{\Omega}^2 + (D k_x - E)\,\bar{\Omega} - F = 0,$$

whose solution, after long and tedious but otherwise straightforward algebra, gives

$$\bar{\Omega}_X = \left[\frac{-1 \pm \sqrt{1+F}}{F}\right]\{\Sigma\,\bar{\Omega} + X\,\Delta\bar{\Omega}\},$$

where $F \equiv \varphi(X^2-1)$, and with a similar form for the other component. We may write both solutions as a single vector equation

$$\begin{aligned}\vec{W}_X &= \left[\frac{-1 \pm \sqrt{1+F}}{F}\right]\{\Sigma\,\vec{W} + X\,\Delta\vec{W}\} = \\ &= [\,]\{\vec{W}_2(X+1) - \vec{W}_1(X-1)\}.\end{aligned} \tag{6-20}$$

We shall from now on denote the intermediate space vector $\vec{W}_X$ with a subscript to emphasize the fact that it is a function of the shape factor X.

The Functions [] and F.

We see from Eq. (6-20) that $\vec{W}_X$ is a function of both the shape factor X and the thickness parameter φ; but although the shape factor occurs in both the brackets and the braces, the thickness parameter occurs only in the function within the brackets. In particular we see that in the limiting case of a thin lens or refracting surface, for which $\varphi = 0$, the value of this function may be obtained by applying the L'Hospital rule

$$\lim_{F\to 0}[\,] = \lim_{F\to 0}\frac{1}{2\sqrt{1+F}} = \frac{1}{2}. \tag{6-21}$$

On the other hand, for $\phi \to \infty$, we see that

$$\lim_{\Phi \to \infty} [\,] = \lim_{\Phi \to \infty} \left(\frac{-1}{\Phi} \pm \sqrt{\frac{1}{\Phi} + \frac{1}{\Phi^2}} \right) = 0. \tag{6-22}$$

The function

$$[\,] = \frac{-1 \pm \sqrt{1 + \Phi}}{\Phi}, \tag{6-23}$$

is a cubic whose graph is given in Fig. 38. The solid line represents the points obtained by choosing the positive sign of the radical, and the dotted line represents the points obtained with the negative sign. It is obvious that only the upper positive sign gives the correct limit for a thin lens, and therefore from now on we shall drop the negative sign in front of the radical in Eq. (6-23).

We also note from this equation that we must have $\Phi > -1$ in order to make the radical a real quantity. This leads to certain restrictions on the values of ϕ and X; these are illustrated by plotting Φ as a function of X, which is a parabola, as shown in Fig. 39.

For the case $\Phi > 0$, we see that the condition

$$\Phi \equiv \phi(X^2 - 1) \geq -1$$

leads to

$$\phi \leq \frac{1}{1 - X^2}, \qquad \text{if } |X| < 1,$$

and for the case $\Phi < 0$, the same condition leads to

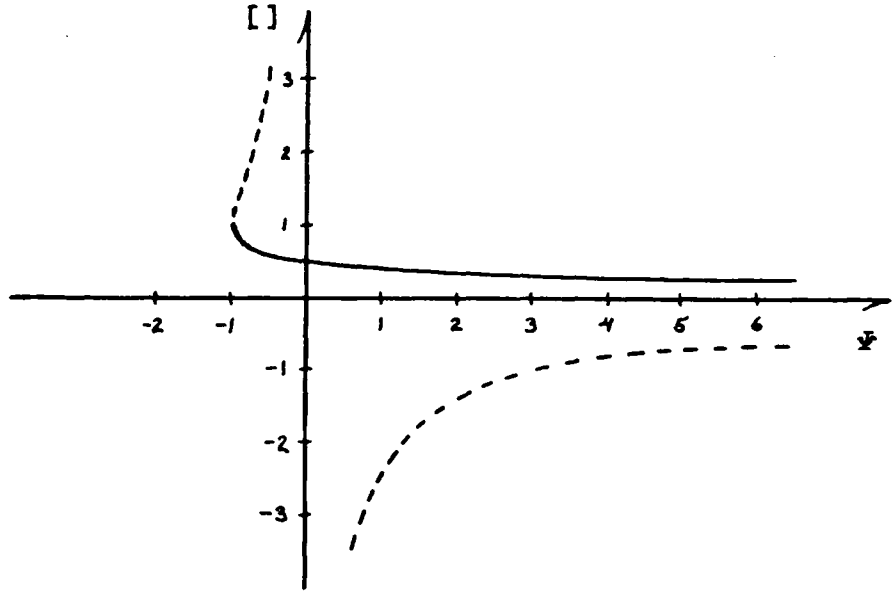

Fig. 38 Graph of the function $[\,] = (-1 \pm \sqrt{1+\Psi})/\Psi$.

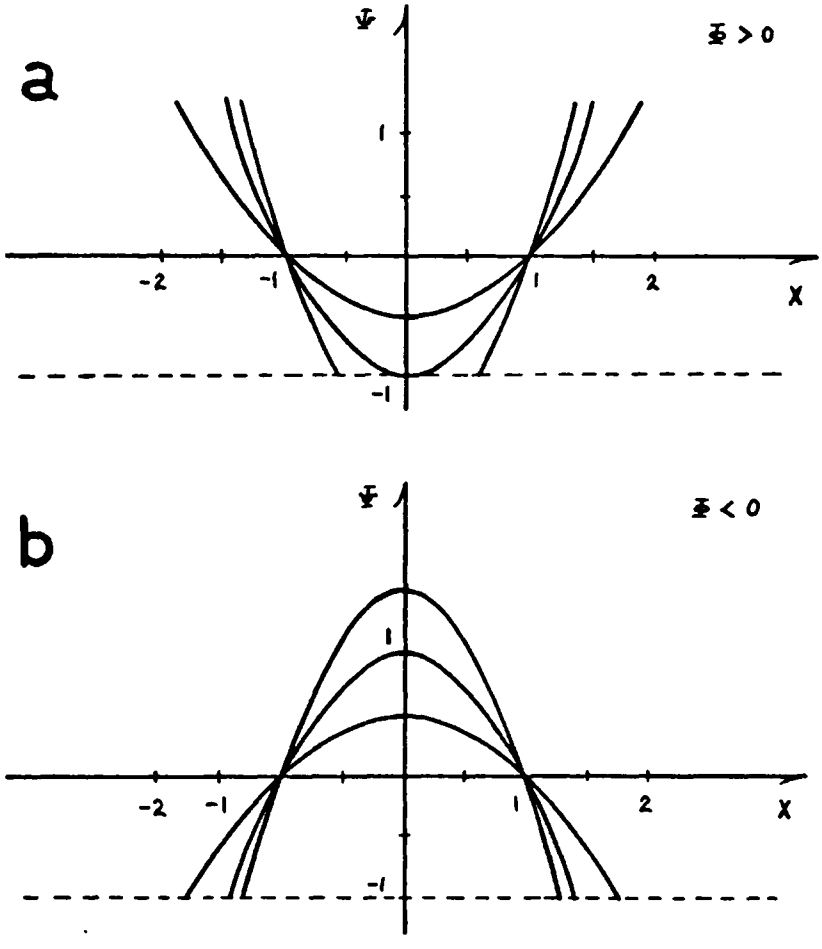

Fig. 39 Ψ as a function of shape factor for different thicknesses. a) For positive power. b) For negative power

$$\varphi \leq \frac{1}{X^2 - 1}, \qquad \text{if} \quad |X| > 1.$$

From Fig. 39 we see what these inequalities mean. Each parabola represents a possible value of φ; $\varphi = 0$ is given by the axis of X, and as the value of φ increases the vertex of the parabola moves along the axis of Ψ, receding from the origin.

For $\Psi > 0$, we see that for a given φ all values of the shape factor are permitted as long as the corresponding parabola does not cross the "forbidden" region below $\Psi = -1$. If we increase the thickness factor φ more and more, the permitted values of X are more and more restricted to the region around $X = +1$ and $X = -1$. This means that really thick lenses, thicker than the focal length of the lens for example, must have one surface of nearly zero curvature, and no biconvex lens of this thickness can exist.

For the case of a lens of negative power, the restriction applies to values of $|X|$ larger than 1, as may be appreciated from Fig. 39b.

Limitations of the Hyperbola in the Ω-$\bar{\Omega}$ Diagram.

Returning to the parametric equation of the hyperbola, Eq. (6-20), we see that

$$\vec{W}_X = \begin{cases} \vec{W}_2, & \text{for} \quad X = +1, \\ \vec{W}_1, & \text{for} \quad X = -1, \end{cases}$$

as in both cases $[\,] = 1/2$, by Eq. (6-21). This is independent of the value of the thickness parameter ϕ. In other words, every hyperbola, each characterized by a value of ϕ, passes through the object and image vectors $\vec{W}_1$, $\vec{W}_2$. In particular, for $\phi = 0$, the hyperbola degenerates into the line $\vec{z}_p$, which passes through these two vectors.

The equations of the chords parallel to this line are important at this time. They may be obtained by considering the general equation of a line in the Ω-$\bar{\Omega}$ diagram, which may be written as

$$\vec{W} \times \Delta\vec{W} = \hat{k}\,\Phi \tag{6-24}$$

by substituting the value of the vector $\vec{z}_p$, given by Eq. (4-17), into the expression for the Lagrange invariant, Eq. (3-7), which represents a straight line in both diagrams.

Then the line parallel to the above and passing through any other given vector $\vec{W}_o$, say, has for equation,

$$|\vec{W}, \Delta\vec{W}| = |\vec{W}_o, \Delta\vec{W}|, \tag{6-25}$$

where we have used the determinant notation.

In the case of the hyperbola, we want the equation of the chord parallel to the line, Eq. (6-24), which represents the thin lens, and passing through the point $\vec{W}_x$; therefore, using Eqs. (6-20) and (6-25), we have

$$|\vec{W}, \Delta\vec{W}| = |\vec{W}_x, \Delta\vec{W}| = 2\,\Phi[\,], \tag{6-26}$$

and we used the fact that $|\Sigma\vec{W}, \Delta\vec{W}| = 2\mathcal{F}$, as may be seen by developing the determinant. Because the right-hand side of Eq. (6-26) is independent of the sign of X, the same chord passes through the point $\vec{W}_{-X}$, whose equation is

$$\vec{W}_{-X} = []\{\Sigma\vec{W} - X\Delta\vec{W}\} = \\ = []\{\vec{W}_1(X+1) - \vec{W}_2(X-1)\}. \tag{6-27}$$

Therefore, the chords parallel to the thin-lens equivalent of the thick lens give the points with symmetric values of X. In particular,

for $X = \pm 1$, $[] = 1/2$, chord passes through $\vec{W}_1, \vec{W}_2$;

for $X = 0$, $[] = (1-\sqrt{q})/p$, chord is tangent to hyperbola;

for $X = \pm\infty$, $[] = 0$, chord passes through origin of coordinates.

So, we see that the hyperbola is limited on the left-hand side by the chord parallel to the thin-lens line and passing through the origin.

On the other hand, when $\mathcal{F} = -1$, $[] = 1$, and this imposes a limitation on the right, defined by the "chord" passing through the point $\Sigma\vec{W} = \vec{W}_1 + \vec{W}_2$. These limitations are illustrated in Fig. 40.

Moreover, the average values of $\vec{W}_X$ and $\vec{W}_{-X}$ define a diameter for these chords

$$\vec{W}_d = 1/2\,(\vec{W}_X + \vec{W}_{-X}) = []\Sigma\vec{W}. \tag{6-28}$$

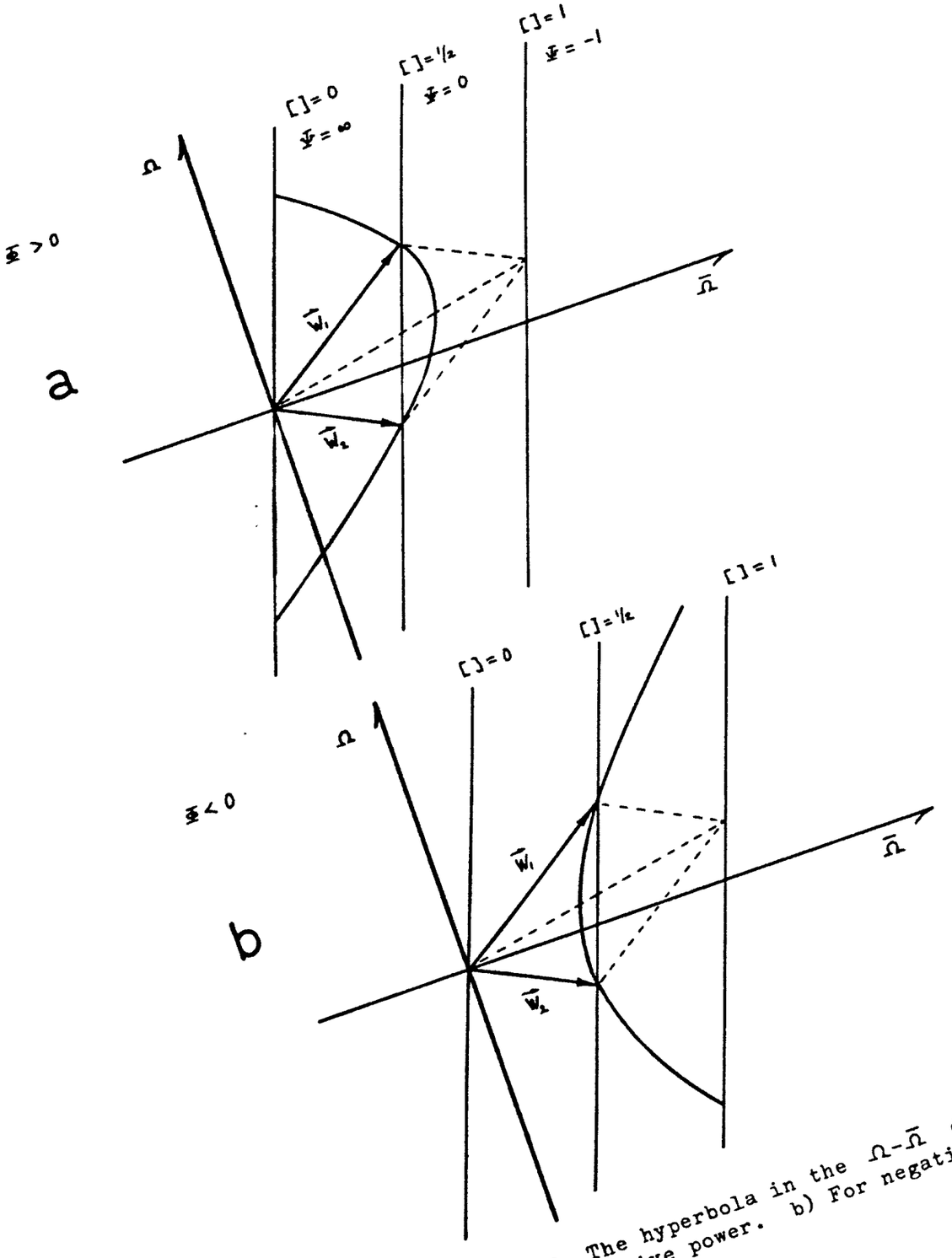

Fig. 40 The hyperbola in the Ω-$\bar{\Omega}$ diagram.
a) For positive power. b) For negative power

Remembering that the shape line (the line representing the shape factor X), Eq. (6-19), reduces to

$$|\vec{W}, \Sigma\vec{W}| = 0, \quad \text{for} \quad X = 0, \tag{6-29}$$

we may substitute the value of $\vec{W}_d$ from Eq. (6-28 into Eq. (6-29) to obtain

$$|\vec{W}_d, \Sigma\vec{W}| = 0.$$

In other words, the points $\vec{W}_d$ satisfy the shape line equation for $X = 0$, and therefore the line given by Eq. (6-29) is a diameter of the conic. Because all hyperbolas pass through $\vec{W}_1$, $\vec{W}_2$, all will have the same chords and therefore this same line is a diameter for all the family; and because all diameters pass through the center of the curve, all the centers of the family lie along this line. Indeed, the coordinates of the center, Eq. (6-15), satisfy the same equation.

It may be easily seen that the vectors $\vec{W}_1, \vec{W}_2$ form a quadrilateral, one of its diagonals being this same diameter (which is the conjugate diameter to the thin-lens line), and the other the thin-lens line. The crossing of these diagonals is the point $\frac{1}{2}(W_1 + W_2)$.

The extreme values of $\vec{W}_X$ when $X = \pm\infty$ may be obtained by rewriting Eq. (6-20) as

$$\vec{W}_X = \left[\frac{-1/X + \sqrt{1/X^2 + p(1 - 1/X^2)}}{p}\right]\left\{\frac{\vec{W}_2}{1 - 1/X} - \frac{\vec{W}_1}{1 + 1/X}\right\},$$

which allows us to take the limit as $X \to \infty$,

$$\vec{W}_{+\infty} = \Delta\vec{W}/\sqrt{p}.$$

To obtain the limit of $\vec{W}_{-\infty}$, we simply exchange $\vec{W}_1$ and $\vec{W}_2$ because of Eq. (6-27),

$$\vec{W}_{-\infty} = -\Delta\vec{W}/\sqrt{p}$$

This means that for $\mathcal{E} < 0$ these points do not exist because in this case the branch of the hyperbola opening to the right is used; the center of the conic then lies to the left. In this case the extreme values of the vector $\vec{W}_X$ will be given by the value of X that will make $\mathcal{F} = -1$ in the bracket function; that is,

$$X_{max} = \pm\sqrt{(1-p)/(-p)}$$

then

$$\vec{W}_{X_{max}} = \{\Sigma\vec{W} + \sqrt{-q/p}\,\Delta\vec{W}\}$$

Because the chords parallel to the thin-lens line $\vec{z}_p$ determine both $\vec{W}_X$ and $\vec{W}_{-X}$, it is obvious that, knowing the position of the chord along the conjugate diameter to $\vec{z}_p$, we should be able to get $\vec{W}_{-X}$ from $\vec{W}_X$ by a simple change of sign. For that purpose we define the vector along the chords as

$$\vec{W}_s = \vec{W}_X - \vec{W}_d = X[\,]\,\Delta\vec{W}\,; \qquad (6\text{-}30)$$

then

$$\begin{aligned} \vec{W}_X &= \vec{W}_d + \vec{W}_s \\ \vec{W}_{-X} &= \vec{W}_d - \vec{W}_s. \end{aligned} \qquad (6\text{-}31)$$

This facilitates the computations, as the factors [] and X[] may be tabulated once and for all for a set of values of φ and X and used for different sets of $\vec{W}_1$, $\vec{W}_2$. Also, the vector lying along the conjugate diameter given by Eq. (6-29) may be used graphically to mark off this diameter with the different values of X; then, chords parallel to the thin lens line through these points will cut the curve at the points $\vec{W}_1$ and $\vec{W}_2$, as shown in Fig. 41.

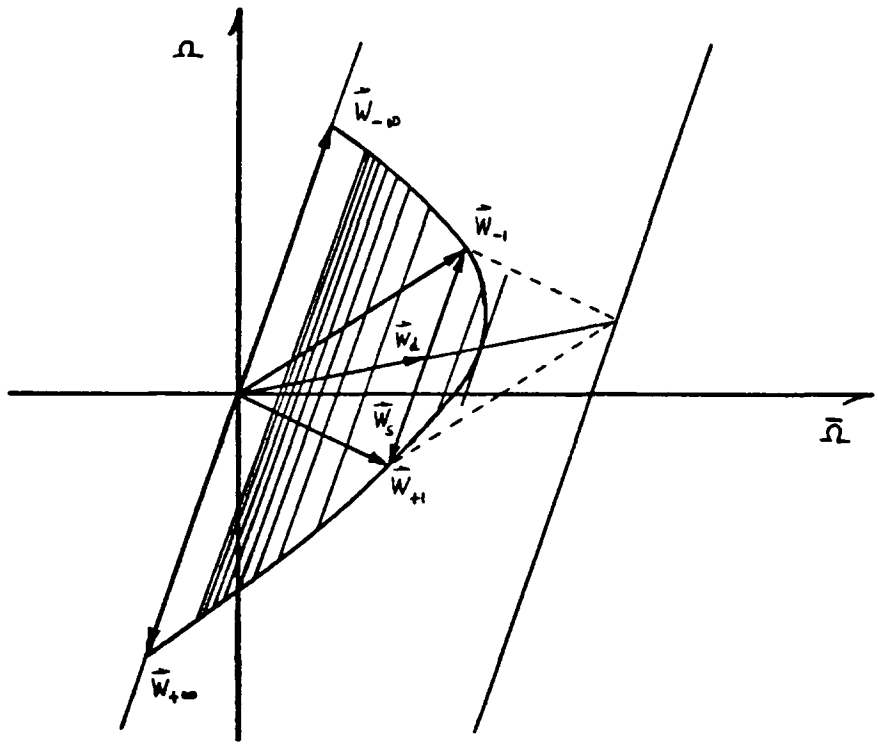

Fig. 41. The chords corresponding to different values of the shape factor

Parametric Equation of the Conic in the y-$\bar{y}$ Diagram

The original line-conic in the Ω-$\bar{\Omega}$ diagram, Eq. (6-10), with coefficients given by Eqs. (6-11), will be transformed into the point-conic whose equation is given by

$$\Delta_A \bar{y}^2 + 2\Delta_B \bar{y} y + \Delta_C \bar{y}^2 + 2\Delta_D \bar{y} + 2\Delta_E y + \Delta_F = 0, \qquad (6\text{-}32)$$

according to Appendix B, and its coefficients are given by Eqs. (6-12).

The invariants of this point-conic are given by

$$\tilde{\Delta} = \Delta^2 = 4\rho^2 q^2 \Phi^2, \qquad (6\text{-}33)$$

$$\tilde{\Delta}_F = 2F\Delta = 4\rho q \Phi^2, \qquad (6\text{-}34)$$

$$\tilde{I} = \Delta_A + \Delta_C = 4q(\bar{W}_1 \cdot \bar{W}_2) - (\Sigma \bar{W})^2. \qquad (6\text{-}35)$$

From Eq. (6-34), we see that the type of the curve will be

for $|\rho| < 1$, ellipse if $\Phi > 0$,
hyperbola if $\Phi < 0$;

for $|\rho| > 1$, hyperbola if $\Phi > 0$,
ellipse if $\Phi < 0$.

We shall restrict ourselves to the case in which $|\rho| < 1$.

Note from Eq. (6-34) that this quantity will be different from zero only for nondegenerate conics, i.e., only central conics transform from one diagram to another without degeneracy.

The center of the conic may be obtained at once, from Eq. (B-5) as

$$(x_c, y_c) = (D/2F, E/2F);$$

in vectorial form, using Eqs. (6-11), and Eq. (4-17), we have

$$\hat{\mathfrak{Z}}_c = -\tfrac{1}{2}\,\Delta\hat{W}/\mathfrak{F} = \tfrac{1}{2}\,\hat{\mathfrak{Z}}_p \qquad (6\text{-}36)$$

which is independent of the thickness or the type of the curve. In other words, all the curves of the family have a common center of symmetry, which is related to the fact that all the original hyperbolas in the Ω-$\bar{\Omega}$ diagram had a common conjugate diameter to the thin-lens line $\hat{\mathfrak{Z}}_p$.

Moreover, as all the line-conics pass through the points $\hat{W}_1$, $\hat{W}_2$ in the Ω-$\bar{\Omega}$ diagram, it follows that all the point-conics will be tangent to the lines $\hat{W}_1$, $\hat{W}_2$ in the y-$\bar{y}$ diagram.

We now proceed to derive the parametric equation of the point-conic. Because of the dual relationship between the two diagrams, the points of one diagram will transform into lines in the other and vice versa. Therefore, given a line conic, we know that tangents to such a curve will transform into the point conic. So, if we start with the line conic, in the Ω-$\bar{\Omega}$ diagram, we may express it in homogeneous coordinates (see Gans, 1969) as

$$(\xi\ \eta\ \zeta)\begin{pmatrix} 2A & B & D \\ B & 2C & E \\ D & E & 2F \end{pmatrix}\begin{pmatrix} \xi \\ \eta \\ \zeta \end{pmatrix} = 0$$

$\backslash D$

The tangent to the curve at the point (ξ_1, η_1, ζ_1) has the equation

$$(\xi\ \eta\ \zeta)\begin{pmatrix} 2A & B & D \\ B & 2C & E \\ D & E & 2F \end{pmatrix}\begin{pmatrix} \xi_1 \\ \eta_1 \\ \zeta_1 \end{pmatrix} = 0,$$

but it also obeys the linear relation

$$(\xi \ \eta \ \zeta)\begin{pmatrix} x' \\ y' \\ z' \end{pmatrix} = 0.$$

In other words, the point coordinates are given by

$$\begin{pmatrix} x' \\ y' \\ z' \end{pmatrix} = \begin{pmatrix} 2A & B & D \\ B & 2C & E \\ D & E & 2F \end{pmatrix}\begin{pmatrix} \xi_1 \\ \eta_1 \\ \zeta_1 \end{pmatrix}. \tag{6-37}$$

In our case,

$$\begin{aligned} \xi_1 &= \Omega_x & x'/z' &= \bar{y} \\ \eta_1 &= -\bar{\Omega}_x & y'/z' &= y \\ \zeta_1 &= 1 \end{aligned} \tag{6-38}$$

Remembering Eq. (6-20), we obtain for the homogeneous coordinates after some algebra

$$\begin{aligned} x' &= -p\,[\,](X\Sigma\bar{\Omega} + \Delta\bar{\Omega}) \\ y' &= -p\,[\,](X\Sigma\Omega + \Delta\Omega) \\ z' &= -2F(1 - [\,]) \end{aligned} \tag{6-39}$$

where $[\,]$ is the same bracket function given by Eq. (6-23).

Taking the ratios indicated in the right-hand set of Eqs. (6-38) and using vectorial notation, we get

$$\vec{z}_x = \frac{p[\,]\{X\Sigma\vec{W} + \Delta\vec{W}\} - \Delta\vec{W}}{2F(1 - [\,])}, \tag{6-40}$$

and for negative X we get the analogous vector

$$\vec{z}_{-x} = \frac{p[\,]\{-X\Sigma\vec{W} + \Delta\vec{W}\} - \Delta\vec{W}}{2F(1 - [\,])}. \tag{6-41}$$

We may then define the vector $\vec{z}_d$ along a diameter as

$$\vec{z}_d \equiv \tfrac{1}{2}(\vec{z}_x + \vec{z}_{-x}) = \left(\frac{1-p[\,]}{1-[\,]}\right)\left(\frac{-\Delta\vec{W}}{2F}\right) \tag{6-42}$$

but

$$\vec{z}_p = -\Delta\vec{W}/F,$$

and putting

$$FZD = \frac{1-p[\,]}{1-[\,]}, \tag{6-43}$$

we obtain

$$\vec{z}_d = \tfrac{1}{2}(FZD)\,\vec{z}_p \tag{6-44}$$

We now define a vector along the chords

$$\vec{z}_s \equiv \vec{z}_x - \vec{z}_d = \left(\frac{p\,X\,[\,]}{1-[\,]}\right)\left(\frac{\Sigma\vec{W}}{2F}\right), \tag{6-45}$$

but by introducing the antiprincipal vector

$$\vec{z}_A = \vec{z}_F - \vec{z}'_F = -\Sigma\vec{W}/F$$

and putting

$$FZS = \frac{p\,X\,[\,]}{1-[\,]} \tag{6-46}$$

we have

$$\vec{z}_s = -\tfrac{1}{2}(FZS)\,\vec{z}_A. \tag{6-47}$$

In analogy to the vector $\vec{W}_x$ we may write

$$\begin{aligned} \vec{z}_x &= \vec{z}_d + \vec{z}_s \\ \vec{z}_{-x} &= \vec{z}_d - \vec{z}_s \end{aligned} \tag{6-48}$$

The Functions FWD, FWS, FZD, FZS

In analogy to Eqs. (6-43) and (6-46), we define

$$FWD \equiv [\,], \tag{6-49}$$

$$FWS \equiv X[\,]. \tag{6-50}$$

The four functions, FWD, FWS, FZD, FZS, are independent of the vectors $\vec{W}_1$, $\vec{W}_2$ and are functions of p and X alone; they can be tabulated once and for all and used for different systems. It is possible to simplify them. By writing

$$Q \equiv 1 + p(X^2 - 1) = q + p X^2 \tag{6-51}$$

where $q \equiv 1 - p$. Then we have

$$\begin{aligned} FWD &= 1/(1 + \sqrt{Q}) \\ FWS &= X/(1 + \sqrt{Q}) \\ FZD &= 1 + q/\sqrt{Q} \\ FZS &= p X \sqrt{Q} \end{aligned} \tag{6-52}$$

Note that FWD and FZD are even functions, whereas FWS and FWD are odd functions of the shape factor X.

It is of interest to tabulate the limiting values of these functions for $p = 0$ and $p = 1$:

$$\text{for } p = 0, \quad \begin{aligned} FWD &= 1/2 \\ FWS &= 1/2\, X \\ FZD &= 2 \\ FZS &= 0 \end{aligned} \tag{6-53}$$

$$\text{for } p = 1, \quad FWD = 1/(1+X), \quad FWS = X/(1+X), \quad F2D = F2S = 1 \tag{6-54}$$

and also to tabulate special values for X:

$$\text{for } X = 0, \quad FWD = 1/(1+\sqrt{q}), \quad FWS = 0, \quad F2D = 1+\sqrt{q}, \quad F2S = 0 \tag{6-55}$$

$$\text{for } X = 1, \quad FWD = FWS = 1/2, \quad F2D = 1+q = 2-p, \quad F2S = p \tag{6-56}$$

$$\text{for } X = \infty, \quad FWD = 0, \quad FWS = 1/\sqrt{p}, \quad F2D = 1, \quad F2S = \sqrt{p} \tag{6-57}$$

Parameters of the Point Conic

Eliminating the parameter X between the two components of the vector $\vec{z}_X$ given by Eq. (6-40), we may obtain the equation of the point conic in the y-$\bar{y}$ diagram, which should reduce to the form given by Eq. (6-32). However, by eliminating the parameter, we obtain expressions for the coefficients that are more convenient than those given by Eqs. (6-12), as will be appreciated presently.

If we use as the center of coordinates the center of the conic $\vec{z}_c$, we may write Eq. (6-40) in the form

$$\vec{z}_x = \frac{-q\,\Delta\vec{W} + p\,\Sigma\vec{W}}{2E\sqrt{Q}} \tag{6-58}$$

or equivalently,

$$\vec{z}_x = \frac{-\sqrt{q}}{2E}\,\Delta\vec{W}\left(\frac{\sqrt{q}}{\sqrt{Q}}\right) + \frac{\sqrt{p}}{2E}\,\Sigma\vec{W}\left(\frac{\sqrt{p}\cdot X}{\sqrt{Q}}\right) \tag{6-59}$$

We see that

$$\left(\frac{\sqrt{q}}{\sqrt{Q}}\right)^2 + \left(\frac{\sqrt{p}\,X}{\sqrt{Q}}\right)^2 = \frac{q + pX^2}{Q} = 1\,;$$

therefore, we may choose some angle such that

$$\sqrt{p}\,X/\sqrt{Q} = \sin\vartheta$$
$$\sqrt{q}/\sqrt{Q} = \cos\vartheta$$

which, substituted into Eq. (6-59), permits us to write

$$\bar{y} = \frac{\sqrt{p}\,\Sigma\bar{\Omega}}{2E}\sin\vartheta - \frac{\sqrt{q}\,\Delta\bar{\Omega}}{2E}\cos\vartheta$$

$$y = \frac{\sqrt{p}\,\Sigma\Omega}{2E}\sin\vartheta + \frac{\sqrt{q}\,\Delta\Omega}{2E}\cos\vartheta$$

Solving for $\sin\vartheta$, $\cos\vartheta$, squaring, and adding them, we may eliminate them, resulting in

$$\frac{|y,\Delta\Omega|^2}{p} + \frac{|y,\Sigma\Omega|^2}{q} = 1$$

which is the equation of the conic with the shape factor eliminated. By expanding the determinants, this may be put into the following form by comparing with Eq. (6-32):

$$-\Delta_A \bar{y}^2 - 2\Delta_B \bar{y} y - \Delta_C y^2 = p q \tag{6-60}$$

where now

$$\begin{aligned} -\Delta_A &= p(\Sigma\Omega)^2 + q(\Delta\Omega)^2, \\ \Delta_B &= p\,\Sigma\bar{\Omega}\cdot\Sigma\Omega + q\,\Delta\bar{\Omega}\cdot\Delta\Omega, \\ -\Delta_C &= p(\Sigma\bar{\Omega})^2 + q(\Delta\bar{\Omega})^2. \end{aligned} \tag{6-61}$$

The invariants of the conic are already given by Eqs. (6-33), (6-34), (6-35), except for the latter which now we write with a change of sign for notational convenience:

$$\tilde{I} = -\Delta_A - \Delta_C = p(\Sigma\vec{W})^2 + q(\Delta\vec{W})^2 \tag{6-62}$$

By defining the quantity

$$\tilde{\mathcal{R}}^2 = \tilde{I}^2 - 4\tilde{\Delta}_F \tag{6-63}$$

we may write the eccentricity, the semimajor and semiminor axes, and the semifocal distance as

$$\begin{aligned} e^2 &= 2\tilde{\mathcal{R}}/(\tilde{I}+\tilde{\mathcal{R}}) \\ a^2 &= (\tilde{I}+\tilde{\mathcal{R}})/8\mathcal{E}^2 \\ b^2 &= (\tilde{I}-\tilde{\mathcal{R}})/8\mathcal{E}^2 \\ c^2 &= \tilde{\mathcal{R}}/4\mathcal{E}^2 \end{aligned} \tag{6-64}$$

This conic is illustrated in Fig. 42 for $\mathcal{E} > 0$, and in Fig. 43 for $\mathcal{E} < 0$. Note that, for positive powers, the ellipse is inscribed in the parallelogram formed by the focal vectors $\vec{z}_F$, $\vec{z}_F'$, and only the part above the line parallel to the antiprincipal vectors $\vec{z}_A$, $\vec{z}_A'$ has physical significance; the lower part corresponds to the values obtained by using the lower sign of the

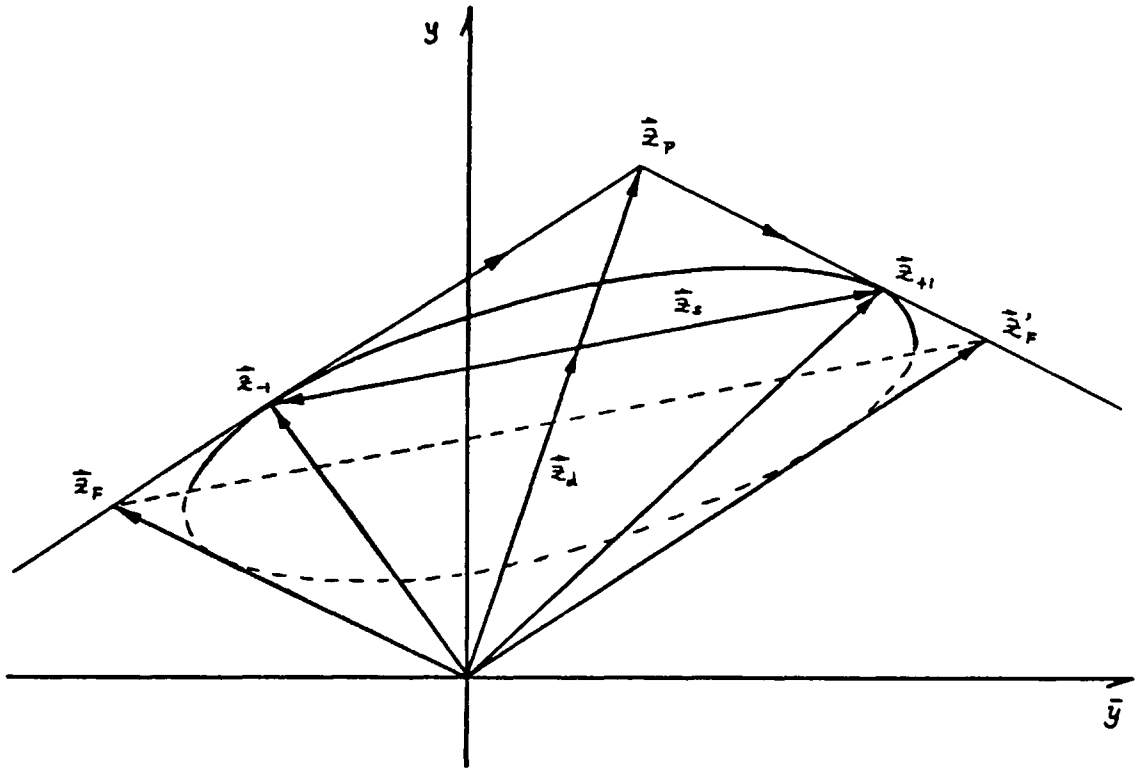

Fig. 42 The ellipse in the $y-\bar{y}$ diagram. (Positive power)

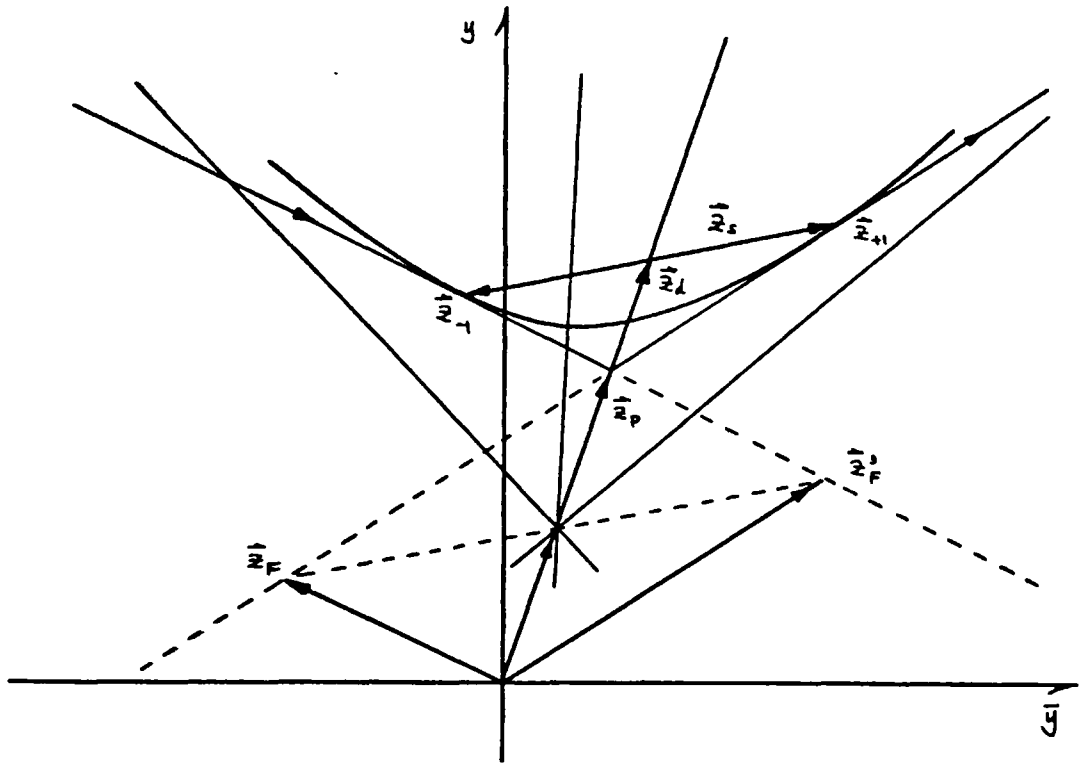

Fig. 43 The hyperbola in the $y-\bar{y}$ diagram. (Negative power)

radical in the bracket function of Eq. (6-23). As the thickness parameter varies, the ellipse changes shape, but it is always confined to the inside of the parallelogram and is tangent to the lines $\vec{W}_1$ and $\vec{W}_2$ precisely for the values of $\vec{z}_X$ for which $X = +1$ and $X = -1$, respectively. When the value of p is close to zero, the ellipse approaches the vector $\vec{z}_P$, and as p approaches unity the ellipse tends to coincide with the vector $\vec{z}_{F'} - \vec{z}_F$. Figure 44 shows the ellipses for several values of p, and Fig. 45 is a plot of the eccentricity of the ellipse as a function of p for the choice of $\vec{W}_1$ and $\vec{W}_2$ vectors of Fig. 42. Figure 42 also illustrates the use of the vectors $\vec{z}_d$ and $\vec{z}_s$ given by Eqs. (6-44) and (6-47) to locate a point on the curve associated with the shape factor X; the tangent to the curve at this point represents the intermediate space within the lens given by the vector $\vec{W}_X$, Eq. (6-20).

Similar comments apply to the curve in Fig. 43 for which $\frac{1}{F} < 0$, except that now the values of the shape factor that are allowed are limited to a maximum, set by the asymptotes to the hyperbola.

Powers and Surfaces of the Thick Lens

We can now compute the powers of, and the vectors representing, the two surfaces of the thick lens as a function of the shape factor X and the thickness parameter p. Remembering that the equation of the intermediate space vector is Eq. (6-20)

$$\vec{W}_X = [\,]\left\{\vec{W}_2(X+1) - \vec{W}_1(X-1)\right\},$$

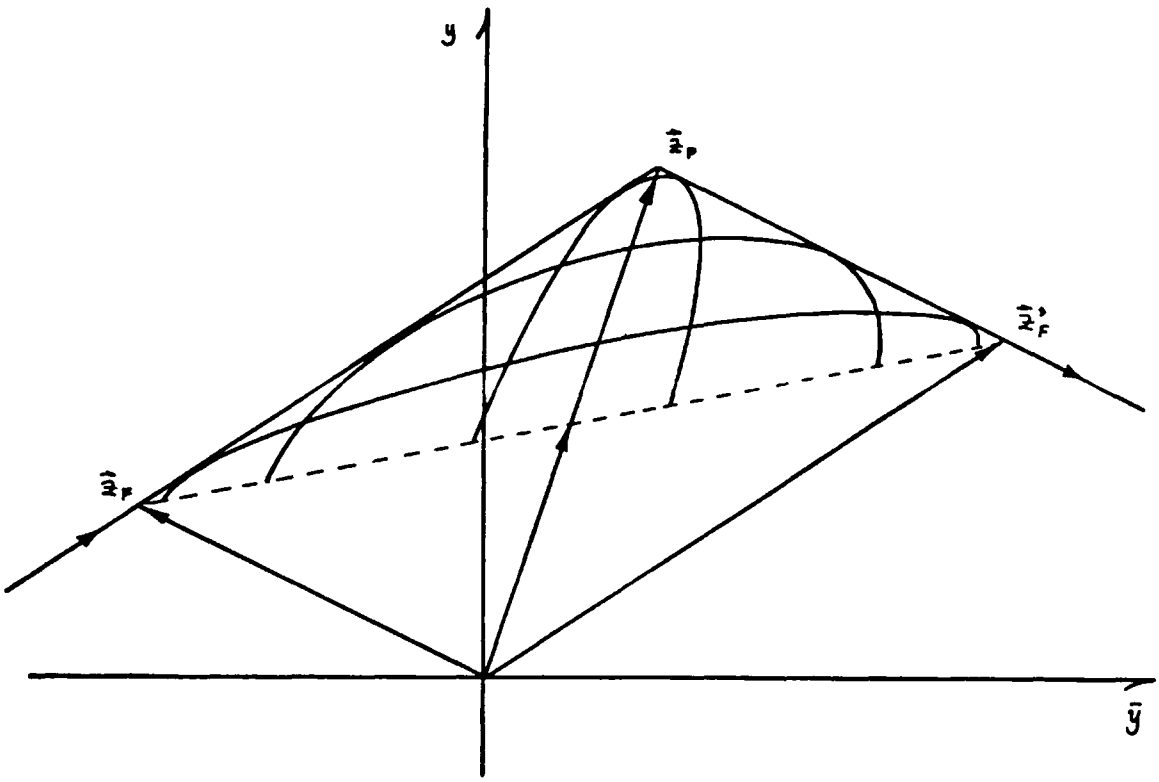

Fig. 44 Different ellipses for different thicknesses

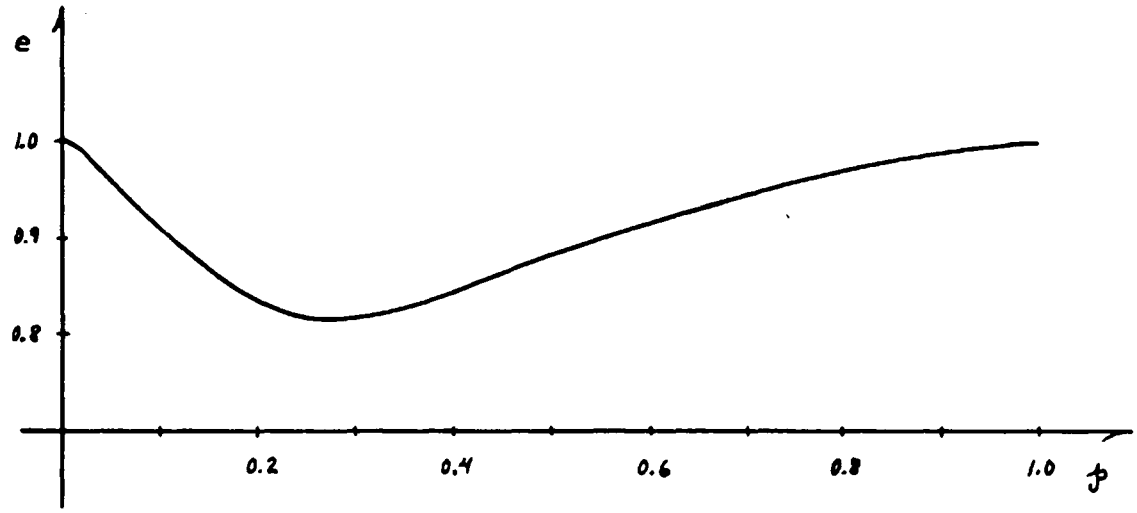

Fig. 45 Excentricity of the ellipse as a function of thickness

the powers at each surface are given by

$$\mathfrak{D}_1 = |\vec{W}_1, \vec{W}_X| = [](X+1)\mathfrak{D} \equiv FW_1\,\mathfrak{D}\,, \tag{6-65}$$

$$\mathfrak{D}_2 = |\vec{W}_X, \vec{W}_2| = -[](X-1)\mathfrak{D} \equiv FW_2\,\mathfrak{D}, \tag{6-66}$$

where we have defined the functions FW_1 and FW_2. Note that

$$FW_1 = FWD + FWS = [](X+1) \tag{6-67}$$

$$FW_2 = FWD - FWS = -[](X-1) \tag{6-68}$$

These may be tabulated once and for all for selected values of and φ and X.

The points representing the surfaces are given by (see Eq. 3-15)

$$\vec{z}_1 = \frac{\vec{W}_X - \vec{W}_1}{-\mathfrak{D}_1} = \\ = \vec{z}_F + \left\{\frac{[](X-1)+1}{[](X+1)}\right\}\vec{z}'_F \equiv \vec{z}_F + (Fz_1)\,\vec{z}'_F \tag{6-69}$$

$$\vec{z}_2 = \frac{\vec{W}_2 - \vec{W}_X}{-\mathfrak{D}_2} = \\ = \left\{\frac{[](X+1)-1}{[](X-1)}\right\}\vec{z}_F + \vec{z}'_F \equiv (Fz_2)\,\vec{z}_F + \vec{z}'_F \tag{6-70}$$

where we have defined the functions Fz_1, Fz_2. These may be simplified to read

$$Fz_1 = (X + \sqrt{Q})/(X+1) \tag{6-71}$$

$$Fz_2 = (X - \sqrt{Q})/(X-1). \tag{6-72}$$

Note that

$$FW_1(-X) = FW_2(+X)$$
$$FW_2(-X) = FW_1(+X)$$
$$F2_1(-X) = F2_2(+X)$$
$$F2_2(-X) = F2_1(+X)$$

and therefore we need to calculate them only for positive values of X.

Stavroudis (1971) has shown that these functions, which are of the general form

$$f_1(x) = f_2(-x)$$

have the general property that f_1 is a sum of an even and an odd function, and f_2 is the difference of the same even and odd functions. This is clear for FW_1, FW_2, but it is not immediately obvious for the others.

It is of interest to tabulate the limiting values of these functions for $p = 0$ and $p = 1$, as well as for some special values of X:

for $p = 0$,
$$FW_1 = \tfrac{1}{2}(X+1)$$
$$FW_2 = -\tfrac{1}{2}(X+1) \qquad (6\text{-}73)$$
$$F2_1 = F2_2 = 1$$

for $p = 1$,
$$FW_1 = 2$$
$$FW_2 = (1-X)/(1+X) \qquad (6\text{-}74)$$
$$F2_1 = 2X/(X+1)$$
$$F2_2 = 0$$

for $X = 0$,

$$FW_1 = FW_2 = 1/(1+\sqrt{q})$$
$$Fz_1 = Fz_2 = \sqrt{q} \qquad (6\text{-}75)$$

for $X = 1$,

$$FW_1 = 1$$
$$FW_2 = 0$$
$$Fz_1 = 1 \qquad (6\text{-}76)$$
$$Fz_2 = q$$

for $X = \infty$,

$$FW_1 = 1/\sqrt{p}$$
$$FW_2 = -1/\sqrt{p} \qquad (6\text{-}77)$$
$$Fz_1 = 1+\sqrt{p}$$
$$Fz_2 = 1-\sqrt{p}$$

Cardinal Points of the Thick Lens

Any two conjugate points with an associated magnification m_T are separated from the surfaces $\hat{z}_1$, $\hat{z}_2$ by

$$|\hat{z}_1, \hat{z}| = |\hat{z}_1, \hat{z}_F| + (1/m_T)|\hat{z}_1, \hat{z}'_F| = \\ = (1/m_T - Fz_1)/\mathfrak{D} \qquad (6\text{-}78)$$

in object space, and by

$$|\hat{z}_2, \hat{z}'| = m_T|\hat{z}_2, \hat{z}_F| + |\hat{z}_2, \hat{z}'_F| = \\ = (Fz_2 - m_T)/\mathfrak{D} \qquad (6\text{-}79)$$

in image space. With these expressions we may calculate the positions of the cardinal points with respect to the surfaces of the lens.

The front focal point has associated with it a magnification $m_T = \infty$; therefore, the front focal distance is given by

$$FFD = (Fz_1)f$$

The rear focal point has an associated magnification $m_T = 0$; therefore, the back focal distance is given by

$$BFD = (Fz_2)f'$$

The principal points are given by setting $m_T = 1$ into Eqs. (6-78) and (6-79)

$$|\tilde{z}_1, \tilde{z}_P| = (1 - Fz_1)/\Phi$$
$$|\tilde{z}_2, \tilde{z}_P| = (Fz_2 - 1)/\Phi$$

But these expressions may be simplified to read as follows

$$(1 - Fz_1)/\Phi = -[](X-1)f_P/\Phi = (FW_2)T$$
$$(Fz_2 - 1)/\Phi = -[](X+1)f_P/\Phi = -(FW_1)T$$

Therefore, the actual distances become

$$\ell_P/n_1 = (FW_2)\tilde{\tau}$$
$$\ell'_P/n_2 = -(FW_1)\tilde{\tau} \qquad (6\text{-}80)$$

where $\tilde{\tau} \equiv \tilde{t}/\tilde{n}$ is the reduced thickness of the thick lens.

The more conventional formulas for these distances (see Born and Wolf, 1970) may be obtained by using Eqs. (6-2) and (6-3) instead of Eqs. (6-78) and (6-79), to yield

$$|\tilde{z}_1, \tilde{z}_P| = T\Phi_2/\Phi$$
$$|\tilde{z}_2, \tilde{z}_P| = -T\Phi_1/\Phi \qquad (6\text{-}81)$$

which in turn may be reduced to Eqs. (6-80) by using the expressions for the powers given by Eqs. (6-65) and (6-66). The

advantage of using Eqs. (6-80) is that the functions FW_1, FW_2 contain explicitly the dependence on φ and X.

Also of interest at this stage is the expression for the separation of the principal points, which is not given directly by the diagram because both principal points, in object and in image space, are represented by the same vector $\bar{\bar{z}}_P$. However, by using the distances given by Eqs. (6-80) we see that

$$\overline{PP'} = \tilde{t} - \ell_P + \ell_P'$$

and by reducing this distance by $\tilde{n}$, the index of refraction in the interior of the lens, and multiplying by the Lagrange invariant, we may write

$$T_{PP} \equiv \mathcal{H}\,\overline{PP'}/\tilde{n} = T\left[1 - \frac{n_1 \Sigma_1 + n_2 \Sigma_1}{\tilde{n}\,\Sigma}\right], \tag{6-82}$$

where we have used the expressions in Eqs. (6-81). By using the expressions for the powers, Eqs. (6-65), (6-66) and the functions FWD and FWS given by Eqs. (6-49), (6-50), we may finally write

$$\overline{PP'} = \tilde{\tau}\left[\tilde{n} - FWD\,(n_1 + n_2) + FWS\,(n_1 - n_2)\right] \tag{6-83}$$

If we restrict ourselves for a moment to the case for which $n_1 = n_2$ (the thick lens in air), we see that

$$\overline{PP'} = \tilde{\tau}\,(\tilde{n} - 2[\,]) \tag{6-84}$$

This equation tells us that the separation between the principal planes will vanish not only for a thin lens ($\tilde{\tau} = 0$) but also for a thickness such that $[\,] = \tilde{n}/2$. It is possible to show that this is the case of a concentric thick lens.

The separations of the nodal points may also be obtained from Eqs. (6-78) and (6-79) by substituting the value $m_T = n_1/n_2$.

Optical Center of the Thick Lens

The optical center of the lens is defined as the point within the thick lens that is conjugate to the nodal points. See Fig. 46. Therefore its location will be given by Eq. (4-24) with $m_T = \mathcal{R} \equiv n_1/n_2$.

$$\vec{z}_{oc} = \frac{\vec{W}_1 - \mathcal{R}\vec{W}_2}{\mathcal{F}_1 + \mathcal{R}\mathcal{F}_2} = \frac{\vec{z}'_N}{[\,]\{(1+\mathcal{R}) + (1-\mathcal{R})X\}} \qquad (6\text{-}85)$$

If $\mathcal{R} = 1$, i.e. $n_1 = n_2$, $\vec{z}'_N = \vec{z}_p$ and Eq. (6-85) reduces to

$$\vec{z}_{oc} = \vec{z}_p/[\,] = (1 + \sqrt{Q})\,\vec{z}_p$$

The distances of the optical center from the surfaces are given by

$$|\vec{z}_1, \vec{z}_{oc}| = \frac{1-\mathcal{R}}{\mathcal{F}[\,]\{\ \}} - \frac{(X-1)\mathcal{R}T}{\{\ \}},$$

$$|\vec{z}_2, \vec{z}_{oc}| = \frac{\mathcal{R}-1}{\mathcal{F}[\,]\{\ \}} - \frac{(X+1)T}{\{\ \}};$$

where the $\{\ \}$ factor is the same as in Eq. (6-85). When $\mathcal{R} = 1$ these distances reduce to

$$|\vec{z}_1, \vec{z}_{oc}| = -\tfrac{1}{2}(X-1)T$$

$$|\vec{z}_2, \vec{z}_{oc}| = -\tfrac{1}{2}(X+1)T.$$

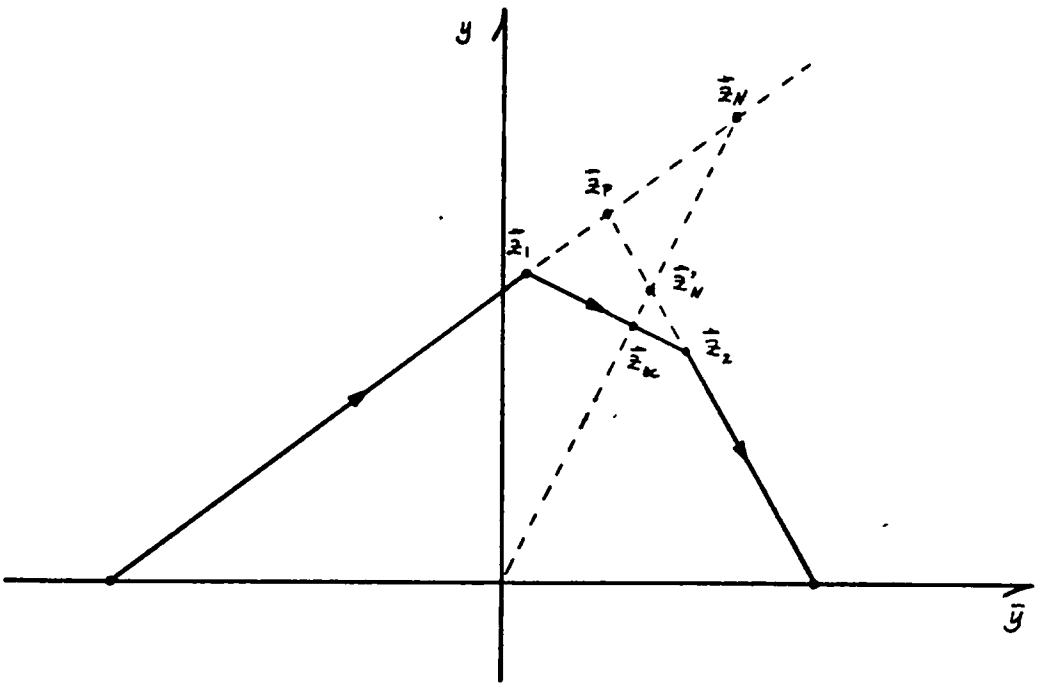

Fig. 46. Optical center of a thick lens

We see from these expressions that when $X = 0$, the optical center lies within the lens; when $X = \pm 1$, it is located at the curved surface of the lens; and if the lens is a meniscus, the optical center is located outside the lens.

We may also note that the ratio of these distances is equal to the ratio of the curvatures of the lens.

$$\frac{|\bar{z}_1, \bar{z}_{oc}|}{|\bar{z}_2, \bar{z}_{oc}|} = \frac{c_2}{c_1} = \frac{r_1}{r_2}.$$

Conclusion

The expressions just derived for a thick lens are completely general with respect to the shape and thickness of the lens. We have restricted ourselves to lenses whose thickness parameter $|\phi| < 1$. This is valid, as practically all of the thick lenses actually used in optical systems belong to this group. On the other hand, little is known about the properties of very thick lenses for which $|\phi| > 1$; this corresponds to axial thicknesses greater than the effective focal length of the lens itself, and they will become the subject of a future investigation.

Several approximations to the expressions developed in this paper are worth noting.

First, we have the "text-book" thin lens, for which $\phi = 0$. In this case $\bar{z}_1$ and $\bar{z}_2$ coincide with $\bar{z}_P$ and the line representing $\bar{W}_X$ pivots on $\bar{z}_P$ as a function of the shape factor X ; all expressions simplify enormously but are of limited application because no actual thin lenses may be fabricated. More interesting is the case where $|\phi| \ll 1$ (which I call "narrow" lenses), as these may be realized in practice and, in fact, a great number of elements in optical systems are indeed of this type. In this case the basic approximation is that of the bracket function, Eq. (6-23) for small values of ϕ ; by expanding the radical in Eq. (6-23) we obtain for the bracket function

$$[\,] \approx 1/2 - 1/8\,\Phi = 1/2\,[1 - 1/4\,\phi(X^2 - 1)] \; ; \qquad (6\text{-}86)$$

being a simpler function of φ and X, each expression involving this bracket function will be simpler.

Another useful approximation of the formulas developed here is that of a mirror; in this case we may also take $\varphi = 0$ as for a thin lens, but we must have $n_2 = -n_1$. This also may be considered as a special case of a single refracting surface, $n_1 \neq n_2$, $\varphi = 0$.

These expressions can also be used in the case of a system of two thin lenses; in this case φ would represent the separation parameter, the product of the actual separation and the power of the combination, and the two thin lenses would take the place of the two refracting surfaces of the thick lens. We still have the freedom of choosing all the three indices $n_1, \tilde{n}, n_2$ equal to or different from each other, i.e., the two thin lenses in air or separating different media.

CHAPTER 7

GENERALIZED BENDING AND THICKENING OF LENSES

The general treatment of a single thick lens in the diagram described in the previous chapter, allows the derivation of expressions for the bending and thickening of lenses. These expressions are completely general and in closed form, without recourse to approximations or iterative procedures, and therefore may be applied either analytically, for the study of properties of thick elements, or in graphical form by means of the diagram, to the analysis and design of optical systems; they may also be incorporated into a computer program.

By bending, we mean the well known procedure used in optical design of changing the curvatures of the surfaces composing the element, without changing its power and the first-order properties of the rest of the system. It is generalized to allow for different indices of refraction before, inside, and after the lens, and in the sense that we permit a more liberal change in the curvatures than the usual small increments in their values. Several attempts have been made at a procedure for "generalized bending" [notably Sutton (1963), but see also Hopkins (1950, p. 111), and Darnauer (1971)], but in our opinion, they are not general enough.

By thickening, we mean any change in the thickness of the lens, including the thickening of a previously thin lens. This has also been attempted before, by Berek (1930, p. 86), Herzberger (1944), Hopkins (1950, p. 114), Hopkins and Rao (1970); but all of them at one stage or another recourse to approximations or iterations.

As may be appreciated from the previous chapter, the bending of the thick lens is completely determined by the shape factor X defined by Eq. (6-18), and the thickening of the lens is controlled by the thickness factor $\phi = T\Phi$. These two parameters are completely independent of each other, but they are intimately related in describing the properties of the thick lens. Therefore, the formulas to be described as an algorithm may be used to vary ϕ and X independently or simultaneously, in one or several elements of an optical system, to adjust the values of the third order aberrations, or to replace a system of ideal thin lenses by a more realistic one of thick lenses, for example.

Bending a Thick Lens

Let us assume for the moment that we fix the value of the thickness factor ϕ, and only change the value of the shape factor X. In other words, we are making a pure bending.

As may be appreciated from the right-hand side of Fig. 36, bending a lens defines a new vector $\vec{W}_X$ for the space within the lens, given by Eq. (6-20). In turn, the line vector $\vec{W}_X$ defines with the object and image vectors $\vec{W}_1$, $\vec{W}_2$ the new points $\vec{z}_1$, $\vec{z}_2$

given by Eqs. (6-69), (6-70). In Fig. 47, we have plotted in a single graph the lines $\vec{W}_X$ and the points $\vec{z}_1, \vec{z}_2$ resulting from different values of the bending factor X, for a fixed set of object and image vectors $\vec{W}_1, \vec{W}_2$. It may be seen from the figure that this small sample already shows how the set of lines produced in this manner envelope a curve, which the analysis of the previous chapter shows to be an ellipse. If we change continuously the shape factor from $X = -\infty$ to $X = +\infty$ we obtain the upper part of the ellipse shown in Fig. 42 defined as the envelope of all its tangents. Note also that each line determines a <u>different</u> set of surface vectors $\vec{z}_1, \vec{z}_2$.

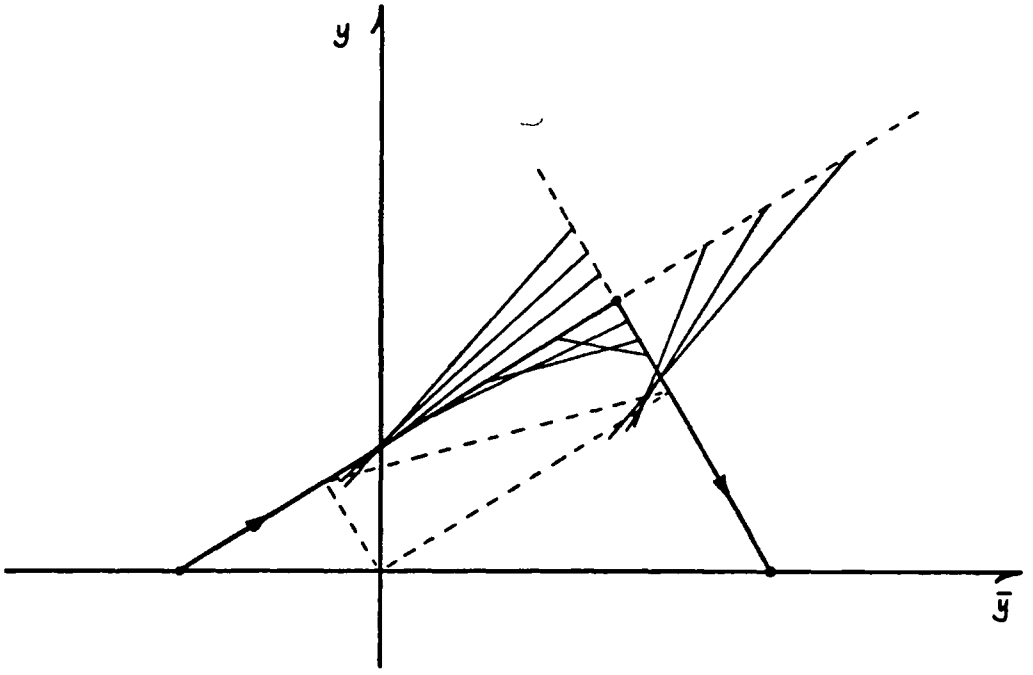

Fig. 47. Same thickness, different shape factors

If we were to change the thickness parameter ρ at the same time we change the value of X, we would define a tangent line $\vec{W}_X$ to a <u>different</u> ellipse. This is in essence what the algorithm proposed by Sutton (1963) does, as he forces the bending (and incidentally, the thickening) in such a manner as to leave the first surface vector $\vec{\mathfrak{r}}_1$ unchanged. Unfortunately, by doing this, he loses the generality of the method, as there is no control over the resulting thickness. This is also the source of the singularity that he has to overcome by a special case. One may remedy the situation by doing a "backward" bending, as defined by Darnauer (1971); however, that complicates the process.

The method here proposed is more general as it permits a better control of the two parameters, the shape factor X and the thickness factor ρ, as the roles of the two are clearly established.

Before we describe the algorithm let us examine the effect of changing only the thickness parameter ρ for a fixed choice of the shape factor.

<u>Thickening a Lens</u>

By looking at the left-hand side diagrams in Fig. 36, we may see that by changing the thickness parameter ρ, and keeping fixed the shape factor X, we in effect are sliding the line parallel to itself. This may be appreciated more clearly in Fig. 48, in which we have plotted in the same graph, the vector $\vec{W}_X$

for different values of ϕ, for the same choice of object and image vectors $\vec{W}_1$, $\vec{W}_2$ as in Fig. 47.

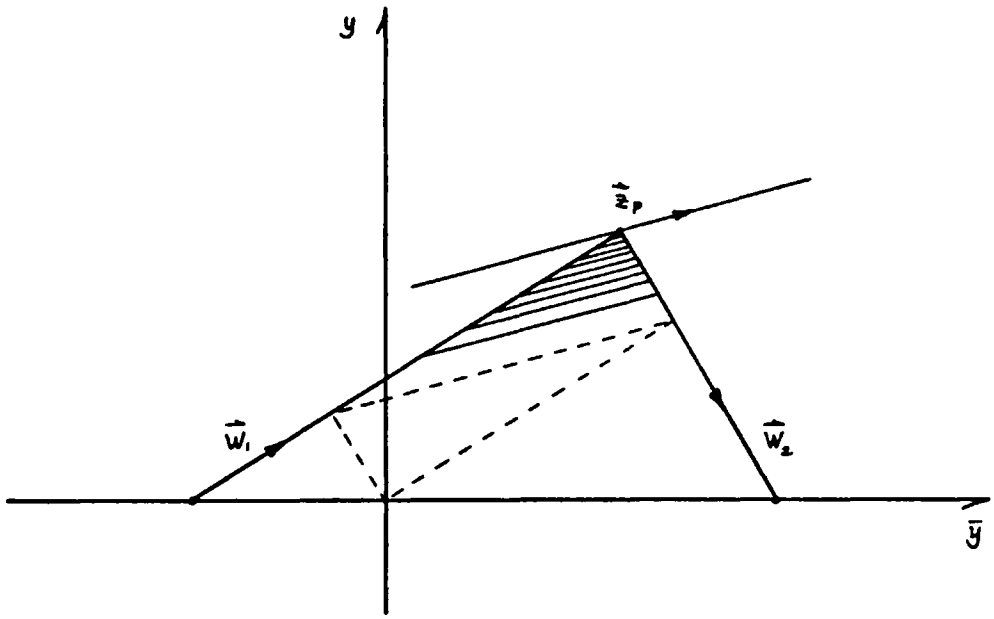

Fig. 48. Same shape factor, different thicknesses

It is clear from Eq. (6-20) that by this operation we are only changing the value of the function [] given by Eq. (6-23) and as the slope of the line $\vec{W}_x$ is determined by the factor in braces in Eq. (6-20), it is clear that the line will remain parallel to itself.

The limiting case of $\phi = 0$ is worth noting; in this case [ ] = 1/2 and $\vec{W}_x$ represents the space within a thin lens. Also $\vec{z}_1 = \vec{z}_2 = \vec{z}_p$, i.e., the two surfaces coincide with the principal points. This illustrates the fact that we may also use this

algorithm to thicken a previously thin lens as well as to change the thickness of an already thick lens. This problem has been attacked before but without the generality and completeness given by the present algorithm. Hopkins and Rao (1970) as mentioned before, use an iterative procedure of successive approximations. Berek (1930) gives a cumbersome method and suggests that an iteration will be necessary when the thickness to be introduced is not sufficiently small. Herzberger (1944) solved this problem quite successfully restricting himself to a fixed value of the shape factor; his formulae may be obtained from the ones presented here by using the ratio of curvatures c_1/c_2 instead of X, by taking it as a constant, and by assuming that the lens is in air, $n_1 = n_2 = 1$. However, instead of leaving his formulae in the general form (at the time of applying them to compute the Petzval sum, for example), he made an approximation too soon, which vitiated his results, as was already pointed out by Rayces (1955). Nevertheless, his general method and expressions may be considered as special cases of those derived in the previous chapter.

The Algorithm

It is clear from the previous paragraphs that the two operations of bending and thickening are independent of each other and may be applied one at a time or both simultaneously to a given system. The generality of this algorithm is based on the fact that each operation is accomplished by a distinct parameter independently of the other.

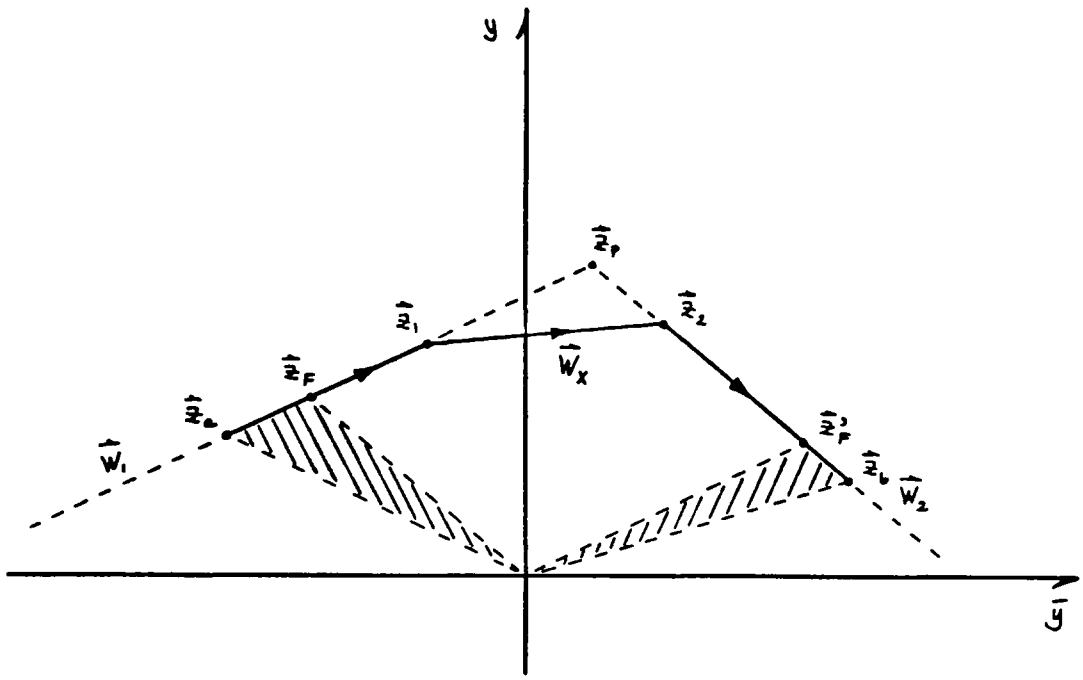

Fig. 49. Definition of variables for thickening or bending

In order to use efficiently the following algorithm we must express first the system under consideration in terms of the $y - \bar{y}$ variables. The system we want to modify is represented in Fig. 49. The two surfaces of the original lens are $\vec{z}_1$ and $\vec{z}_2$; the object and image lines are $\vec{W}_1$ and $\vec{W}_2$ with corresponding indices n_1 and n_2; the surface previous to $\vec{z}_1$ will be designated by $\vec{z}_a$ and that following $\vec{z}_2$ by $\vec{z}_b$. The space within the lens will be given by $\vec{W}_x$ with index $\tilde{n}$.

We assume that the object and image lines $\vec{W}_1, \vec{W}_2$ are fixed, and therefore the power of the lens Φ, and the focal points $\vec{z}_F$, $\vec{z}'_F$ remain fixed throughout any change considered by

this algorithm; this assures the continuity with, and the invariance of the first-order properties of the rest of the system. In particular, the distances between the surfaces $\vec{z}_a$ and $\vec{z}_F$ here designated by T_{AF}, and between $\vec{z}'_F$ and $\vec{z}_b$ (T_{FB}), will not change. Therefore, for any change of ϕ or X that defines a new set of $\vec{z}_1, \vec{z}_2$ only the back and front focal distances from these surfaces will be required.

Given then the above points $\vec{z}_a, \vec{z}_1, \vec{z}_2, \vec{z}_b$, we calculate first the object and image lines,

$$\vec{W}_1 = \frac{\vec{z}_1 - \vec{z}_a}{T_1} = \frac{\vec{z}_1 - \vec{z}_a}{|\vec{z}_a, \vec{z}_1|}, \tag{7-1}$$

$$\vec{W}_2 = \frac{\vec{z}_b - \vec{z}_2}{T_b} = \frac{\vec{z}_b - \vec{z}_2}{|\vec{z}_2, \vec{z}_b|}; \tag{7-2}$$

which in turn give the power of the lens

$$\Phi = |\vec{W}_1, \vec{W}_2|. \tag{7-3}$$

Next, we calculate the intermediate vector $\vec{W}_X$, and the thickness of the lens,

$$\vec{W}_X = \frac{\vec{z}_2 - \vec{z}_1}{\tilde{T}} = \frac{\vec{z}_2 - \vec{z}_1}{|\vec{z}_1, \vec{z}_2|}. \tag{7-4}$$

If the original lens is thin $\tilde{T} = 0$, and Eq. (7-4) will be undefined. However, as in that case $[\,] = 1/2$, the intermediate vector will be given by

$$\vec{W}_X = 1/2 \{ \vec{W}_2 (X + 1) - \vec{W}_1 (X - 1) \}, \tag{7-5}$$

where we must know or assume a shape factor for the thin lens.

Next, we calculate the powers at each surface,

$$\Phi_1 = |\vec{W}_1, \vec{W}_X| \tag{7-6}$$

$$\Phi_2 = |\vec{W}_X, \vec{W}_2| \tag{7-7}$$

and the shape factor, if it is not already known,

$$X = \frac{\Phi_1 - \Phi_2}{\Phi_1 + \Phi_2}. \tag{7-8}$$

It is also convenient to calculate the focal vectors

$$\hat{z}_F = -\vec{W}_2/\Phi, \tag{7-9}$$

$$\hat{z}'_F = +\vec{W}_1/\Phi, \tag{7-10}$$

and the separations of these points from the previous and following surfaces $\hat{z}_a$, $\hat{z}_b$,

$$T_{AF} = |\hat{z}_a, \hat{z}_F| = \text{const} \tag{7-11}$$

$$T_{FB} = |\hat{z}'_F, \hat{z}_B| = \text{const} \tag{7-12}$$

which will remain constant during bending or thickening.

Note that some of these quantities may already be known by previous analysis and some of the above steps might be eliminated.

We are now ready to proceed with the changes. At this point we introduce a new value of $\tilde{T}$, or X, or both.

We define the thickness parameter

$$\rho = \tilde{T}\Phi \tag{7-13}$$

and the quantity

$$Q = 1 + \rho(X^2 - 1) \tag{7-14}$$

to get the bracket function

$$[] = \frac{1}{1 + \sqrt{Q}} \tag{7-15}$$

We may now define the functions

$$FW_1 = [](X + 1) \tag{7-16}$$

$$FW_2 = -[](X - 1) \tag{7-17}$$

$$F\mathcal{Z}_1 = (X + \sqrt{Q})/(X + 1) \tag{7-18}$$

$$F\mathcal{Z}_2 = (X - \sqrt{Q})/(X - 1) \tag{7-19}$$

which allows to write the new values for the powers

$$\mathcal{P}_1 = (FW_1)\,\mathcal{P}, \tag{7-20}$$

$$\mathcal{P}_2 = (FW_2)\,\mathcal{P}, \tag{7-21}$$

in terms of the power of the lens given by Eq. (7-3). From these we get the new curvatures

$$c_1 = \frac{(FW_1)\varphi}{\tilde{n} - n_1}, \tag{7-22}$$

$$c_2 = \frac{-(FW_2)\varphi}{\tilde{n} - n_2}. \tag{7-23}$$

The value of the new intermediate vector $\vec{W}_X$ will be given by

$$\vec{W}_X = (FW_1)\,\vec{W}_2 + (FW_2)\,\vec{W}_1 ; \tag{7-24}$$

and the new surfaces will be:

$$\vec{\mathcal{Z}}_1 = \vec{\mathcal{Z}}_F + (F\mathcal{Z}_1)\,\vec{\mathcal{Z}}'_F , \tag{7-25}$$

$$\vec{\mathcal{Z}}_2 = (F\mathcal{Z}_2)\,\vec{\mathcal{Z}}_F + \vec{\mathcal{Z}}'_F . \tag{7-26}$$

The new front and back focal distances will be given by

$$FFD = (Fz_1)f, \tag{7-27}$$

$$BFD = (Fz_2)f', \tag{7-28}$$

as may be seen from the equations following Eq. (6-79). Therefore, the separations from the previous and following surfaces $\tilde{z}_a$, $\tilde{z}_b$ will be

$$T_1 = |\tilde{z}_a, \tilde{z}_1| = T_{AF} + (Fz_1)/\tilde{\varphi} \tag{7-29}$$

$$T_b = |\tilde{z}_2, \tilde{z}_b| = T_{FB} + (Fz_2)/\tilde{\varphi} \tag{7-30}$$

where the constant distances T_{AF}, T_{FB} are given by Eqs. (7-11), (7-12).

By introducing the indices of refraction and the Lagrange invariant, the actual separations t_1, t_b may be obtained.

Finally, the new separation of the principal points will be given by

$$T_{PP} = \frac{\varphi}{\tilde{n}} \left\{ \tilde{n} - n_1(FW_1) - n_2(FW_2) \right\}. \tag{7-31}$$

This completes the algorithm. Note, that by keeping $\tilde{T} = const$, and varying X we get bending and a graph will look as in Fig. 47 with several such changes. For thickening we set $X = const$ and vary $\tilde{T}$; several such changes are shown in Fig. 48. It should be noted that the new values obtained after a change of φ or X do not depend at all on the old values of φ and X.

Minimum Thickness for a Narrow Lens

When thickening a previously thin lens, the question arises as to what should be the minimum thickness attached to it.

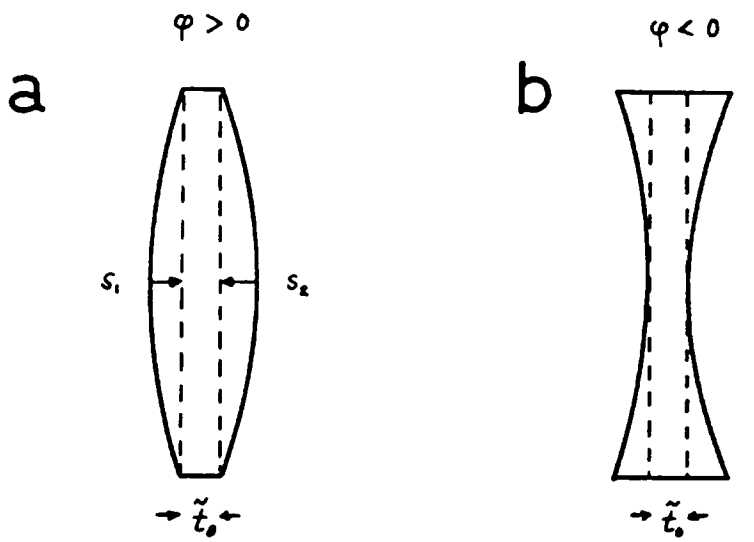

Fig. 50. Minimum thickness.
a) For a positive lens. b) For a negative lens

As seen in Fig. 50, if the lens is positive this minimum thickness includes the sagittae of the two surfaces plus some construction thickness for the rim, that we shall call $\tilde{t}_o$. If the lens is negative the construction thickness $\tilde{t}_o$ will be sufficient.

Therefore the minimum thickness $\tilde{t}$ will be given by

$$\tilde{t} = s_1 - s_2 + \tilde{t}_o \quad , \text{ for a positive lens,}$$

$$\tilde{t} = \tilde{t}_o \quad , \text{ for a negative lens.}$$

An expression may be developed for this thickness in terms of the parameters of the lens. Noting that the sagittae may be written as

$$s \approx \tfrac{1}{2} c h^2 = \tfrac{1}{2} c \{ |\bar{y}| + |y| \}^2, \tag{7-32}$$

where h is the minimum clear aperture of the lens to avoid vignetting, we may write,

$$\begin{aligned} \tilde{T} &= \tilde{T}_0 + \frac{\mathcal{H}}{\tilde{n}} (s_1 - s_2) = \tilde{T}_0 + \frac{\mathcal{H}}{\tilde{n}} (c_1 - c_2) \frac{h^2}{2} = \\ &= \frac{\mathcal{H}^2 h^2 \mathcal{E}}{4\tilde{n}} [\,] \left\{ \frac{X(n_1 - n_2) + 2\tilde{n} - (n_1 + n_2)}{(\tilde{n} - n_1)(\tilde{n} - n_2)} \right\}. \end{aligned} \tag{7-33}$$

If the lens is sufficiently narrow, $\tilde{T} \ll 1$ then $[\,] \approx 1$. And if we consider the case of the lens in air, $n_1 = n_2 = 1$, then

$$\tilde{T} \approx \frac{\mathcal{H}^2 h^2 \mathcal{E}}{2\tilde{n}(\tilde{n} - 1)} + \tilde{T}_0, \tag{7-34}$$

which is independent of the shape factor.

We may use this value for thickening a previously positive thin lens to produce a sufficiently narrow but otherwise realistic thick lens. If the thin lens is negative, we neglect the first term on the right-hand side of Eq. (7-34).

CHAPTER 8

THE PROGRAM YYRANCH

The computer program YYRANCH ($y-\bar{y}$ Representation ANd Computational Handling), written entirely in FORTRAN for the CDC 6400 Computer is basically a program for the numerical analysis of given optical systems, although it has several design features that allow the modification of the given system towards a desired design.

It is entirely based on the formulae developed in the previous chapter of this work, and should be considered as a numerical application of the $y-\bar{y}$ method to the analysis and design of optical systems.

The program is a multipurpose program being capable of performing a series of tasks sequentially and controllable entirely by data cards. For this purpose the program is composed of an ensemble of subroutines, each of which performs a specific task. All the subroutines have been grouped in 12 subprograms as listed in Table I, to facilitate the flow of the program and the internal transfer of information among the different subroutines; for example, most of the transferring from one part of the program to another is done through labelled COMMON, to avoid the calling lists associated with the subroutines.

TABLE I

LIST OF THE SUBPROGRAMS CONTAINED IN THE PROGRAM YYRANCH

ONE	TWO	THREE	FOUR	TASK1	TASK2
INVARNT	BENDING	SEIDEL	FROM 12	Z FROM X	SEIDEL G
TO READ Z	CARDNAL	MERIT	FROM PP	Z FROM Y	SEIDEL 1
TO GET Z	TO LIST Z	WAVE CF	TO VARY	Z FROM KC	SEIDEL 2
TO GET W	NEW ZHE	CHANGE Z		S SHIFT	SEIDEL 3
TO SHIFT	NEW RN	CHANGE W		C SHIFT	SEIDEL 4
NORMAL	FOR BX	CHANGE N		Z ABS	SEIDEL 5
THIN	FOR SP	CHANGES		Z ORD	SEIDEL L
TH AND CV	TO SAVE	VIGNETT			SEIDEL T
PARAX	NEW DECK				DERIVAT
THICKEN	RESTORE				

DIAGRAM	FIRST	SECOND	THIRD	FOURTH	FIFTH
DIAGRAM	CENTER	TITLES	AXIS X	TO IMBED	DECIMAL
RECOVER	CNTROID	TO CLEAR	AXIS Y	PACKING	DIGITS
NEW ZOOM	FOR ZOOM	FRAME XY	FOR XMOD	MASKING	
ENLARGE	SCALES	FRAME Y	FOR YMOD		
	TO PRINT	PLOT XY	TO LASTX		
	REJECT	FOR LINE	TO LASTY		
		FOR AXES	LABELS X		
			LABELS Y		
			X POINTS		
			Y POINTS		

The program YYRANCH proper, acts as a driver and control for all the rest of the subroutines and can call upon any part of any subprogram with very few restrictions. In turn, a given subroutine can call any other in another subprogram without going back to the main program.

The upper part of Table I contains all the operations pertaining to the handling of the y-$\bar{y}$ diagram variables. The lower part of the table lists the subprograms necessary for the production of the y-$\bar{y}$ or Ω-$\bar{\Omega}$ diagrams as cartesian graphs plotted in the printer. Therefore, they are not absolutely essential to the analysis of optical systems, if one does not desire the graphs, or if there are other means of plotting those graphs. These latter routines, although written in FORTRAN, depend heavily on the internal structure of the CDC 6400 computer.

All the tasks performed by the YYRANCH program are controllable through data cards which are all of the same format: two alphanumeric fields and five numerical fields, which are read under the format 2A8, 5E12.6; the last 4 columns may be used for identification. Thus, the two labels should be punched starting in columns 1 and 9 respectively, and the five variables should be punched starting in columns 17, 29, 41, 53, 65, respectively. The identification may be started in column 77.

In the following examples of input cards the first two labels will be typed as they should appear in the data cards, and the numerical variables will be listed as a sequence, separated by commas. When a variable may be absent, this will

be indicated by a long dash. Sometimes the names in the labels are optional, in the sense that as far as the program is concerned they may be absent, although its presence is a good guidance for the user. This will be indicated by an asterisk after those names.

Among the many tasks that the program YYRANCH performs we may mention the derivation of first-order properties of a given y-$\bar{y}$ or Ω-$\bar{\Omega}$ diagram; the normalization of the diagram; its graphical representation; a shift of the object or of the stop; the derivation of a diagram from a given set of curvatures and spacings; the derivation of the Seidel coefficients for each surface and all of the surfaces together; and the bending and thickening of lenses.

We now proceed to describe the input cards to achieve these tasks.

The very first card of a given input deck must be of the form

NEW DECK* (8-1)

this initializes several counters and sets the value of $\mathcal{H}$ to unity. The very last card of the deck must be

END DECK* (8-2)

to properly stop the program.

Several systems may be processed in a single run. Each one must begin with a card of the form (8-1), to properly

initialize the counters. However, only one END card must be present, the very last one, as this card stops the program.

Immediately following a NEW card, the program expects to find a card of the form

TITLE ____ Some appropiate title beginning after column 17 (8-3)

The contents of this TITLE card will be used as a label for all listings and graphs pertaining to the particular system that it precedes. If this card is left out the title label will be left blank.

When asking for graphs of the diagram there is an option for a card of similar format

MESSAGE ____ Some appropiate message beginning after column 17 (8-4)

which is used to put a required label at the bottom of the graphs to distinguish them from one another.

Options for Input

The input to the YYRANCH program may take three forms: We may input the set of points $\vec{z}$ representing the optical system in the y-$\bar{y}$ diagram, or the set of line vectors $\vec{W}$ representing the same system in the n-$\bar{n}$ diagram, or the set of surface curvatures and separations, from which the y-$\bar{y}$ diagram may be constructed by the ray trace of marginal and chief rays. At the same time we read the values of the different indices of refraction involved.

To read a set of points $\hat{\mathfrak{x}}$ we start by reading a card of the form

OBJECT POINT* $\quad \bar{y}_o\ ,\ 0.,\ \_\_\_\_,\ \_\_\_\_,\ \_\_\_\_.$ (8-5)

We next read as many cards as points are in the diagram, representing either surfaces or thin lenses. If the point read is to represent a surface, the data card takes the form

SURFACE* j* $\quad \bar{y}_j\ ,\ y_j\ ,\ n_j\ ,\ \nu_j\ ,\ \_\_\_\_.$ (8-6)

Instead, if the point represents a thin lens, the input card should be

LENS j* $\quad \bar{y}_j,\ y_j\ ,\ \tilde{n}_j\ ,\ \tilde{\nu}_j\ ,\ X_j\ .$ (8-7)

In these cards, ($\bar{y}_j$, y_j) are the coordinates of point j, n_j , ν_j , are the index of refraction and dispersion constant of the space before point j, or $\tilde{n}_j$, $\tilde{\nu}_j$ for the thin lens, (see Appendix A for nomenclature), and X_j is the shape factor of lens j.

After all points representing surfaces or thin lenses are read the set is closed with a card of the form

IMAGE POINT* $\quad \bar{y}_I\ ,\ 0.,\ \_\_\_\_,\ \_\_\_\_,\ \_\_\_\_.$ (8-8)

This card signals the end of the input set and the program then proceeds to calculate the lines $\vec{W}$ connecting the points and the derived quantities T and Φ, according to Eqs. (3-9), (3-14), (3-11).

If instead of points $\hat{\mathfrak{x}}$ we wish to read the lines $\vec{W}$ we begin with a different object card:

OBJECT LINE $\quad \bar{\Omega}_1\ ,\ \Omega_1\ ,\ n_1\ ,\ \nu_1\ ,\ \_\_\_\_.$ (8-9)

Then the intermediate lines are read as

RAY* j* $\bar{\Omega}_j$, Ω_j, n_j, ν_j, ____. (8-10)

and finally we close with an image card that has the same function as the one in (8-8),

IMAGE LINE* $\bar{\Omega}_I$, Ω_I, n_I, ν_I, ____. (8-11)

From here, the program proceeds to calculate the vectors $\bar{\bar{z}}$ and the quantities T and Φ.

When we wish to read the input in the conventional manner by giving the curvatures and separations of the surfaces composing the system, we begin by reading an object card of the form

OBJECT HEIGHT $\bar{y}_0$, $\bar{u}_1$, u_1, n_1, ν_1. (8-12)

Where $\bar{u}_1$, u_1, are the chief and marginal ray angles in the first space, expressed in radians. This card is valid for an object at a finite distance. If the object is located at infinity, this object card takes the form

OBJECT HEIGHT y_E, $\bar{u}_1$, $0.$, n_1, ν_1. (8-13)

Here, y_E is the height of the marginal ray at the entrance pupil.

After reading either of the two object cards we proceed with alternating thickness and curvature cards of the form

TH* ____ t_j, ____, ____, ____, ____. (8-14)

for the separation t_j, and

CV* ____ c_j, n_{j+1}, ν_{j+1}, ____, ____. (8-15)

for the curvature c_j, and the index for the next spacing. The set ends with an image card of the form

IMAGE HEIGHT* (8-16)

with this card the program proceeds to trace a marginal and chief rays through the system and from them get all the values of $\hat{\mathfrak{Z}}$, $\hat{W}$, T and $\mathfrak{T}$.

To complete the specification of the system we must input the value of the Lagrange invariant used to reduce the set of points or lines in the y-$\bar{y}$ diagram to the physical set of curvatures and spacings or vice versa.

As mentioned before, at the beginning of the program H is set equal to unity. Another given value of H can be introduced with the card

CHANGE ZHE H , 0. , ____, ____, ____. (8-17)
1. list

The second variable allows the printing of a new τ and t lists, (see below).

Another way of introducing a value of the Lagrange invariant is by specifying the focal length of the system f', the f-ratio N, and the field angle $\bar{u}_1$, as follows

INVARNT ____ N , f', $\bar{u}_1$, ____, ____. (8-18)

The invariant is computed from

$$H = n_1 \bar{u}_1 f'/2N.$$

However, the card (8-18) does much more than just introducing a new value of H. After the value of H has been computed, the whole set of points and lines $\hat{\mathfrak{Z}}$ and $\hat{W}$ are normalized, according

to the rule given in Chapter 5, and then rescaled with the new value of $\mathcal{H}$ using the expressions developed in the same Chapter 5. Obviously this operation cannot be carried out before the points and the lines are defined, and therefore an INVARNT card must follow the OBJECT through IMAGE cards.

On the other hand, if the input is given in terms of thicknesses and separations it will be necessary to introduce a Lagrange invariant <u>before</u> we read the input set in order to get realistic values for the variables $\bar{z}$ and $\bar{W}$ of the y-$\bar{y}$ diagram. This is most conveniently done by introducing the value of through a card of the type (8-17).

If any of the points in the y-$\bar{y}$ diagram represents a thin lens this should be indicated by the card

THIN LENS* j , 0. old data
1. new data, $\tilde{n}_j$, $\tilde{\nu}_j$, X_j. (8-19)

which follows the OBJECT through IMAGE cards. In this card if the second numerical variable is absent or zero means that we take the data for the thin lens ($\tilde{n}_j$, $\tilde{\nu}_j$, X_j) from the card (8-7); otherwise, they are given in this card (8-19).

When all the points defined in the input set are thin lenses then it is sufficient to use the card

THIN ALL* (8-20)

These cards (8-19), (8-10) have the effect of defining two coincident points which represent the two surfaces of the thin lens of strictly zero thickness. The line vector

representing the space within the lens is computed with the help of the shape factor X by means of Eq. (7-5).

One word about default conditions. In the great majority of cases, when a numerical variable is left blank, it is read by the program as zero (actually, negative zero). One notable exception is the cards containing indices of refraction; when these are left blank, they are set equal to unity by the program and the corresponding dispersion factor is set as $\nu = 90$. In the same way, when we define points to be thin lenses, by means of cards (8-7) or (8-19), the neighboring indices of refraction are set equal to unity. If different indices are desired surrounding a thin lens, these may be introduced with a card of the form

$$\text{CHANGE INDEX} \qquad j, n_j, \nu_j, \begin{matrix} 0. \\ 1. \text{ list} \end{matrix}, \text{——}. \qquad (8\text{-}21)$$

The fourth variable allows printing of a new t list, (see below).

Once the input to the program is specified by means of the above cards, we may proceed to analyze the contents of the diagram or to modify it by certain operations. Before we describe these modifications let us look into the options of output and the analysis features of the program.

Options for Output

The output may take the form of listing of several types or the form of graphs of the y-$\bar{y}$ or Ω-$\bar{\Omega}$ diagrams. Several of the listings are the result of other operations carried out on part or the whole of the diagram, but a direct command may produce

the listing of the variables in the y-$\bar{y}$ diagram by means of the card

LIST ____ 1. T list, ____, ____, ____, ____ (8-22)
2. τ list
3. t list

The T list refers to the listing of the quantities $\bar{y}$, y, T, $\bar{\Omega}$, Ω, and Φ, which are directly derivable from the set of points $\bar{z}$. The τ list consist of the reduced quantities τ, $\bar{\omega}$, ω, and φ, which are derived from the T list by inserting the value of the Lagrange invariant $\mathcal{H}$. Finally, the t list is a listing of the quantities t, $\bar{u}$, u, f', c, γ, obtained from the τ list by inserting the appropiate indices of refraction.

If the numerical variable is left blank, it is interpreted by the program as unity and therefore, a T list is implied.

To obtain the graphical output we use the card

DIAGRAM YYBAR 0. 0. 0. 0. 0.
OMEGA 1. graph 1. scales 1. T list 1. rejected 1. message
2. τ list
3. t list (8-23)

According to (8-23) if the second name is YYBAR we obtain a y-$\bar{y}$ diagram and if it is OMEGA we get an Ω-$\bar{\Omega}$ diagram. If the first variable is different from zero, the graph will be printed, otherwise it will be calculated and saved, either for subsequent modification or for future printing. The second variable controls the printing of the scale used for the graph. The third variable serves to produce the listings described before for card (8-22); if it is blank, no lists will be produced. The

fourth variable controls the printing of the points that fall outside the frame defining the graph. Finally, the fifth variable permits the printing of a message read immediately after card (8-23) under the format (8-4).

The graph previously calculated or printed has a fixed scale of one unit per inch, and is centered at the origin of coordinates. Sometimes this is not convenient and a modification either before or after printing is possible with a card of the form

ZOOM TO CNTROID NEW CTR OLD CTR RECOVER	Scale x ,	Scale y ,	0. 1.	graph	, x_c , y_c .	(8-24)

When the second name is CNTROID, the graph will be translated, with new scaling (scale x , scale y) if necessary, to the centroid of the points in the diagram. If it is desired to have the scaling unchanged, we must put scale x = scale y = 1. The printing of the graph is controlled with the third variable.

When the second name is NEW CTR, a new center is defined by variables 4 and 5, with or without scaling and printing.

When the second name is OLD CTR, the center of the previous graph is used, and only the scaling is changed.

Finally, when the second name is RECOVER, the original graph is recovered.

Two more cards may be used when controlling the output. The following card

PRINT DECK*

allows the printing of the set of points and indices of refraction in the same format as would be used as input for a following run. This listing is different from a T list in the sense that the values appear with six figures after the decimal point.

Sometimes, when a printing option is called for, the output would be printed immediately below the last printed results. If it is desired to print these results in a different page, the following card may be used just before using the option in question:

SKIP PAGE*

This will allow the printer to start any subsequent output in a new page.

Analysis Features

Aside from the above options of output which may be used as analysis tools, the YYRANCH program provides for a number of operations and listings that permits the detailed study of an optical system represented in the $y-\bar{y}$ diagram. The most important of these are the computation and listing of the first- and third-order properties of the optical system. But before describing these we shall mention two options that are useful in practice.

When we consider that the optical system consists of lens elements either thin or thick, sometimes it is important before proceeding, to calculate the shape and thickness factors of the lens, given by Eqs. (7-8) and (7-13) respectively. This is

accomplished by the two following cards, one for each element considered

SHAPE ____ j, ____, ____, ____, ____. (8-25)

SP ____ j, ____, ____, ____, ____. (8-26)

Note that the inclusion of these two cards will not produce any printed output. Its inclusion is mandatory when the quantities X or p are necessary for further computations, and the powers or the separations have been changed by previous calculations.

The first order properties of a system may be computed by a card of the form

FIRST ORDER* 0. , ____, ____, ____, ____. (8-27)
1. T list
2. τ list
3. t list

After reading this card the program will proceed to make the listings indicated by the first variable, according to the rules given above for card (8-22); if this variable is blank or zero these lists will be omitted.

Proceeding, the program will calculate all the first order parameters of the system taking the first line as object ray and the last one as image ray. The formulae developed in Chapter 4 are used to calculate all the cardinal points, the object and pupil magnifications, the refraction invariant, etc., as well as the location of all points from the first and last surfaces of the system. The distances are also displayed in the

three formats of T list, τ list, and t list. Finally the location of the stop of the system is printed at the bottom of the page.

It is also possible to calculate the cardinal points and other first order parameters for a pair of given line vectors taken as object and image rays; this may be accomplished with a card of the form

CARDNAL POINTS* j, k, ____, ____, ____. (8-28)

This card will calculate the cardinal points corresponding to the "system" formed by the rays $\vec{W}_j$, $\vec{W}_k$.

If it becomes necessary to construct a vignetting diagram of the system, the program will calculate and print the necessary quantities to produce a drawing as in Fig. 32 by reading a card of the form

VIGNETT ____ j, CA_j, ____, ____, ____. (8-29)

for each surface of the system. The second variable gives the prescribed clear aperture of the system; if it is absent the program will set it at its minimum value as given by Eq. (4-41).

The third-order coefficients of the system will be calculated by means of a card of the form

THIRD ORDER* ____, k, ____, ____, ____. (8-30)

this card will signal the program to calculate the Seidel coefficient S_k (see below) for all surfaces. If $k=0$, all Seidel coefficients will be computed for all surfaces and printed; however if $k=0$, the result will <u>not</u> be printed.

The Seidel coefficients are computed from the following expressions, which are essentially those given by Hopkins (1950, pp. 87-88), properly scaled by the Lagrange invariant, and in terms of the quantities intrinsic to the diagram. The coefficient for distortion is differently expressed to avoid a singularity.

Using the variables defined in Chapter 4, we have for each surface:

Spherical aberration, $S_1 \equiv S_I = y\,\Delta I^2$

Coma, $S_2 \equiv S_{II} = y\,\Delta \bar{I} I$

Astigmatism, $S_3 \equiv S_{III} = y\,\Delta \bar{I}^2$

Petzval, $S_4 \equiv S_{IV} = P = -\mathcal{R}\Phi/n^2$

Distortion, $S_5 \equiv S_V = y\,\bar{\Delta}\bar{I}^2 - \bar{y}\,\bar{I}P$

Longitudinal color, $S_6 \equiv C_L = y\,I\left(\delta n'/n' - \delta n/n\right)$

Transverse color, $S_7 \equiv C_T = y\,\bar{I}\left(\delta n'/n' - \delta n/n\right)$

Summing over all surfaces we obtain the wave aberration coefficients as follows, (Hopkins, 1950, p. 50)

$$W_{040} = -1/8\ \mathcal{H}^3 \Sigma S_I$$

$$W_{131} = -1/2\ \mathcal{H}^3 \Sigma S_{II}$$

$$W_{222} = -1/2\ \mathcal{H}^3 \Sigma S_{III}$$

$$W_{220P} = -1/4\ \mathcal{H}^3 \Sigma S_{IV}$$

$$W_{311} = -1/2\ \mathcal{H}^3 \Sigma S_V$$

$$\delta(W_{020}) = -1/2\, \mathcal{H} \Sigma C_L$$

$$\delta(W_{111}) = -1/2\, \mathcal{H} \Sigma C_T$$

These aberration coefficients may be combined in some "figure of merit" to give an idea of the performance of the system. We chose as a figure of merit the following "mean squared spot size" referred to the image centroid in the gaussian image plane:

$$\sigma_e^2 = \left(\frac{\bar{y}_I}{\mathcal{H}}\right)^2 \Big\{ 2\left[(W_{020} + 4/3\, W_{040}) + (W_{220P} + W_{222})\beta^2\right]^2 +$$

$$+ 1/2\,(W_{222}\beta^2)^2 + 4/9\,(W_{040})^2 +$$

$$+ \left[(W_{111} + W_{131})\beta + W_{311}\beta^3\right]^2 + 2/3\,(W_{131}\beta)^2 \Big\},$$

where β is the fractional size of the aperture, and where we have taken $W_{111} = \delta(W_{111})$ and $W_{020} = \delta(W_{020})$, using the C and F lines as extremes and the d line as reference. This quantity is computed by the program for the values $\beta = 0,\ 0.5,\ 0.7,\ 1.0$.

After calculating these quantities the program prints the Seidel coefficients for each surface, their sums, the wave aberration coefficients and the merit function.

Design Features

We include as design features all the operations and changes in the diagram that will lead to a desired configuration. These include bending and thickening of lenses, and shifts of the

stop or the object. Each type of change may be accomplished with a different card or set of cards. We describe them in this section.

Many times it is convenient to work with a normalized diagram in the manner described in Chapter 5. A normalization of the diagram is accomplished with the following card

NORMAL _____ (8-31)

Arbitrary changes in the variables may be made with the following cards; however they are of limited value in the present use of the program, because after the data cards have been read in the machine, the user has no control whatsoever over that run. Nevertheless some times it is desirable to include those changes in the same run to see how the diagram is evolving.

We already mentioned the cards used to change the Lagrange invariant, card (8-17), or a given index of refraction (8-21).

If we wish to change a point we use the cards

CHANGE POINT 1., j, $\bar{y}_j$, y_j, ____.
CHANGE POINT 2., j, k, $\bar{y}_j$, ____.
CHANGE POINT 3., j, k, y_j, ____.
CHANGE POINT 4., j, k, Δz, ____. (8-32)

When the first variable is unity, the new value of $\hat{z}_j$ will be given by variables 3 and 4. When the first variable is 2, the $\hat{z}_j$ is moved along the line $\hat{W}_k$ until it has a value $\bar{y}_j$ given by variable 4. Similarly, when variable 1 is 3, $\hat{z}_j$ moves along line

$\vec{W}_k$ until it has a value of y_j given by variable 4. Finally, when the first variable is 4, $\vec{z}_j$ moves along $\vec{W}_k$ a distance Δz.

A change in a line vector $\vec{W}$ may be made with a card of the form

CHANGE LINE 1., j, $\bar{\Omega}_j$, Ω_j, ____. (8-33)

Of more important applicability is the bending or thickening of lenses. The bending of a lens according to the rules given in Chapter 7, may be obtained with the card

BENDING LENS* j, T_{j+1}, X_j, 0. old T, 0.
1. new T, 1. print (8-34)

where X_j is the new bending factor for lens j. A lens is considered to be composed of surfaces $\vec{z}_j$ and $\vec{z}_{j+1}$. If the fourth variable is blank, the bending will be done without changing the thickness of the lens. If however a thickening as well as a bending is desired, this variable (4) will be different from zero and the new thickness in the form $T = \mathcal{H} t/n$, must be punched as variable 2. The fifth variable controls the printing of the results.

For thickening, we use a card of similar format

THICKEN LENS* j, T_{j+1}, X_j, 0. old shape, 0.
1. new shape, 1. print (8-35)

The new thickness is T_{j+1} and the possible new shape is given by X_j.

We may use either of these two cards also to thicken or bend a previous thin lens, by giving the new thickness or bending

required. However if we wish to give the thin lens the minimum thickness required, as explained at the end of Chapter 7, we use the card

THICKEN MINIMUM j, $\tilde{t}_o$, ____, ____, 0. / 1. print (8-36)

Where $\tilde{t}_o$ is the physical rim thickness. See the last section of Chapter 7.

The shifts of the object or the stop may be accomplished by many different options, each more convenient than the others in different applications. The cards are of the following format either for the object or the stop shift:

SHIFT OBJECT / STOP 1., $\bar{k}'$ / k', ____, ____, ____. (8-37)

The second name controls the type of shift, and the first variable the option. For card (8-37), the slope of the new axis is given, and the formulae of Chapter 4 are used to calculate the new values of $\bar{y}$ or y variables.

SHIFT OBJECT / STOP 2., $\bar{y}_s$, y_s, ____, ____. (8-38)

This card says that the new axis passes through the point $(\bar{y}_s, y_s)$

SHIFT OBJECT / STOP 3. / 4., $\bar{\Omega}_s$, Ω_s, ____, ____. (8-39)

In this card if the first variable is 3, the new axis is parallel to $(\bar{\Omega}_s, \Omega_s)$; if it is 4, the new axis is perpendicular to $(\bar{\Omega}_s, \Omega_s)$.

SHIFT OBJECT STOP	5., j, ____, ____, ____. 6. 7.	(8-40)

This card determines that, according to the first variable, the new axis passes through the point $\bar{z}_j$ (5), or is parallel (6) or perpendicular (7) to the line $\bar{w}_j$.

SHIFT STOP	8., j, t_s, ____, ____.	(8-41)

This card can only be used for a stop shift and says that the stop should be located at the distance t_s from the point $\bar{z}_j$.

SHIFT OBJECT STOP	9., m_o / m_E, ____, ____, ____.	(8-42)

This card expresses the fact that the new axis is the conjugate line whose magnification is m_o or m_E.

SHIFT OBJECT STOP	10., γ / ζ, ____, ____, ____.	(8-43)

Finally, this card says that the new axis should be the conjugate line whose magnification ratio is either γ or ζ given respectively by

$$\gamma \equiv \frac{\Omega_2 + \Omega_1}{\Omega_2 - \Omega_1} = \frac{1 + m_o}{1 - m_o}$$

$$\zeta \equiv \frac{\bar{\Omega}_2 + \bar{\Omega}_1}{\bar{\Omega}_2 - \bar{\Omega}_1} = \frac{1 + m_E}{1 - m_E}$$

These factors are very convenient in expressing certain properties of optical systems. See Hopkins (1950, p. 120).

Note that these SHIFT cards do not produce any printed or graphical output. If the results of these operations need to be

checked the appropiate cards should be used to display the information.

One last word of caution: any variable punched in the five numerical fields should be always punched as a floating point number, i.e., with a decimal point, or located within its own field as to satisfy the implied format E12.6. This is particularly important for those numbers that appear as subscripts or integers in the cards described above.

APPENDIX A

NOMENCLATURE

General

Quantities pertaining to a ray refer to the marginal ray if written without a bar and to the chief ray if written with a bar.

Quantities without a prime refer to the space before the refracting surface under consideration, and primed quantities refer to the space after the surface.

Subscripts

The first physical surface is denoted by the subscript 1. An intermediate surface is labeled as the j^{th} surface with the subscript j, or if necesary as the i^{th} surface with the subscript i. The last surface is denoted by the subscript k.

The object plane or surface is denoted by O and the image plane or surface by O' or I.

The surface or plane of the physical stop is denoted by a subscript S.

The surface or plane of the entrance pupil is denoted by a subscript E, that of the exit pupil by a subscript E'.

Quantities Belonging to a Surface

r, radius of curvature

$c = 1/r$, curvature

$y, \bar{y}$, height of the marginal and chief rays

$CA = |\bar{y}| + |y|$, clear aperture

$\mathcal{R} = n/n'$ refractance

Quantities Defined in the Spaces Between the Surfaces

$u, \bar{u}$, angle between ray and optical axis

$i, \bar{i}$, angle of incidence; note that

$$i = u + c y \ , \qquad \bar{i} = \bar{u} + c \bar{y}$$

$i', \bar{i}'$, angle of refraction

n, n', indices of refraction before and after the surface

t, t', axial distances before and after the surface

Note that $u'_j = u_{j+1}$, $n'_j = n_{j+1}$, $t'_j = t_{j+1}$.

Reduced Quantities

$$\omega \equiv n u \ , \qquad \bar{\omega} \equiv n \bar{u}$$

$$\tau \equiv t/n$$

$$\varphi \equiv (n' - n) c \ , \quad \text{power}$$

Lagrange Invariant

$$\mathcal{H} = \bar{\omega} y - \bar{y} \omega$$

Quantities Derivable from the y-$\bar{y}$ Diagram

$$\Omega \equiv \omega/\mathcal{H} \ , \qquad \bar{\Omega} \equiv \bar{\omega}/\mathcal{H}$$

$$T \equiv \mathcal{H} \tau$$

$$\Phi \equiv \varphi/\mathcal{H}$$

APPENDIX B

DUAL TRANSFORMATIONS OF CONICS

Before we derive the transformations of conics from point to line coordinates and vice versa, we shall quote the formulae necessary to analyze a conic when we are given its general form

$$A x^2 + B xy + C y^2 + D x + E y + F = 0. \tag{B-1}$$

These formulae are derived in books on analytic geometry (e.g., Spain, 1957; Garnier, 1946); and we shall restrict ourselves to summarize them indicating a logical sequence for their use. They are based on the existence of certain quantities which remain invariant when we apply the transformations of rotation and translation to the general Eq. (B-1).

Starting from the general equation of a second degree curve in the cartesian plane, Eq. (B-1), we form the following determinant with its coefficients:

$$\Delta = \begin{vmatrix} 2A & B & D \\ B & 2C & E \\ D & E & 2F \end{vmatrix}, \tag{B-2}$$

which is called the "General Discriminant." From this determinant we now define the following minors

$$\begin{aligned} \Delta_A &\equiv 4CF - E^2, \\ \Delta_B &\equiv DE - 2BF, \\ \Delta_C &\equiv 4AF - D^2, \end{aligned} \tag{B-3}$$

$$\Delta_D \equiv BE - 2CD,$$
$$\Delta_E \equiv BD - 2AE, \qquad \text{(B-3)}$$
$$\Delta_F \equiv 4AC - B^2.$$

We also define the two quantities

$$I \equiv A + C,$$
$$\Delta_{AC} \equiv \Delta_A + \Delta_C. \qquad \text{(B-4)}$$

The quantities Δ, Δ_F, I, and the sign of Δ_{AC}, are invariant under the transformations of rotation and translation, and therefore may be used to classify the different types of conics available. Table II gives such a classification (p. 194; or see Korn and Korn, 1968, p. 42). The curves for which $\Delta_F \neq 0$, are also called "central conics" and in this case, the most common for our application. It is more convenient to carry out first a translation of the origin to the center of the curve and then a rotation of the axes about this center.

The center of the curve is given by

$$(x_0, y_0) = (\Delta_D/\Delta_F, \Delta_E/\Delta_F). \qquad \text{(B-5)}$$

When the translation to this point has been carried out the equation of the curve takes the form

$$Ax'^2 + Bx'y' + Cy'^2 + \Delta/2\Delta_F = 0. \qquad \text{(B-6)}$$

The rotation of the curve through an angle $|\varphi| < \pi/2$ can be used to eliminate the coefficient B in Eq. (B-6). This is accomplished by solving the "characteristic equation,"

$$\lambda^2 - I\lambda + \tfrac{1}{4}\Delta_F = 0. \qquad \text{(B-7)}$$

The roots of this equation λ_1, λ_2 permit us to write Eq. (B-6) in the following form

$$\lambda_1 x''^2 + \lambda_2 y''^2 + \Delta/2\Delta_F = 0. \tag{B-8}$$

Note that these roots may be written also as

$$\lambda_{1,2} = \tfrac{1}{2}(I \pm R), \tag{B-9}$$

where

$$R^2 = I^2 - \Delta_F. \tag{B-10}$$

The choice of the roots is arbitrary, and we shall adopt the following notation: For the ellipse, $\lambda_1 \leq \lambda_2$ and for the hyperbola, $\lambda_1 > 0$, $\lambda_2 < 0$.

The equation of the major axis, that is, the new x-axis after translation and rotation, is

$$y - y_0 = \frac{B}{2(\lambda_1 - C)}(x - x_0), \tag{B-11}$$

and the equation of the minor axis is given by

$$y - y_0 = \frac{B}{2(\lambda_2 - C)}(x - x_0).$$

The angle of inclination of the major axis may also be expressed as

$$\tan\varphi = \frac{B}{2(\lambda_1 - C)} = \frac{A - C + R}{-B}, \tag{B-12}$$

where R is given by Eq. (B-10).

The eccentricity of the conic is given by

$$e = \sqrt{1 - \lambda_1/\lambda_2}. \tag{B-13}$$

Then, we have for the ellipse,

$$\begin{aligned} &\text{the semi-major axis:} && a^2 = -\Delta/(2\lambda_1 \Delta_F), \\ &\text{the semi-minor axis:} && b^2 = a^2(1-e^2), \\ &\text{the semi-focal distance:} && c = ae. \end{aligned} \tag{B-14}$$

And for the hyperbola,

$$\begin{aligned} a^2 &= -\Delta/(2\lambda_1 \Delta_F), \\ b^2 &= a^2(e^2-1), \\ c &= ae. \end{aligned} \tag{B-15}$$

The asymptotes of the hyperbola are given by

$$2Ax + (\mathcal{B} \pm \sqrt{-\Delta_F})\, y = 2A x_0 + (\mathcal{B} + \sqrt{-\Delta_F})\, y_0, \tag{B-16}$$

or alternatively,

$$(\mathcal{B} \pm \sqrt{-\Delta_F})\, x + 2Cy = (\mathcal{B} \pm \sqrt{-\Delta_F})\, x_0 + 2C y_0. \tag{B-17}$$

For the case of a parabola $(\Delta_F = 0)$, we have to proceed in a different way, as there is not a center defined in this case (in fact, it is located at infinity). We must first rotate the axis and then carry out a translation of origins, usually to the vertex of the parabola, the new x-axis being the axis of symmetry of the curve.

We shall not quote the formulae for the parabolic case, as they are not of interest for the present investigation, and the interested reader may find them in the books quoted above. However, we shall quote the only case that may find application in our work, namely when $\Delta_F = 0$ <u>and also</u> $\Delta = 0$.

In this case, as may be appreciated from the Table B-1, the parabola has degenerated in a pair of straight lines, whose equations are

$$\sqrt{A}\,x \pm \sqrt{C}\,y + \frac{\sqrt{A}\cdot D \pm \sqrt{C}\cdot E}{2I} = \frac{\pm\sqrt{-I\cdot\Delta_{Ac}}}{2I}, \qquad \text{(B-18)}$$

where the negative sign of $\sqrt{C}$ is to be chosen when $B < 0$.

We shall now proceed to see how these conics transform from point coordinates to line coordinates and vice versa. For that purpose we shall make use of the concept of homogeneous coordinates; see Gans (1969), and Chapter 2 of this work. The point coordinates will be denoted by (x,y,z) and the line coordinates by (ξ,η,ζ).

The equation of a straight line will be given by

$$x\xi + y\eta + z\zeta = 0, \qquad \text{(B-19)}$$

which may be written in the matrix form

$$(x \;\; y \;\; z)\begin{pmatrix}\xi\\ \eta\\ \zeta\end{pmatrix} = 0. \qquad \text{(B-20)}$$

The equation of the point conic, as defined in Eq. (B-1), in homogeneous coordinates is given by

$$Ax^2 + Bxy + Cy^2 + Dxz + Eyz + Fz^2 = 0. \qquad \text{(B-21)}$$

Note that we may recover the cartesian form of Eq. (B-1) from this expression by setting $z = 1$.

Equation (B-21) may also be written in matrix form as:

$$(x\ y\ z)\begin{pmatrix} 2A & B & D \\ B & 2C & E \\ D & E & 2F \end{pmatrix}\begin{pmatrix} x \\ y \\ z \end{pmatrix} = 0. \qquad \text{(B-22)}$$

The equation of the tangent to this conic at the point (x_1, y_1, z_1), is given by

$$(x\ y\ z)\begin{pmatrix} \xi \\ \eta \\ \zeta \end{pmatrix} = (x\ y\ z)\begin{pmatrix} 2A & B & D \\ B & 2C & E \\ D & E & 2F \end{pmatrix}\begin{pmatrix} x_1 \\ y_1 \\ z_1 \end{pmatrix} = 0; \qquad \text{(B-23)}$$

comparing both sides of this expression we see that

$$\begin{pmatrix} \xi \\ \eta \\ \zeta \end{pmatrix} = \begin{pmatrix} 2A & B & D \\ B & 2C & E \\ D & E & 2F \end{pmatrix}\begin{pmatrix} x_1 \\ y_1 \\ z_1 \end{pmatrix} \qquad \text{(B-24)}$$

and solving for the point of tangency,

$$\begin{pmatrix} x_1 \\ y_1 \\ z_1 \end{pmatrix} = \begin{pmatrix} 2A & B & D \\ B & 2C & E \\ D & E & 2F \end{pmatrix}^{-1}\begin{pmatrix} \xi \\ \eta \\ \zeta \end{pmatrix}; \qquad \text{(B-25)}$$

But the point (x_1, y_1, z_1) is on the line (ξ, η, ζ), whose equation is given by

$$(\xi\ \eta\ \zeta)\begin{pmatrix} x_1 \\ y_1 \\ z_1 \end{pmatrix} = 0. \qquad \text{(B-26)}$$

Substituting Eq. (B-25) into Eq. (B-26) we have therefore

$$(\xi\ \eta\ \zeta)\begin{pmatrix} 2A & B & D \\ B & 2C & E \\ D & E & 2F \end{pmatrix}^{-1}\begin{pmatrix} \xi \\ \eta \\ \zeta \end{pmatrix} = 0, \tag{B-27}$$

which is the equation of the conic in terms of its tangents, or in other words, is the equation of the line conic. This is the equation of the conic in the dual space.

The inverse of the matrix of the coefficients of the conic, defined by Eq. (B-24), may be expressed in terms of its minors defined in Eq. (B-3). Let us call the original matrix M; then

$$M^{-1} \equiv \begin{pmatrix} 2A & B & D \\ B & 2C & E \\ D & E & 2F \end{pmatrix}^{-1} = \frac{1}{\Delta}\begin{pmatrix} \Delta_A & \Delta_B & \Delta_D \\ \Delta_B & \Delta_C & \Delta_E \\ \Delta_D & \Delta_E & \Delta_F \end{pmatrix}, \tag{B-28}$$

where Δ is given by Eq. (B-2) and is the determinant of the matrix M. Let us call $\tilde{M}$ the matrix whose elements are the minors of M and whose form is given in Eq. (B-28). Its determinant will be denoted by $\tilde{\Delta} \equiv |M|$ and its corresponding minors will be $\tilde{\Delta}_A$, $\tilde{\Delta}_B$, etc. We may rewrite Eq. (B-28) as follows

$$M^{-1} = \tilde{M}/\Delta \tag{B-29}$$

We wish to find now the determinant of the inverse,

$$|M^{-1}| = |\tilde{M}/\Delta| = |\tilde{M}|/\Delta^3 = \tilde{\Delta}/\Delta^3. \tag{B-30}$$

For this purpose we remember that

$$M M^{-1} = M\tilde{M}/\Delta = \text{the unit matrix}, \tag{B-31}$$

and

$$|M M^{-1}| = |M| \cdot |\tilde{M}/\Delta| = \tilde{\Delta}/\Delta^2 = 1 \tag{B-32}$$

therefore

$$\tilde{\Delta} = \Delta^2. \tag{B-33}$$

Also, note that

$$\left(M^{-1}\right)^{-1} = M = \Delta \cdot M^{-1} = \frac{\Delta}{\tilde{\Delta}} \begin{pmatrix} \tilde{\Delta}_A & \tilde{\Delta}_B & \tilde{\Delta}_D \\ \tilde{\Delta}_B & \tilde{\Delta}_C & \tilde{\Delta}_E \\ \tilde{\Delta}_D & \tilde{\Delta}_E & \tilde{\Delta}_F \end{pmatrix} = \begin{pmatrix} 2A & \mathcal{B} & \mathcal{D} \\ \mathcal{B} & 2C & E \\ \mathcal{D} & E & 2F \end{pmatrix}, \tag{B-34}$$

therefore,

$$\begin{aligned} \tilde{\Delta}_A &= 2A \cdot \Delta \\ \tilde{\Delta}_B &= \mathcal{B} \cdot \Delta \\ \tilde{\Delta}_C &= 2C \cdot \Delta \\ \tilde{\Delta}_D &= \mathcal{D} \cdot \Delta \\ \tilde{\Delta}_E &= E \cdot \Delta \\ \tilde{\Delta}_F &= 2F \cdot \Delta \end{aligned} \tag{B-35}$$

As a check we may calculate from these expressions the value of the determinant $\tilde{\Delta}$:

$$\begin{aligned} \tilde{\Delta} &= \Delta_D \cdot \tilde{\Delta}_D + \Delta_E \cdot \tilde{\Delta}_E + \Delta_F \cdot \tilde{\Delta}_F = \\ &= \Delta \left(\mathcal{D} \Delta_D + E \Delta_E + 2F \Delta_F \right) = \Delta^2, \end{aligned} \tag{B-36}$$

which agrees with the value obtained in Eq. (B-33).

Using Eq. (B-28) and Eq. (B-27), we see that the equation of the conic in the dual space (ξ, η, ζ) is given by

$$(\xi \;\; \eta \;\; \zeta) \begin{pmatrix} \Delta_A & \Delta_B & \Delta_D \\ \Delta_B & \Delta_C & \Delta_E \\ \Delta_D & \Delta_E & \Delta_F \end{pmatrix} \begin{pmatrix} \xi \\ \eta \\ \zeta \end{pmatrix} = 0; \tag{B-37}$$

or written in expanded form for cartesian coordinates ($\zeta = 1$), we have

$$\Delta_A \xi^2 + 2\Delta_B \xi\eta + \Delta_C \eta^2 + 2\Delta_D \xi + 2\Delta_E \zeta + \Delta_F = 0. \tag{B-38}$$

This is the dual transform of the conic given by Eq. (B-1), which is also a conic as expected (see Basset, 1901, p. 30, and Zwikker, 1950, p. 76).

We finish this appendix by noting that the coordinates (x,y,z) and (ξ, η, ζ) are interchangeable, due to Eq. (B-19). Thus, the conic

$$A\xi^2 + B\xi\eta + C\eta^2 + D\xi + E\eta + F = 0, \tag{B-39}$$

is transformed into the conic

$$\Delta_A x^2 + 2\Delta_B xy + \Delta_C y^2 + 2\Delta_D x + 2\Delta_E y + \Delta_F = 0. \tag{B-40}$$

TABLE II

CLASSIFICATION OF CONICS
IN TERMS OF Δ, Δ_F, I, AND Δ_{Ac}

1. $\Delta_F > 0$, elliptic curve:

   a) $I\Delta < 0$; real ellipse, ($I^2 = \Delta_F$, circumference).

   b) $I\Delta = 0$; a point, punctual ellipse.

   c) $I\Delta > 0$; no geometric locus, imaginary ellipse.

2. $\Delta_F < 0$, hyperbolic curve:

   a) $\Delta \neq 0$; real hyperbola, ($I = 0$, equilateral hyperbola).

   b) $\Delta = 0$; two intersecting straight lines, the asymptotes.

3. $\Delta_F = 0$, parabolic curve:

   a) $\Delta \neq 0$; real parabola

   b) $\Delta = 0$; degenerate parabola:

      i) $\Delta_{Ac} < 0$; two parallel straight lines.

      ii) $\Delta_{Ac} = 0$; a single straight line, coincident parallels.

      iii) $\Delta_{Ac} > 0$; no geometric locus, imaginary parallels.

LIST OF REFERENCES

Basset, A. B. (1901), An Elementary Treatise on Cubic and Quartic Curves. Cambridge: Deighton.

Berek, M. (1930), Grundlagen der Praktischen Optik, Analyse und Synthese Optischer Systeme. Berlin: De Gruyter.

Born, M. and E. Wolf. (1970), Principles of Optics. London: Pergamon Press.

Brouwer, W. (1964), Matrix Methods in Optical Instrument Design. New York: Benjamin.

Chrétien, H. (1958), Calcul des Combinaisons Optiques. Paris: Sennac.

Coxeter, H. S. M. (1969), Introduction to Geometry. New York: Wiley (2nd. Ed.).

Darnauer, J. H. (1971), Properties of Generalized Bending. Optical Sciences Center Technical Report No. 64. Tucson: University of Arizona.

Delano, E. (1963), "First Order Design and the y-$\bar{y}$ Diagram," Applied Optics. Vol. 2, No. 12, p. 1251.

Gans, D. (1969), Transformations and Geometries. New York: Appleton-Century-Crofts.

Garnier, E. (1946), La Matematica che Serve. Milano: Hoepli.

Goldstein, H. (1953), Classical Mechanics. Cambridge, Mass: Addison-Wesley.

Herzberger, M. (1944), "Replacing a Thin Lens by a Thick Lens," Journal of the Optical Society of America. Vol. 34, No. 2, p. 114.

Hopkins, H. H. (1950), Wave Theory of Aberrations. Oxford: Clarendon Press.

Hopkins, H. H. and V. V. Rao. (1970), "The Systematic Design of Two Component Objectives," Optica Acta. Vol. 17, No. 7, p. 497.

Hopkins, R. E. and R. Hanau. (1962), "First Order Optics," Ch. 6 in Military Standardization Handbook on Optical Design. Washington, D. C. Defense Dept.

Korn, G. A. and T. M. Korn. (1968), Mathematical Handbook for Scientists and Engineers. New York: McGraw-Hill, (2nd. Ed.)

López-López, F. J. (1970a), "Normalization of the Delano Diagram" Applied Optics. Vol. 9, No. 11, p. 2485. Optical Sciences Center Technical Report No. 57.

López-López, F. J. (1970b), "A New Tool for the Teaching of Geometrical Optics" (A), Journal of the Optical Society of America. Vol. 60, No. 11, p. 1564. American Journal of Physics. Vol. 38, No. 12, p. 1500.

López-López, F. J. (1971a), "Use of the Normalized Delano Diagram in the Design of a Two Mirror System of the Schwarzschild Concentric Type" (A), Journal of the Optical Society of America. Vol. 61, No. 5, p. 661.

López-López, F. J. (1971b), "Vectorial Representation of the Delano (y-$\bar{y}$) Diagram" (A), Journal of the Optical Society of America. Vol. 61, No. 5, p. 685.

López-López, F. J. (1971c), "General Treatment of the Thick Lens in the Delano Diagram" (A), Journal of the Optical Society of America. Vol. 61, No. 11, p. 1566.

López-López, F. J. (1971d), "Notes on the y-$\bar{y}$ Diagram. Vector Complex Number, and Matrix Representations." Optical Sciences Center Newsletter. Vol. 5, No. 3, p. 101, Tucson: University of Arizona.

López-López, F. J. (1972a), "Generalized Bending and Thickening of Lenses" (A), Journal of the Optical Society of America. Vol. 62, No. 5, p. 712.

López-López, F. J. (1972b), "Notes on the y-$\bar{y}$ Diagram. General Properties of a Thick Lens." Optical Sciences Center Newsletter. Vol. 6, No. 2, p. 51. Tucson: University of Arizona.

López-López, F. J. (1972c), "The Application of the Delano (y-$\bar{y}$) Diagram to Optical Design" (A), Journal of the Optical Society of America. Vol. 62, No. 11, p. 1348.

López-López, F. J. (1972d), "Inhomogeneous Media in the y-$\bar{y}$ Diagram" (A), Journal of the Optical Society of America. Vol. 62, No. 11, p. 1375.

López-López, F. J. and T. Sette Jr. (1972), "Stop Shift and Conjugate Shift are not Commutative," Optical Sciences Center Newsletter. Vol. 6, No. 1, p. 9.

Maxwell, E. A. (1963), The Methods of Plane Projective Geometry Based on the Use of General Homogeneous Coordinates. Cambridge: University Press.

O'Neill, E. L. (1963), Introduction to Statistical Optics. Reading, Mass.: Addison-Wesley.

Pegis, R. J., T. P. Vogl, A. K. Rigler and R. Walters. (1967), "Semiautomatic Generation of Optical Prototypes," Applied Optics. Vol. 6, No. 5, p. 969.

Powell, F. M. (1970), "y-$\bar{y}$ Diagram Analysis of Two-surface Optical Systems with Zero Third-order Spherical Aberration." Optical Sciences Center Technical Report No. 55.

Rayces, J. L. (1955), "Petzval Sum of Thick Lenses," Journal of the Optical Society of America. Vol. 45, No. 9, p. 774.

Shack, R. V. (1972), "Optical System Layout" in New Methods in Optical Design and Engineering, (Short Course Notes) Optical Sciences Center. Tucson: University of Arizona.

Spain, B. (1957), Analytic Conics. London: Pergamon.

Stavroudis, O. N. (1971), University of Arizona. Private communication.

Sutton, L. E. (1963), "A Method for Localized Variation of the Paths of Two Paraxial Rays," Applied Optics. Vol. 2, No. 12, p. 1275.

Zwikker, C. (1950), Advanced Plane Geometry. Amsterdam. North-Holland. (Republished 1963, as The Advanced Geometry of Plane Curves and their Applications. New York: Dover.)